NTNU – Trondheim
Norwegian University of
Science and Technology

Bucket Foundation in Clay for OWT Subjected to Combined Cyclic Loads

Ying Chen

Wind Energy
Submission date: June 2014
Supervisor: Torgeir Moan, IMT
Co-supervisor: Hans Petter Jostad, BAT
Kristoffer Skjolden Skau, Norwegian Geotechnical Institute

Norwegian University of Science and Technology
Department of Marine Technology

Master of Science Thesis

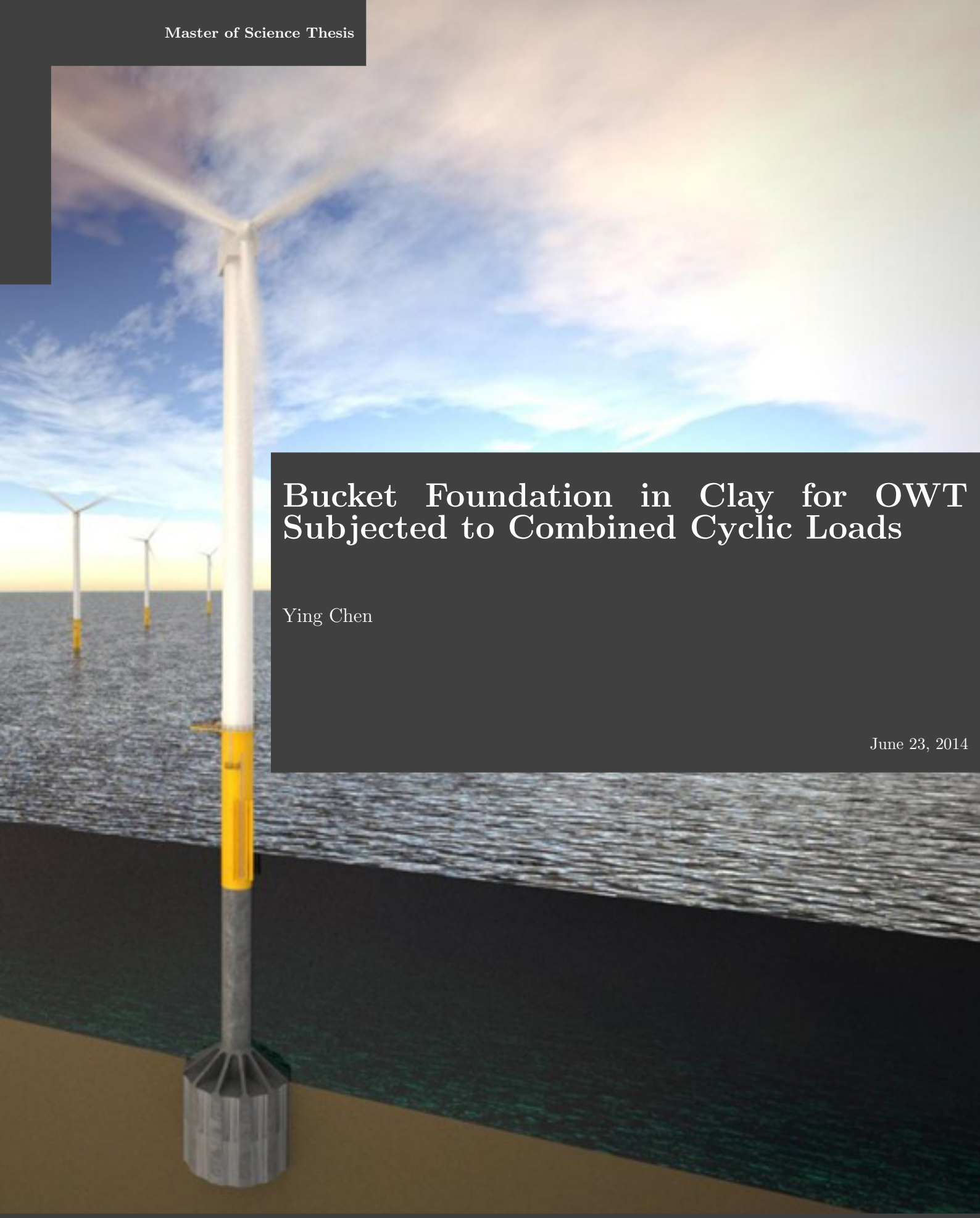

Bucket Foundation in Clay for OWT Subjected to Combined Cyclic Loads

Ying Chen

June 23, 2014

European Wind Energy Master - EWEM - Offshore Engineering Track

Bucket Foundation in Clay for OWT Subjected to Combined Cyclic Loads

Master of Science Thesis

For obtaining the degree of Master of Science in Offshore Engineering at Delft University of Technology and in Technology-Wind Energy at Norwegian University of Science and Technology.

Ying Chen

June 23, 2014

European Wind Energy Master - EWEM

Delft University of Technology
Faculty of Mechanical, Maritime and Materials Engineering
Department of Maritime and Transport Technology
Section of Offshore and Dredging Engineering

Norwegian University of Science and Technology
Faculty of Engineering Science and Technology
Department of Marine Technology

Cover photo - The Bucket Foundation, courtesy of Universal Foundation

European Wind Energy Master - EWEM
Of
Offshore Engineering Track

The undersigned hereby certify that they have read and recommend to the European Wind Energy Master - EWEM for acceptance a thesis entitled **"Bucket Foundation in Clay for OWT Subjected to Combined Cyclic Loads"** by **Ying Chen** in partial fulfillment of the requirements for the degree of **Master of Science**.

Dated: June 23, 2014

Supervisor: _____
Prof. A. Metrikine of TU Delft

Supervisor: _____
Prof. H.P. Jostad of NTNU

Daily supervisor: _____
K.S. Skau of NGI

Reader: _____
Dr.Ir. R.B.J. Brinkgreve of TU Delft

Reader: _____
Dr.Ir. W. Broere of TU Delft

Summary

The need for cost reduction of OWT has been a great priority for the wind industry since the early beginning of the development of OWT. The foundation, account for around one third of total cost of offshore wind turbine system, is an important part to be optimized to bring down the cost of OWT systems. Bucket foundations have been given much attention recently due to its low cost and easy installation method. However, the cyclic loading conditions experienced by OWT should be investigated more before applying it to commercial wind farms.

This thesis project investigates the bucket foundation in clay subjected to cyclic loads. The cyclic irregular loading history in this thesis was represented by the equivalent number of cycles N_{eq} with a certain level of cyclic to average stress ratio τ_{cy}/τ_a which can be derived using cyclic shear strain accumulation procedure developed in NGI. The first part is the bearing capacity analysis of bucket foundation in clay. The second part is to produce the displacement contour diagrams.

The bearing capacity analysis used in-house software BIFURC from NGI. The normalized failure envelopes were investigated for different degree of cyclic degradation expressed by N_{eq}, soil profiles and bucket foundation geometry h/D. The two soil profiles used in this thesis project were constant cyclic shear strength with depth for OCR=40 and linearly increase cyclic shear strength with depth for OCR=1 & 40. Drammen clay was used as basis for the evaluation.

The mobilized ultimate capacity were plotted for pure horizontal load, pure vertical load and pure overturning moment. The loads were applied in the decoupling point, meaning that the pure horizontal load fail under pure sliding. It was found that the three load component were equally influenced by cyclic degradation and that the increase and reduction in the total failure as function of N_{eq} and F_{cy}/F_a could be defined by one curve for a given OCR.

The cyclic effect during combined loading was studied through normalized failure envelopes. The normalized failure envelopes do not change for changing cyclic loading history for the same soil profile. The normalized failure envelopes changed in HM load plane due to different h/D and different soil profiles. The failure envelopes describes a

full surface in the 3D load space HVM. Besides, the failure envelopes could be described by formulas suggested by Gourvenec and Barnett with some modifications for the failure envelopes in HM plane.

Displacement contour diagrams were produced for a wide range of load combination in HVM load space. MATLAB was used to interpolate the results from bearing capacity analysis to produce the displacement contour diagrams. The displacement contours gives the stiffness for bucket foundation under cyclic loading.

In the end of this thesis, a procedure was made to account cyclic loading to determine the bearing capacity and stiffness for bucket foundation for OWT. The cyclic loads as input parameters are represented by N_{eq} and F_{cy}/F_a. The other input parameters are bucket foundation geometry h/D and soil profile.

Suggestions for further work can be found in Section 6.2.

Acknowledgements

I would like to express my deep gratitude to Kristoffer Skjolden Skau and Professor Hans Petter Jostad from NGI, for proposing this thesis topic, for their daily supervision and for reviewing on my report.

I also would like to appreciate the valuable comments from Professor Andrei Metrikine, Dr.Ir.Ronald Brinkgreve and Dr.Ir.Wout Broere from TU Delft. I want to thank to all the EWEM coordination members and 2012-2014 EWEM cohorts for their help during last two years.

I would like to thank NGI for offering the opportunity for me to join the professional geotechnical working environment, the chances to attend many lectures offered from geotechnical experts around the world. I also want to thank all the friendly employees and their weekly cake from CGM in NGI.

Last but not least, I would like to thank to my parents for their encouragement and support for my study.

Oslo, Norway
June 23, 2014

Ying Chen

Nomenclature

Latin Symbols

F_a	Average load on the bucket foundation
F_{cy}	Cyclic load on the bucket foundation
H_{ult}	Ultimate horizontal capacity
$K_0^{'}$	Coefficient of earth pressure at rest
M_{ult}	Ultimate overturnning moment
N_{eq}	Equivalent number of cycles
N_F	Number of cycles
s_u	Undrained static shear strength
s_u^C	Undrained static shear strength under triaxial compression
s_u^{DSS}	Undrained static shear strength under direct simple shear
s_u^E	Undrained static shear strength under triaxial extension
u_{cy}	Cyclic pore pressure component
u_p	Permanent pore pressure
$v_{'}$	Poissons ratio
V_{ult}	Ultimate vertical capacity
d	Wall thickness of bucket foundation
u	Horizontal displacement
w	Vertical displacement

Greek Symbols

α	soil-skirt roughness factor
α_{bs}	Reduction factor for shear on structure outside area
α_{ss}	Reduction factor for shear on soil side areas
γ	Shear strain
$\gamma^{'}$	Soil effective unit weight
γ_C	Shear strain at failure in triaxial compression
γ_f^{DSS}	Shear strain at failure in direct simple shear
γ_f^E	Shear strain at failure in triaxial extension
$\sigma_H^{'}$	Horizontal effective stresses
$\sigma_v^{'}$	Vertical and horizontal effective stresses
$\tau_{f,cy}^C$	Cyclic shear strength under triaxial compression
$\tau_{f,cy}^{DSS}$	Cyclic shear strength under direct simple shear
$\tau_{f,cy}^E$	Cyclic shear strength under triaxial extension
τ_0	Initial consolidation shear stress
$\tau_{a,f}$	Average shear strength at failure
τ_a	Average shear stress
$\tau_{cy,f}$	Cyclic shear strength at failure
τ_{cy}	Cyclic shear stress
τ_{static}	Static shear strength
θ	Rotational radian

Abbreviations

1P	First excitation frequency of wind turbines,Rotor rotational frequency
2D	2 Dimensional
3D	3 Dimensional
3P	Second excitation frequency of wind turbines,Rotor blade passing frequency
ALS	Accidental Limit State
CGM	Computational Geomechanics
C	Triaxial Compression
DNV	Det Norske Veritas
DSS	Direct Simple Shear
D	Diameter
EU	European Union
EWEM	European Wind Energy Master
E	Triaxial Extension
FEA	Finite Element Analysis

FEM	Finite Element Method
FLS	Fatigue Limit State
GW	Gigawatt
HM	Horizontal-overturning Moment
HVM	Horizontal-Vertical-overturning Moment
HV	Horizontal-Vertical
h	Height
NGI	Norwegian Geotechnical Institute
NTNU	Norwegian University of Science and Technology
OCR	Over Consolidation Ratio
OWF	Offshore Wind Farms
OWT	Offshore Wind Turbines
RP	Reference Point
SLS	Serviceability Limit State
TU Delft	Delft University Of Technology
ULS	Ultimate Limit State
VM	Vertical-overturning Moment

Contents

List of Figures

List of Tables

Chapter 1

Introduction and literature study

1.1 General introduction

1.1.1 Problem definition

Cyclic loading of soils and foundations has been investigated by many researchers around the world. This research include different approaches to describe cyclic soil behaviour, such as cyclic constitutive models, foundation models, pore pressure accumulation diagrams etc. The accumulation procedure developed at NGI is one such method. The method has been widely used and validated through several model tests and field tests. However, the method is developed on soil element level and there is still need to describe effects of cyclic loading on foundation level. This thesis investigates the effect of cyclic loading on the foundation capacity and the foundation stiffness for bucket foundations in clay. Combined loading of vertical, horizontal and moment loads were considered.

A common way to express foundation capacity for combined loading is to establish failure envelopes. There is however to the authors knowledge no existing failure envelopes were adjusted for cyclic loading.

Foundation stiffness can be described using displacement contour diagrams which is similar to strain contour diagrams used for soil element.

1.1.2 Limitations

The limitations for bucket foundation in clay subjected to combined cyclic loads investigated in this thesis are as follows:

- The study in this thesis is based on Drammen clay data;
- The soil is assumed to be perfectly undrained condition when bucket foundation subjected to cyclic loads;

- The combined cyclic loads are assumed in-plane loading condition, namely the three loads are applied to the foundation in the same plane.
- Two idealized soil profiles are used in this thesis. One soil profile has linear increase cyclic shear strength with depth for both normal consolidated clay(OCR=1) and heavily over consolidated clay(OCR=40) and another soil profile has constant cyclic shear strength with depth for heavily over consolidated clay(OCR=40).

1.1.3 Objectives

The first object is to investigate the cyclic loading effects on pure loading situations which are pure horizontal load, pure vertical load and pure overturning moment load. The ultimate cyclic capacity for horizontal, vertical and moment will be compared to the corresponding ultimate static capacity.

The second objective of this thesis is to produce failure envelopes for bucket foundation subjected to combined cyclic load for different soil profiles and different bucket foundation geometries. This thesis aims to investigate whether the failure envelopes will be changed due to the cyclic loads, the bucket foundation geometry and the soil profile.

The third objective of this thesis was to produce the displacement contour diagrams for varying cyclic load history and bucket foundation geometry h/D. The displacement contour diagram gives the soil-structure stiffness which can be used in bucket foundation design phase.

If possible, it was also a final objective to systemize and organize the results so it could be used efficiently for approximations of bucket capacity and foundation stiffness of a foundation subjected to cyclic loading.

The rest of this chapter is the literature study on the bucket foundation for OWT subjected to combined cyclic loads.

1.2 Offshore wind energy development

Offshore wind power has developed fast the last decade in Europe. Figure 1.1 shows that the annual offshore wind power installations (red columns) has been increased from 1% of the annual EU wind energy installation in 2001 up to 14% in 2013. Because of the total offshore wind power installation targets of 40 GW produced within 2020 for EU, it is expected to drive the offshore wind energy production to increase in the coming years.

Figure 1.2 shows OWT are installed in continually deeper water. Deeper water will impose higher loads on the foundation which may change the foundation methods for OWT. Figure 1.3 shows typical foundation concepts for OWT suitable for different water depth. The wind industry is forced to reduce the cost of offshore wind to make it a more competitive renewable energy source. Figure 1.4 gives the breakdown cost for typical wind turbines and the cost of foundation is around 30%. Reducing foundation cost will therefore significantly reduce the overall cost for OWT.

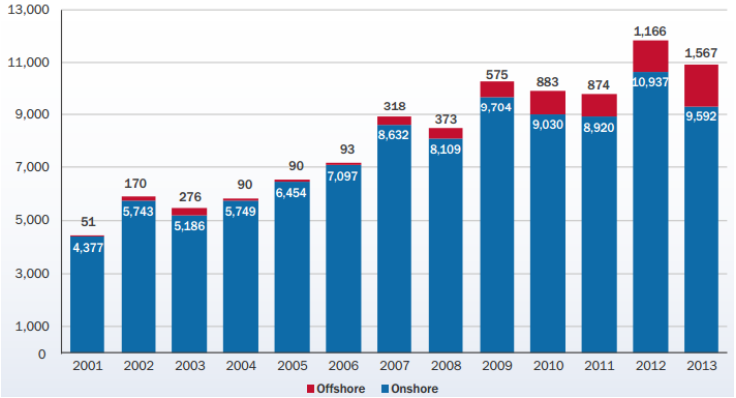

Figure 1.1: *Annual onshore and offshore installations[4]*

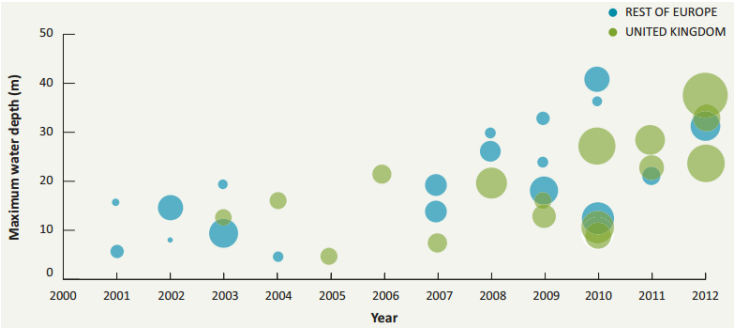

Figure 1.2: *Water depth tend for OWT[5]*

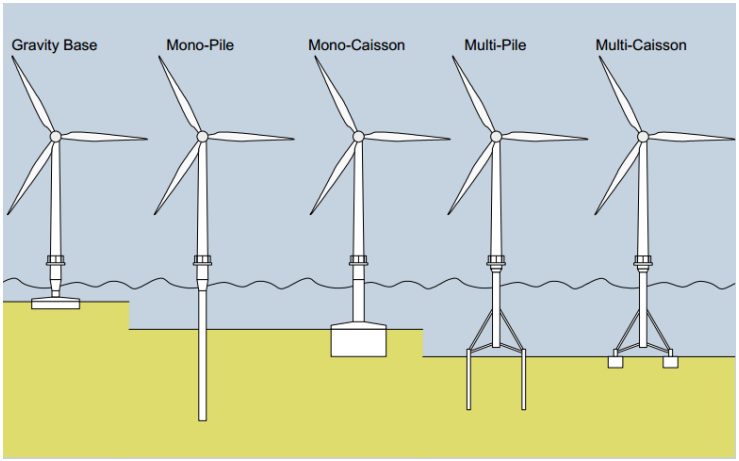

Figure 1.3: *Different foundation types for OWT from Byrne [6]*

1.3 Foundation types for OWT

Gravity based, mono-pile and multi-pile foundations have been applied in offshore wind farms (OWF) while caisson type foundations have not been used in commercial wind farms until now. However, one prototype of wind turbine with bucket foundation has been installed in the test field in Frederikshavn in December 2002[1]. Figure 1.5 shows

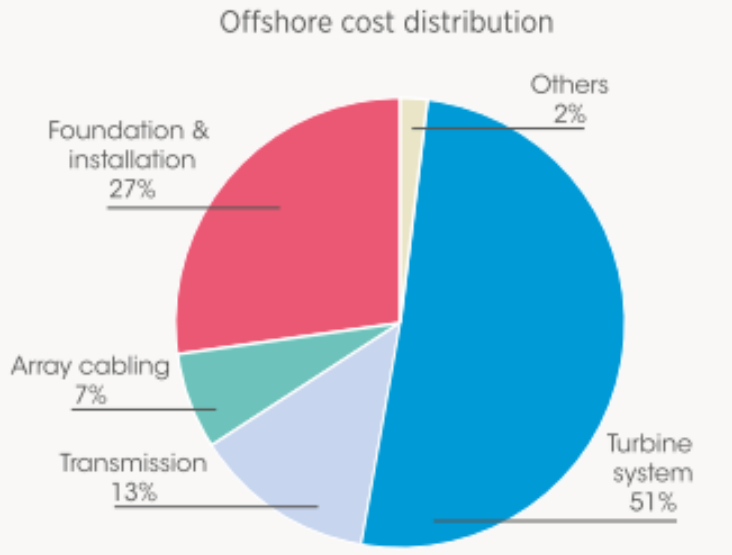

Figure 1.4: *Capital cost for a typical offshore wind system[7]*

that the dominating foundation type up to now has been mono-piles. Different foundation concepts are described briefly in the following sections.

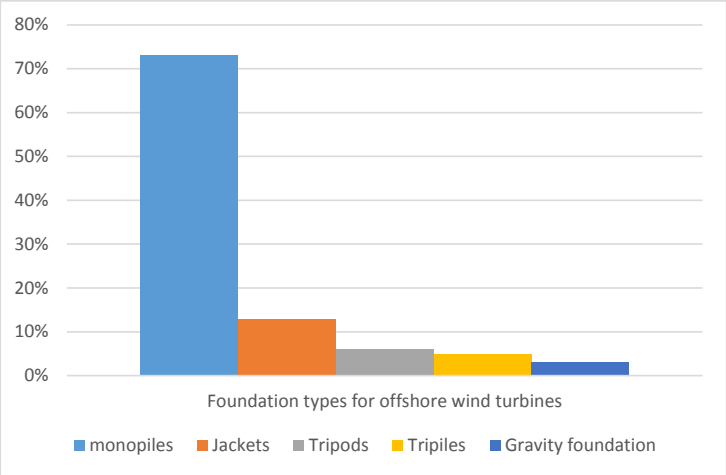

Figure 1.5: *Foundations used for OWT until 2012[4]*

1.3.1 Gravity based foundation

Most of the gravity based foundations (Figure 1.3) are made of concrete with or without skirts which can be ballasted with sand to obtain sufficient dead weight to resist the horizontal load and overturning moment. It was first applied for OWT in 1990s at the world first offshore wind farm Vindeby in Denmark.

The gravity based foundation has lots of advantages and is still developing to be suitable in deeper water and to be able to easy install. The suitable water depth of gravity based

foundation can vary from several meters to hundred meters. The installation generates low noise which has small environment impact. It is durable and has low maintenance requirement. It can be designed to support large wind turbines like 8MW and it has low fatigue sensitivity.

However, as OWT go to deeper water and harsh environment, the gravity foundation also faced lots of challenges, such as heavy installation vessels which can transport and install the giant gravity foundation. The decommissioning also caused troubles for gravity foundations as it is not easy to take away.

1.3.2 Mono-pile foundation

Mono-pile foundation shown in Figure 1.3 is normally made of cylindrical steel where the tip is connected to the transition piece or to the tower directly and the end is penetrated into the seabed to provide sufficient capacity. It is a relative simple structure and is the most common foundation type in OWF. The typical water depth for mono-pile foundation is from 0 to around 35m. The installation is typically carried out by hammer driving. The noise generated by the driving activities has raised environment concerns. The fabrication and installation challenges of large diameter piles required for large water depth may limit the use in the future.

The mono-pile foundations are flexible and the natural frequency of the OWT should be designed to avoid the resonance with the rotor rotational frequency 1P and blades passing frequency 3P as well as wave frequency. This may represent a challenge in deep water and for large OWT with higher loads.

1.3.3 Multi-pile foundation

Multi-pile foundation can be used with jacket and tri-pile support structures. The multi-pile support structures are generally stiffer and the resonance is less problematic for multi-pile foundation compared to the mono-pile foundations.

In addition, the loading regime, which is different when compared to mono-pile foundations. The global overturning moment at mudline is taken up by vertical compression and extension force. The tri-pile foundation has been used in BARD Offshore 1 wind farm in Germany in 2013.

1.3.4 Bucket foundation

Bucket foundation is also called suction caisson or skirted foundation. Bucket foundations are usually a cylindrical segment of steel or concrete. The cylinders are open at the bottom and closed at the top. It has been used wildly in offshore oil&gas industry in almost 30 years. The applicability of bucket foundations for OWT is still on research level and not taken into commercial use. Relative low costs and easy installation make bucket foundation interesting for OWT. Its main characteristic are as follows:

- Low fabrication because of low metal usage[8];

- Low installation cost;
- No driving/drilling means low noise emission;
- Easy removal during decommissioning.

However, it can be very sensitive to the soil conditions compared to other foundation types. The detailed discussion of bucket foundation for OWT will be given in the following sections.

1.4 Load conditions for foundations for OWT

According to DNV[9], the geotechnical investigation should include both laboratory test and in-situ testing. The main geotechnical data should be included as follows:

- Data for soil classification and description;
- Shear strength and deformation properties, as required for the type of analysis to be carried out;
- In-situ stress conditions.

In terms of soil shear strength, DNV mentions that the shear strength should be determined properly due to cyclic loading. The cyclic shear strength might be smaller than static shear strength due to the large cyclic horizontal force and overturning moment[10].

OWT are normally subjected to a combination of wave, current and wind loads. The loads can be divided into permanent loads and environment loads.

The permanent loads are as follows[9]:

- dead weight of structure;
- dead weight of permanent ballast and equipment;
- External and internal hydrostatic pressure of a permanent nature being a reaction to the above, e.g. articulated tower base reaction;

The environment loads are as follows[9]:

- wind loads;
- hydrodynamic loads induced by waves and current, including drag forces and inertia forces;
- earthquake loads;
- current-induced loads;
- tidal effects;

- marine growth;

- Snow and ice loads;

The cyclic environmental loads dominant the loads applied to OWT. The cyclic loads consist of both wave and wind loads, making the frequency content complex. The cyclic nature of the loads significantly influence the soil and foundation behaviour.

1.5 Bucket foundation for OWT

Bucket foundation shown in Figure 1.6 has been discussed as a foundation method for OWT for many years[1]. It has been used widely for offshore structures like suction piles and suction anchors for oil & gas platforms and mooring systems, respectively. Nevertheless, the design of bucket foundation for offshore wind turbine is different compared to foundation design for conventional offshore structures where the dominate force is self-weight. The dominant forces for OWT are horizontal force and overturning moment.

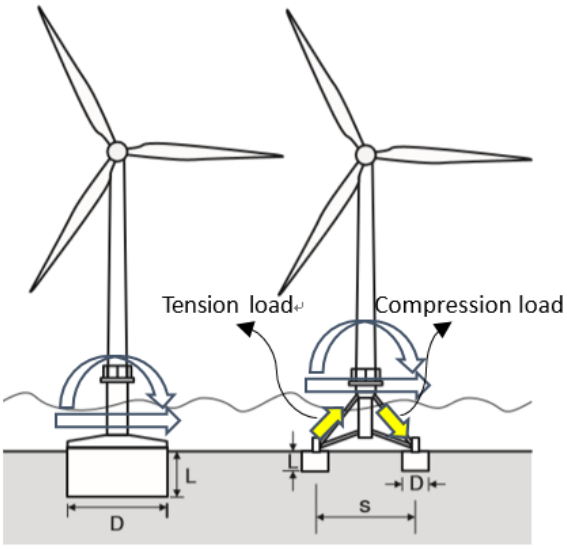

Figure 1.6: *Bucket foundations for a wind turbine: left: monopod, right: tripod[1]*

1.5.1 Loads on bucket foundations for OWT

The critical load applied to a mono bucket foundation and multi-leg support structure are different. The critical loads are horizontal load and overturning moment for the mono bucket foundation. While the tension and compression loads may occur at some legs for multi-leg support structures in addition to horizontal loads and overturning moment. Figure 1.6 shows load regimes for bucket foundations with monopod support structure and multi-leg support structure, respectively.

1.5.2 Geotechnical design aspects of bucket foundation for OWT

The design of bucket foundation can be divided into three phases which are design basis, conceptual design and detailed design. This project cannot include all of them due to the time limitation.

This thesis focus on the ultimate limit state(ULS) design for undrained condition which is part of the conceptual design to determine the dimensions of the bucket foundation. The other aspects in the conceptual design phase are loading combinations, other limite states(SLS,ALS,FLS) and the installation study[1].

The bearing capacity in ULS analysis of bucket foundation is usually determined either by limiting equilibrium methods or FEM[11].

For the undrained condition, the capacity is governed by an undrained cyclic shear strength, the load combinations and the bucket foundation geometry[11]. The determination of undrained cyclic shear strength is the first part of the undrained bearing capacity analysis. Then the undrained bearing capacity can be analysed for a specific bucket foundation geometry under certain loading combinations.

1.6 Summary

This chapter gives information about this thesis topics and objectives. Besides, the literature study also presented in this chapter.

The literature study includes the offshore wind energy development and different foundations for fixed OWT. The features for different foundations were included to compare with the bucket foundation which was investigated in this thesis.

For the bucket foundation, the development of bucket foundation and advantages of using bucket foundation were enclosed in this chapter. The loading regimes were introduced here for using bucket foundation for mono-pod and jacket support structure for OWT respectively.

The next chapter presents the soil behaviour under cyclic loading. A NGI accumulation procedure method for predicting soil behaviour under cyclic loading was enclosed in the next chapter.

Chapter 2

Soil behaviour under cyclic loads

Cyclic loading is important for offshore foundation design as it may reduce the soil shear strength as well as stiffness[12].

The reason for reduced shear strength and stiffness is that the cyclic loading tends to breakdown the soil structure and increase the pore pressure during undrained conditions. The left picture in Figure 2.1 shows the stress history with constant average shear stress,τ_a and constant cyclic shear stress,τ_{cy}. The right picture in Figure 2.1 gives the pore pressure change due to the stress history.

According to Figure 2.1, the permanent pore pressure,u_p increases with time in addition to a cyclic pore pressure component, u_{cy} fluctuates on top of the permanent pore pressure. The increase of pore pressure leads to increasing cyclic and average strain.

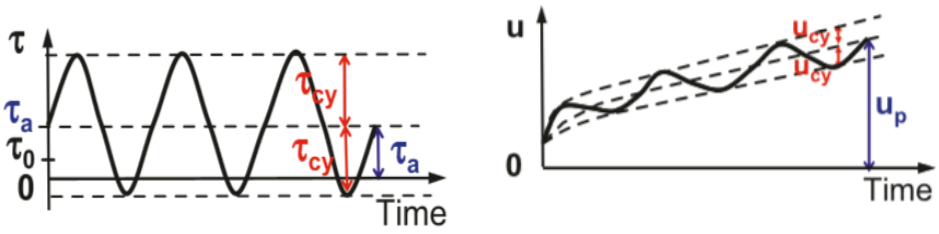

Figure 2.1: *Pore pressure as function of time under cyclic loading. u_p, permanent pore pressure,τ_0, initial consolidation shear stress,u_{cy}, cyclic pore pressure[12]*

Soil response can be assumed to be perfectly undrained for clay during a storm period. Figure 2.2 presents the development of cyclic shear strain and average shear strain for two different stress ratio. The shear failures are large cyclic shear strain in the left and large average strain in the right. The shear failure defined by either large average shear strain or large cyclic shear strain or combination of two, depending on the cyclic to average stress ratio, τ_{cy}/τ_a applied to the soil element[13]. NGI uses shear strain level of 15% for either the average shear strain or the cyclic shear strain as the failure criteria. Figure 2.3 shows

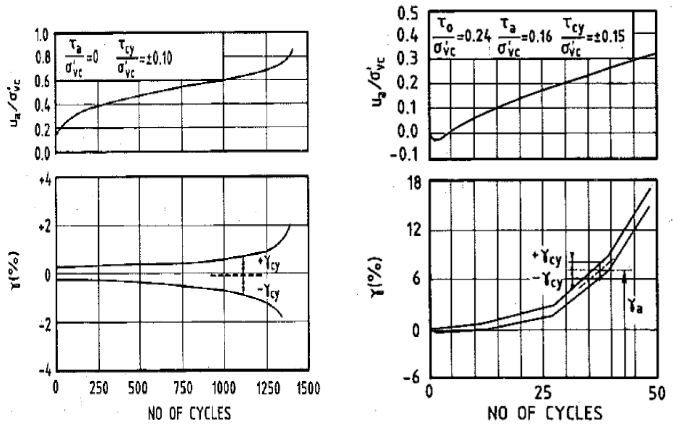

Figure 2.2: *Shear failure, (left) Large cyclic strain, (right) Large average strain*

the failure contours which defined by number of cycles, N_F, and various combination of τ_a and τ_{cy}. The evolution of cyclic strain γ_{cy} and average strain γ_a are indicated on Figure 2.3 with the dashed lines.

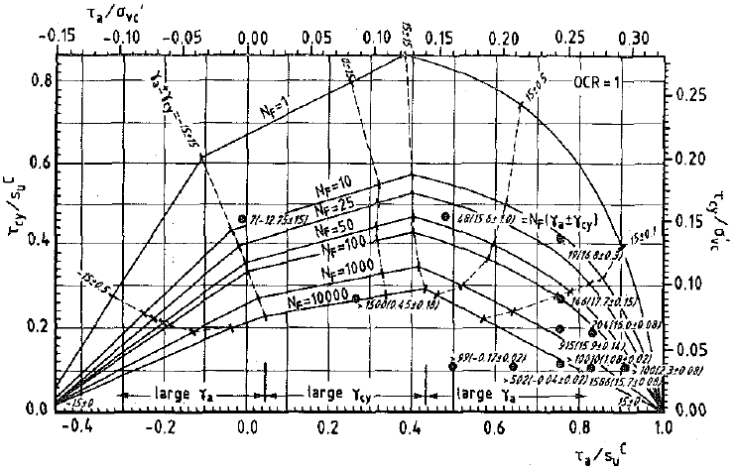

Figure 2.3: *Number of cycles to failure, N_F for various combinations of τ_a and τ_{cy} in triaxial tests on normally consolidated Drammen Clay[13]*

The cyclic shear strength is then be defined as $\tau_{f,cy} = (\tau_a + \tau_{cy})_f$, where $(\tau_a + \tau_{cy})_f$ is the sum of the average and cyclic shear stress at failure after given certain number of cycles and cyclic to average ratio[14].

2.1 Cyclic shear strain accumulation procedure for predicting soil behaviour

It is easy to use Figure 2.3 to determine cyclic shear strength based on a regular loading history with constant cyclic stress and constant average stress. However, real load histories

for OWT are irregular and difficult to directly apply to Figure 2.3 to calculate the cyclic shear strength. Accumulation procedures[2] is therefore developed to allow the cyclic strength to be calculated for cyclic stress histories with variable amplitude and average stress.

Before applying the accumulation procedures, the irregular loading histories are organized into many parcels with constant cyclic shear stress. Then, those parcels are applied to the strain contour diagrams or pore pressure contour diagrams by assuming the soil element remember the effects from previous loading parcels. Between different loading parcels, the shear strain or the pore pressure are assumed constant for shear strain contour diagram and pore pressure diagrams, respectively. After applying all the load parcels, the final number of cycles is the equivalent cycles N_{eq}, the final cyclic stress τ_{cy} and average shear stress τ_a, which then is assumed to represent the full load history. Applying N_{eq} together with cyclic to average ratio τ_{cy}/τ_a in Figure 2.3, the cyclic shear strength can be determined. The same procedure can be used to calculate the cyclic shear strength for both triaxial and DSS stress path.

The shear strain accumulation and pore pressure accumulation has been used both for clay and sand. The shear strain accumulation procedure uses permanent or cyclic shear strain as the memory parameter to do the accumulation while pore pressure accumulation procedure uses pore pressure as the memory parameter.The cyclic shear strain accumulation procedure is suitable for clay because shear strain can be measured accurately while pore pressure accumulation might difficult to precisely measure. The strain contour or the pore pressure contour diagrams are determined based on cyclic triaxial and DSS laboratory test. The following part illustrates how to use the cyclic shear strain contour diagram to determine the equivalent number of cycles N_{eq}.

The equivalent number of cycles N_{eq} with a corresponding cyclic and average shear stress is defined to have the same effect as the actual stress history. N_{eq} is determined by the cyclic shear strain accumulation procedure developed by Andersen [15]The example below describes the process of predicting the soil behaviour using cyclic shear strain accumulation with irregular cyclic loads [2].

1) The irregular load history which is shown in the left of Figure 2.4 can be transformed into the table in right of Figure 2.4 using rain flow counting method;

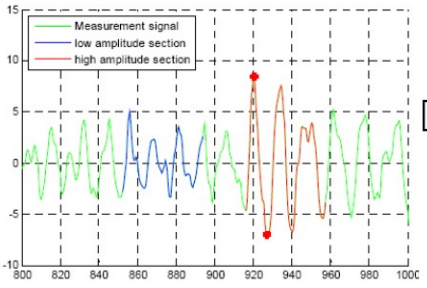

N	τ_{cy}(kPa)
100	36
35	41

Figure 2.4: *Irregular load history with* $\tau_a = 0$

2) From Figure 2.5, the cyclic shear stress 36kPa with 100 cycles can be applied in the cyclic shear strain contour diagram which is shown in path A to B. Then the

shear stress increase to 41kPa with constant cyclic shear strain at point C. Point D is the start point of next load parcel which is 41kPa with 35 cycles and this load lead to point E which is 70 cycles with cyclic shear strain of 1.5%. This 70 cycles is the equivalent cyclic numbers N_{eq}. The equivalent cycles $N_{eq} = 70$ with the cyclic shear stress in the last load parcel of $\tau_{cy} = 41kPa$ has the same effect as the irregular load histories shown in Figure 2.4 and can be used later for determining cyclic shear strength.
The second load parcel start from point D rather than point C was because the cyclic shear strain increased due to change to the higher cyclic shear stress which can be determined from the left picture of Figure 2.5. Then the cyclic shear strain changed from pont C point D without shear strength degradation.

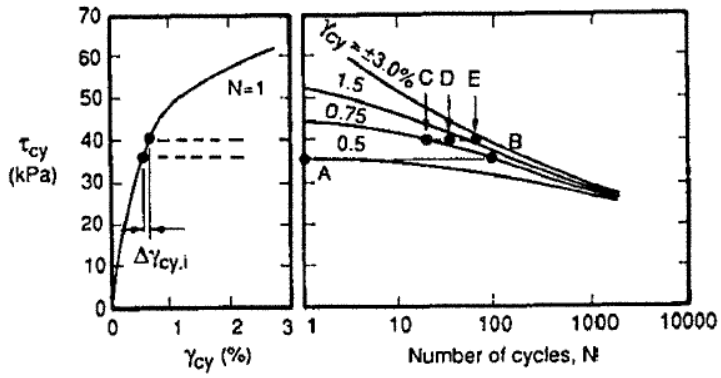

Figure 2.5: *Principle for cyclic shear strain accumulation[2]*

The procedure can be used with both permanent strain and pore pressure as memory or 'accumulation' parameter. However, a small correction has to be included when cyclic shear strain as parameter. the correction account for increasing cyclic shear strain from increasing shear stress without degradation. The cyclic shear strain changes as cyclic shear stress changes even without cyclic degradation as shown in Figure 2.6[2].There is an immediate increase in cyclic shear strain $\Delta\gamma_{cy,i}$ when the cyclic shear stress increases from τ_{cy}^{A} to τ_{cy}^{B}.

To find N_{eq} at failure, the strain contours have to be scaled down so the accumulation ends up at failure. This means the material factor account for uncertainties in the full cyclic behaviour and not only the final maximum load.

2.2 Implimentation of soil cyclic behaviour in foundation design

Some soil elements along the potential failure surface below bucket foundation experience different stress conditions which are shown in Figure 2.7. Therefore, the anisotropic cyclic shear strength determine the failure of bucket foundation. The strain compatibility needs to be considered when using anisotropic stress dependent undrained shear strength[13]. It means that the failure cyclic shear strain and average shear strain $\gamma_{cy} + \gamma_a$ on the

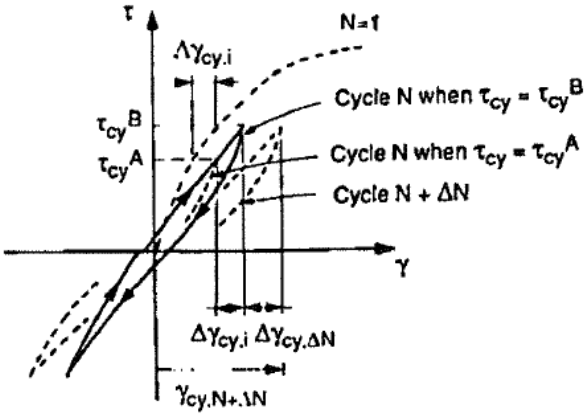

Figure 2.6: *cyclic shear stress-strain curves when cyclic shear stress is increased from τ_{cy}^{A} to τ_{cy}^{B}*

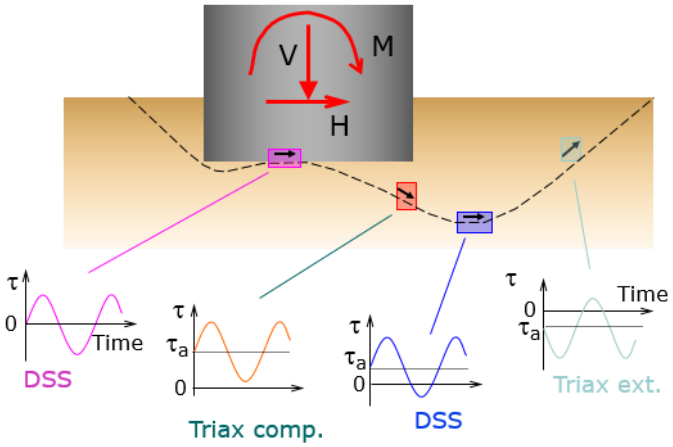

Figure 2.7: *simplified stress conditions along potential failure surface in the soil for the foundation subjected to combined cyclic loading*

failure surface should be the same in a different stress element. This will lead to stress redistribution, and may change the τ_{cy}/τ_a, along the potential failure surface[13].

2.2.1 Simplified procedure for strain compatibility

To account for the strain compatibility in shear strength determination, redistribution mechanisms can be followed in a full boundary value problem. In this project, a simplified procedure was used to account for the strain compatibility by assuming a stress path based on the global loads F_{cy}/F_a in DSS contour diagram was also applied to triaxial contour diagram. A detailed explanation is in the next section.

After calculating the cyclic shear strength, FEM or equlibrium method can be used to calculate the bearing capacity and load-displacement curves for bucket foundation subjected to cyclic loads.

The FEA program BIFURC will be used for analysis in this thesis project. BIFURC is developed in NGI. It is a computer program using FEM for determining of undrained bearing capacity of embedded structures. BIFURC is a 2D program that takes into account 3D effects using side shear roughness factors[11].

2.3 Soil cyclic shear strength and stress-strain curve

2.3.1 Anisotropic static shear strength

Drammen Clay contour diagrams has been used in study because of its extensive database of cyclic tests[12, 14]. Cyclic soil shear strength might be lower or higher than static shear strength due to cyclic loading. The cyclic shear strength was determined prior to the bearing capacity analysis. The following section describes the determination of cyclic shear strength.

Figure 2.8 shows the compression, extension and DSS static shear strength for Drammen Clay with different OCR. The diagram can be approximated by the SHANSEP formula[16] as follows:

$$s_u/\sigma_{vc}^{'} = A \cdot OCR^B \tag{2.1}$$

Where, $\sigma_{vc}^{'}$ is the vertical effective consolidation stress; A, B are the coefficients need to be decided; OCR is over-consolidation ratio.

Coefficient A is obtained from Figure 2.8 by setting OCR=1. The B coefficient was determined from the average results giving different OCR. The normalized anisotropic strength is shown in Table 2.1 as function of OCR.

Table 2.1: *Relation between OCR and normalized shear strength*

Type of loading	Normalized static shear strength
Triaxial compression C	$S_u^C/\sigma_{vc}^{'} = 0.32 \cdot OCR^{0.82}$
Direct simple shear DSS	$S_u^{DSS}/\sigma_{vc}^{'} = 0.22 \cdot OCR^{0.83}$
Triaxial extension E	$S_u^E/\sigma_{vc}^{'} = 0.17 \cdot OCR^{0.84}$

2.3.2 Anisotropic cyclic shear strength and stress strain curve

The strength and stress-strain curves were derived using the cyclic test data on Drammen Clay which has been well documented from K.H. Andersen[14]. Simplified procedures were used in this thesis project to derive the cyclic shear strength and stress-strain curves.

The cyclic shear strength was defined as, $\tau_{f,cy} = \tau_{a,f} + \tau_{cy,f}$, where $\tau_{a,f}$ is average shear strength at failure, $\tau_{cy,f}$ is the cyclic shear strength at failure. The combination of average shear strength and cyclic shear strength is given in Figure 2.9 for different number of cycles to failure N_F and different cyclic to average stress ratios τ_{cy}/τ_a. Cyclic shear strength and average shear strength at failure can be obtained for specific N_{eq} and τ_{cy}/τ_a.

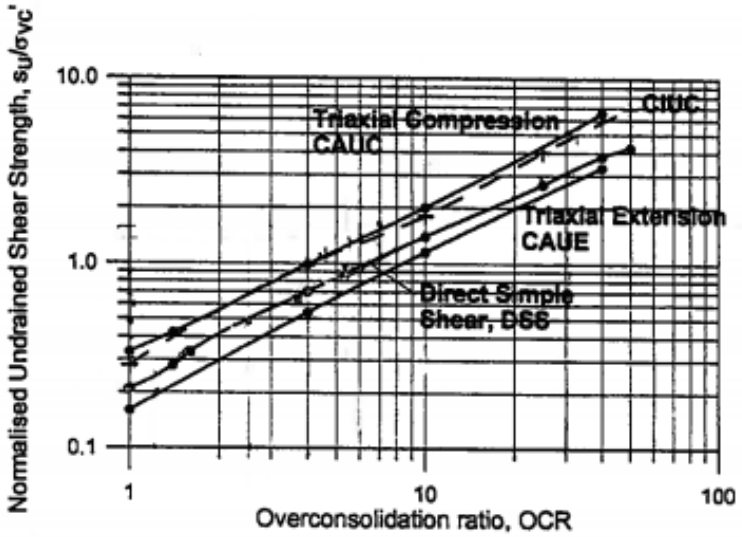

Figure 2.8: *Undrained DSS and triaxial monotonic shear strength of Drammen Clay as function of OCR[10]*

The cyclic shear strength was derived assuming that the strain from the given τ_{cy}/τ_a ratios were governing for the problem. The average shear strain at failure $tau_{a,cy}$ and cyclic shear strain at failure $\tau_{cy,f}$ which is obtained from DSS contour diagram (Figure 2.9) based on the τ_{cy}/τ_a ratio under consideration were used in the compression and extension contour diagrams(Figure 2.9) to acquire compression cyclic shear strength $\tau^C_{f,cy} = \tau^C_{a,f} + \tau^C_{cy,f}$ and extension cyclic shear strength $\tau^E_{f,cy} = \tau^E_{a,f} + \tau^E_{cy,f}$. The normalized cyclic shear strength

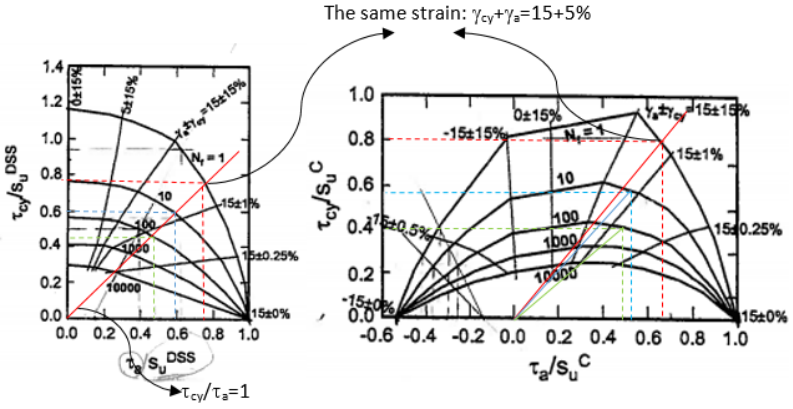

Figure 2.9: *Results from cyclic DSS test and cyclic triaxial test on Drammen Clay with OCR=4[10]*

for all the cases considered in this thesis project are given in Appendix A.

The stress strain curves were generated to represent the characteristic stress paths in the contour diagrams. The path should at the τ_0 relevant.

Figure 2.10 shows one of the stress-strain curves used in this thesis project. All the stress-strain curves used are shown in Appendix B.

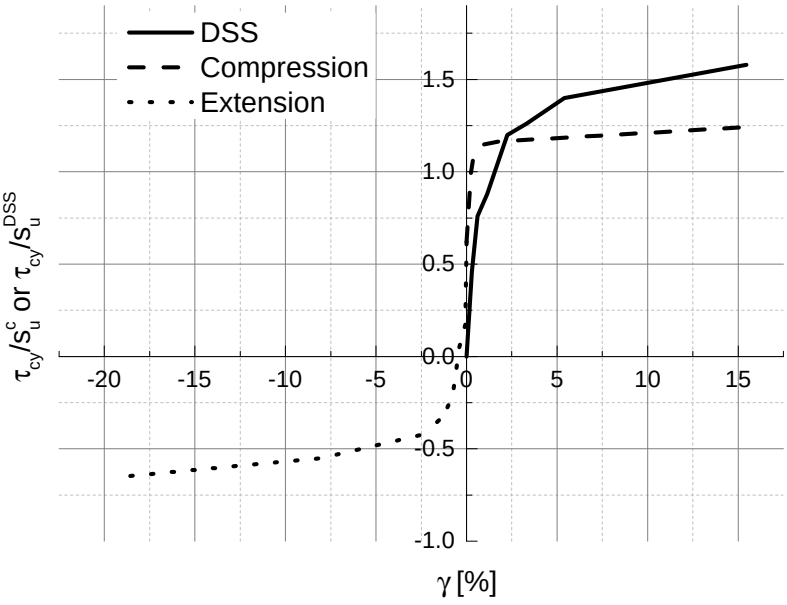

Figure 2.10: *Stress-strain curve for OCR=1,* $N_{eq} = 1$, $\tau_{cy}/\tau_a = 1$

2.4 Summary

This chapter shows the theory to predict soil behavior under cyclic loading developed in NGI which is used in this thesis. This cyclic shear strain accumulation procedure changes the irregular loading history into an equivalent number of cycles N_{eq} with a certain level of cyclic shear stress τ_{cy} and average shear stress τ_a. It means that an irregular loading history with many different loading amplitude and cycles can be represented by one N_{eq} with a specific τ_{cy}/τ_a using the cyclic shear strain accumulation procedure.

The next chapter introduces the in-house software BIFURC developed in NGI to do the bearing capacity analysis for general cyclic loading conditions which was represented by varying N_{eq} and τ_{cy}/τ_a.

Chapter 3

FEA in BIFURC

The bearing capacity of the buckets were computed with BIFURC. BIFURC is a 2D program using FEM by taking 3D effects into consideration using side shear roughness factors. BIFURC can produce the 3D bearing capacity envelop efficiently relative to other full 3D programs.

3.1 BIFURC introduction

BIFURC is a finite element program for failure analysis of materials with anisotropic shear strength as well as consolidation analysis[3].

The basis of the material model used are as follows:

- A yield criterion based on the Tresca criterion;
- An anisotropic shear strength;
- An associated flow rule;
- A hardening rule based on a relationship between the mobilized shear strength and the plastic shear strain;
- An isotropic initial shear modulus;
- An unloading modulus equal to the initial shear modulus Plane strain condition[3].

The soil elements used in BIFURC are 8-node isoparametric Serendipity element with numerical integration of 2×2 Gauss points[3]. This element is different than the normal plane element since it has thickness in the y-direction and shear stresses on the two surfaces perpendicular to the y-direction (Figure 3.1). The interface element is 6-node isoperimetric element (Figure 3.2) and it is used to model sliding between two 8-node elements.

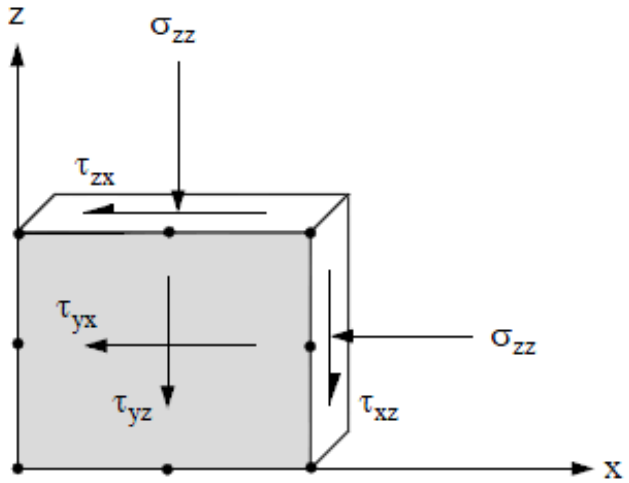

Figure 3.1: *8-node plane element with side friction[3]*

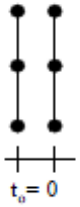

Figure 3.2: *6-node interface element*

PLAXIS is developed from PLAXIS BV in The Netherlands. And all the relevant information are well documented in their manuals which can be download from their home website which is http://www.plaxis.nl/.

3.1.1 2D simplification with side shear roughness factors

BIFURC bring 3D effects into calculation using side shear roughness factors which are shown in Figure 3.3. There are three side shear roughness factors in BIFURC which are reduction factor for shear on structure outside area α_{bs}, reduction factor for shear on structure inside side area, reduction factor for shear on soil side areas α_{ss}. α_{bs} is at the two plane vertical sides of the bucket foundation and α_{ss} is at sides of the active and passive zones. Figure 3.3 shows the side shear roughness factors at the two plane sides of the failure body for shallow foundation.

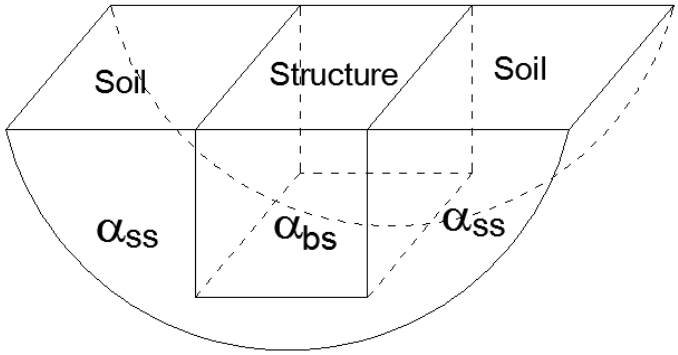

Figure 3.3: *Side shear roughness factors*

3.2 Comparison of BIFURC with PLAXIS

The side shear roughness factors has been extensively be verified from K.H. Andersen and H.P. Jostad[11]. This section compared the ultimate capacity results using BIFURC with roughness factors recommended from K.H. Andersen and H.P. Jostad[11] to PLAXIS.

The finite element models were established in PLAXIS 2D, PLAXIS 3D and BIFURC. The soil profile used in this section was OCR=1. The load condition was $\tau_a/\tau_{cy} = F_{cy}/F_a = 1$ and equivalent cycles N_{eq}=1. BIFURC calculates the ultimate bearing capacity with side shear roughness factors shown in Table3.1.

Table 3.1: *Side shear roughness factors in BIFURC*

Reduction factor for shear on structure outside area α_{bs}	0.5
Reduction factor for shear on structure inside side area	0.727
Reduction factor for shear on soil side areas α_{ss}	0.5

The mesh in PLAXIS 2D and PLAXIS 3D are sufficient to produce the ultimate bearing capacity analysis. The vertical ultimate bearing capacity using BIFURC was compared to the result from PLAXIS 2D shown in Figure 3.4. The bearing capacity using BIFURC was 4% higher than the bearing capacity from PLAXIS 2D.

For the moment bearing capacity, the overshoot from PLAXIS 3D compare to BIFURC was 5% which is shown in Figure 3.5. The bearing capacity using BIFURC with side shear roughness factors shown in Table 3.1 agreed well with PLAXIS 2D and PLAXIS 3D. The overshoot around 5% can be neglected and may be due to the different element and interface in BIFURC and PLAXIS.

The agreement was considered to be sufficient for this study and the roughness factors in Table 3.1 was used in the analysis presented herein.

3.3 Summary

This chapter introduces the material model in BIFURC and elements used in BIFURC. This chapter also describes how the 2D element can take 3D effects by side shear roughness

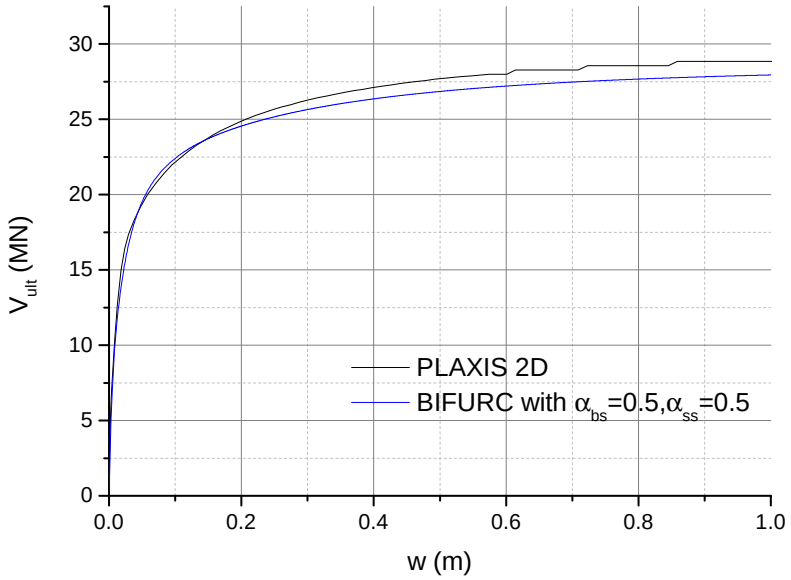

Figure 3.4: *Vertical bearing capacity between PLAXIS 2D and BIFURC*

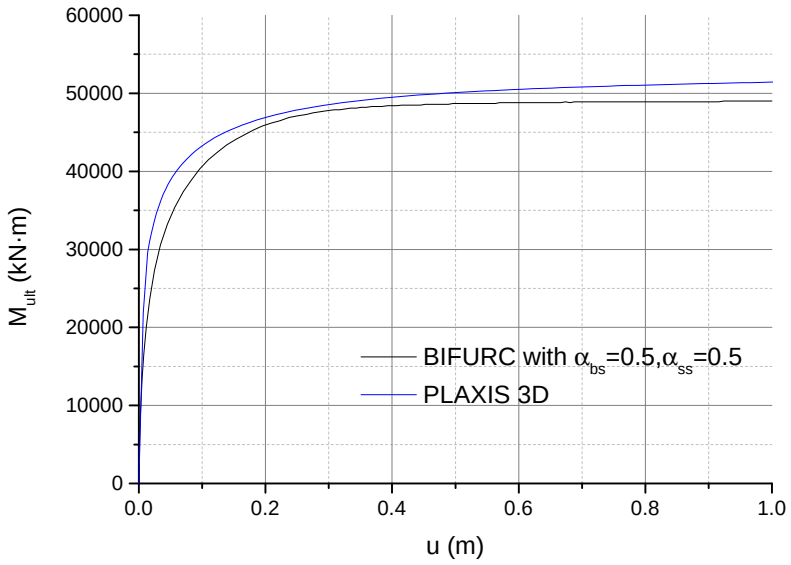

Figure 3.5: *Overturning moment capacity between PLAXIS 3D and BIFURC*

factors into consideration for bearing capacity analysis.

Besides, PLAXIS 2D and PLAXIS 3D were used in this chapter to do the robustness check for the roughness factors used in BIFURC. The good agreement between each other shows the good applicable of using BIFURC to do further analysis.

The next chapter presents the bearing capacity analysis for varying N_{eq} & τ_{cy}/τ_a, soil profiles and bucket foundation geometry h/D.

Chapter 4

Failure envelopes determination

This chapter presents the normalized bearing capacity envelopes in three load dimensions,VHM. V_{ult}, H_{ult} and M_{ult}, denote pure vertical load, pure horizontal load at reference point, RP, and pure moment load(Figure 4.1). The RP is the determined as the point where a horizontal load can be applied and cause a pure horizontal sliding without rotation. The RP was change from 2/3h for linear increasing $\tau_{f,cy}$ with depth to 1/2h for constant $\tau_{f,cy}$ with depth shown in Figure 4.2. The assumption used in the analysis is that the cyclic to average stress ratio τ_{cy}/τ_a applied to the soil element equals the cyclic to average global load ratio F_{cy}/F_a applied to the foundation.

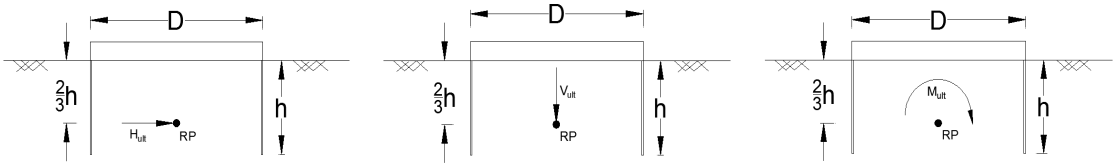

Figure 4.1: *Three ultimate loading conditions for linear increase cyclic shear strength with depth*

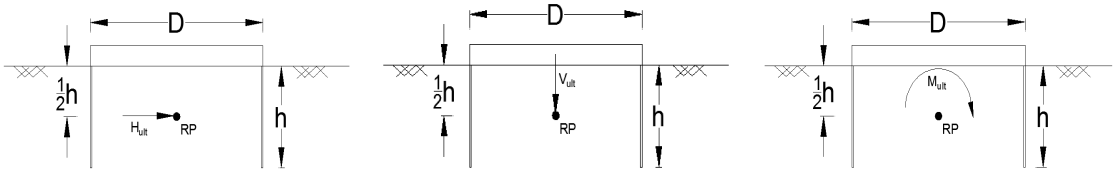

Figure 4.2: *Three ultimate loading conditions for constant cyclic shear strength with depth*

For combined loading conditions shown in Figure 4.3, horizontal, vertical load and overturning moment were applied on the RP.

The analyzed cases in this thesis project are listed in Table 4.1.The soil-skirt roughness factor α is set to 0.65 for all cases.

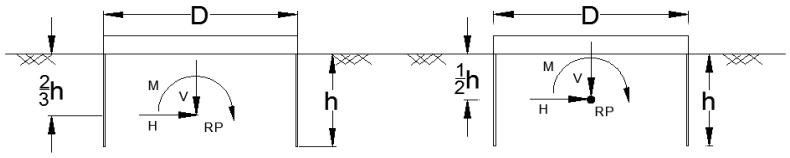

Figure 4.3: *General loading conditions for linear increasing $\tau_{f,cy}$ with depth(left) and constant $\tau_{f,cy}$ with depth(right)*

Table 4.1: *Analyzed cases*

h/D	1 & 0.5		
$\tau_{f,cy}$	Linear increasing with depth		Constant with depth
	OCR=1	OCR=40	OCR=40
N_{eq}	1, 10 ,100	1, 10, 100	10
τ_{cy}/τ_a	1,2,0,$\tau_a = 0$	1	1,2

4.1 FE-model in BIFURC

The bucket foundation geometry of embedment depth to diameter ratios h/D are 0.5 and 1. For OWT it is more realistic to use shallow foundations for monopod structure since the dominant load usually is overturning moment. The model idealization used embedded solid structure. The failure surface is outside the bucket where the bucket was assumed to have inside stiffener which prevents the failure mode to go up between the skirts.

The undrained cyclic shear strength are taken from previous section where it considered loading history and OCR. The undrained shear strength is assumed constant from mudline down to 1m and linearly increases with depth. Figure 4.4 shows the bucket foundation geometry and the corresponding assumed soil condition.

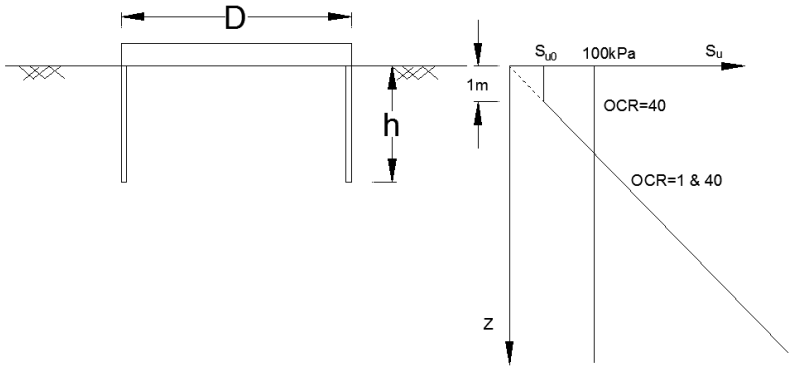

Figure 4.4: *Bucket foundation geometry and assumed soil conditions*

4.1.1 Batch processing using MATLAB

In order to plot the full failure envelopes, different load combinations were applied to calculate the failure load for each load history and OCR. Many load combinations were considered, and batch processing using MATLAB script were developed to reduce the calculation time.It writes loads into BIFURC loads file and then activates the executive file from BIFURC. The user only need to input predefined approximate loads for pure horizontal load, pure vertical and pure overturning moment. MATLAB writes the ultimate loads into the excel file. The rest general load combinations were based on the three ultimate loads. MATLAB reads again the load combination excel file and write each load combination into load file for BIFURC and call BIFURC to calculate.

The results were written into the workspace in MATLAB. Finally, all the load-displacement results were written into one of the sheets in an excel file after calculation finished for all the load combinations for one soil profile. The MATLAB code for the batch processing is shown in Appendix C.1.

4.2 Cyclic loading effects on ultimate capacity

The effects of cyclic loads on the ultimate capacity were investigated by comparing results from different F_{cy}/F_a and N_{eq}.The ratios between cyclic ultimate capacity and static ultimate capacity which are M_{ult}/M_{static}, H_{ult}/H_{static} and V_{ult}/V_{static} are almost the same for horizontal, vertical and overturning moment loading. The effect of cyclic loading expressed as N_{eq} and F_{cy}/F_a can therefore be reduced to two figures shown in Figure 4.5. This figure also represent the effects on M_{ult}/M_{static} and V_{ult}/V_{static}.

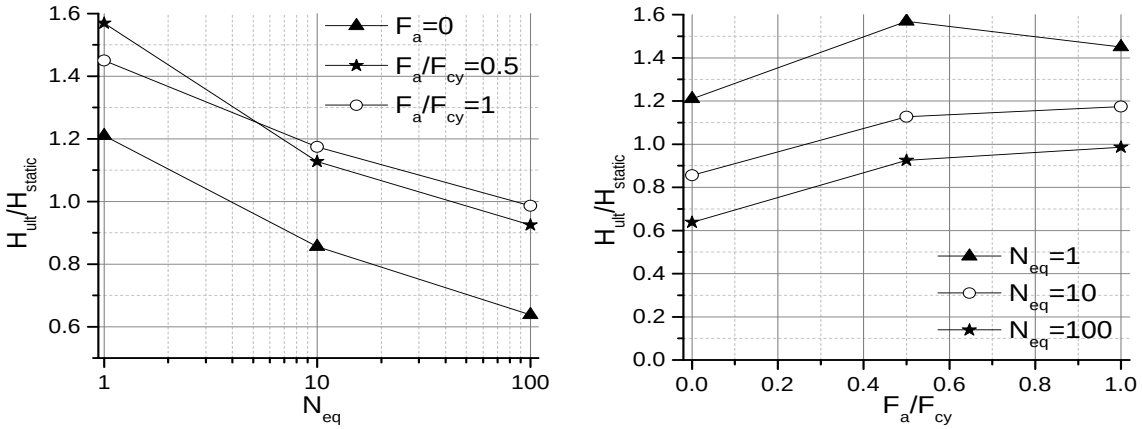

Figure 4.5: *Mobilized ultimate capacity with for OCR=1*

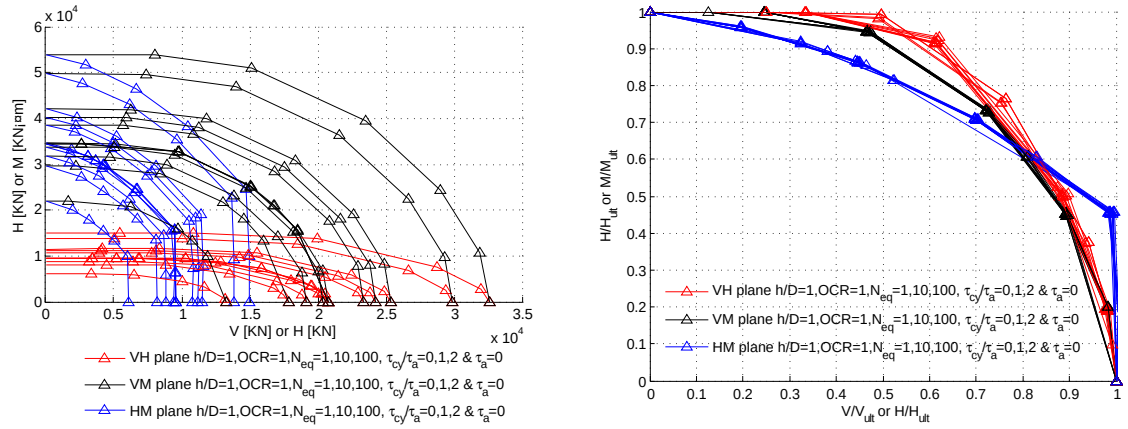

Figure 4.6: *Failure envelopes for different load planes for h/D=1*

4.3 Failure envelopes for linear increasing cyclic shear strength with depth

Failure envelopes were computed for different OCR, N_{eq}, F_{cy}/F_a and the bucket geometry h/D. The input cyclic shear strength can be found in Appendix A. The combined bearing capacity was normalized by the corresponding ultimate bearing capacity. The shape of the failure envelopes were first investigated in two load planes. Then the combined three loading conditions was further applied to the bucket foundation.

4.3.1 Failure envelopes for different N_{eq}, τ_{cy}/τ_a

This section investigate whether cyclic loading expressed as τ_{cy}/τ_a and N_{eq}, has influence the failure envelopes.

The failure envelopes are shown in the left of Figure 4.6 in real number. The normalized failure envelopes for different N_{eq} and τ_{cy}/τ_a were plotted in the right of Figure 4.6 in HM, VH and VM load plane for N_{eq} =1, 10,100 and $\tau_{cy}/\tau_a = 0, 1, 2$,$\tau_a = 0$ respectively. The normalized failure envelopes are almost identical in the same load plane for different N_{eq} and τ_{cy}/τ_a. The cyclic loads do not influence too much on the normalized failure envelopes for the same bucket foundation geometry h/D.

4.3.2 Failure envelopes for different OCR

Figure 4.7 shows the failure envelopes in VH,VM and HM plane not change due to higher OCR which gives a higher cyclic shear strength gradient.

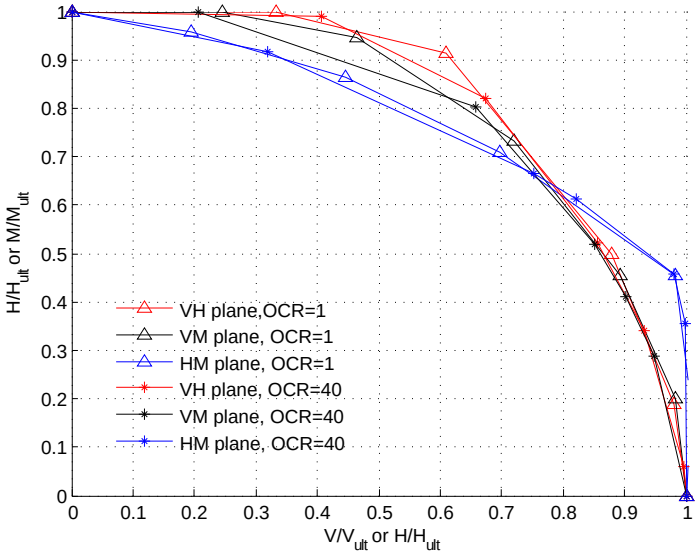

Figure 4.7: *Failure envelopes for h/D=1, $N_{eq} = 10$, $\tau_{cy}/\tau_a = 2$*

4.3.3 Failure envelopes for different h/D

Both failure envelopes and the normalized failure envelopes for h/D=0.5 and 1 were analyzed in this section for OCR=1, $\tau_{cy}/\tau_a = 2$. Figure 4.8 shows the failure envelopes in real numbers and normalized failure envelopes. The shapes of the failure envelopes in VH and VM planes in Figure 4.8 almost identical which might be due to the geometry change is small. The failure mechanisms in VH plane and VM plane stays almost the same for bucket foundation geometry h/D=0.5 and 1.

The failure shape in HM plane significantly changes between h/D=0.5 and 1 which can be seen from Figure 4.8. The coupling between horizontal load and moment load becomes less when h/D goes small namely more shallow foundation.

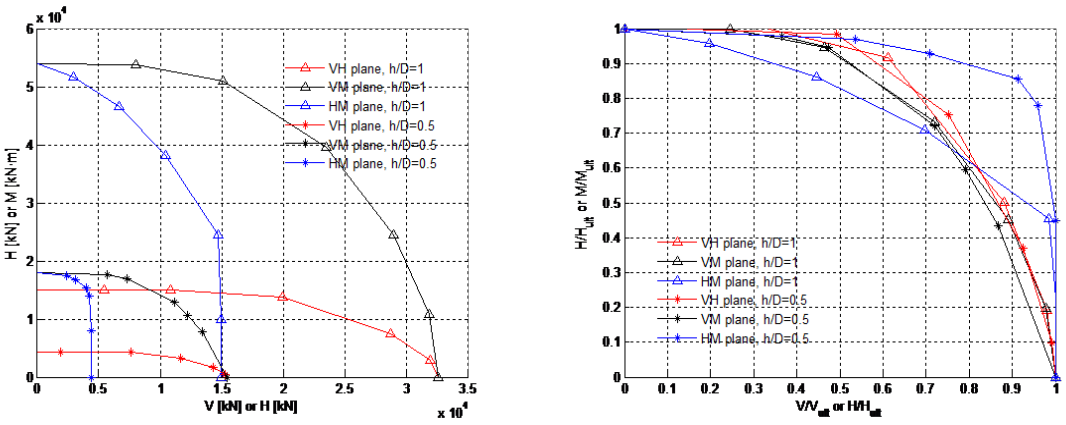

Figure 4.8: *Failure envelopes for OCR=1,$N_{eq} = 1$ $\tau_{cy}/\tau_a = 2$*

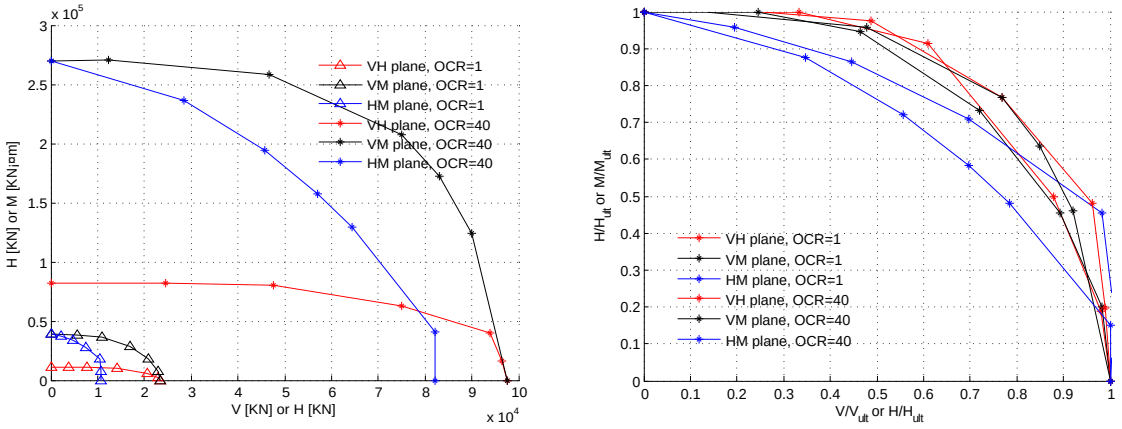

Figure 4.9: *Failure envelopes for h/D=1,* $N_{eq} = 10$, $\tau_{cy}/\tau_a = 2$

4.4 Failure envelopes for constant cyclic shear strength with depth

For OCR=40, the high gradient of cyclic shear strength used in previous section was somewhat unrealistic and a constant shear strength profile with compression cyclic shear strength $\tau^c_{f,cy} = 100kPa$ was used herein. As the failure envelopes only change due to h/D from analysis in previous sections, this section compared the failure envelopes between constant $\tau_{f,cy}$ with depth and linear increase $\tau_{f,cy}$ with depth and failure envelopes for different h/D for constant $\tau_{f,cy}$ with depth.

4.4.1 Failure envelopes between linear increase $\tau_{f,cy}$ and constant $\tau_{f,cy}$ with depth

The failure envelopes for constant cyclic shear strength was compared to linear increase cyclic shear strength are shown in Figure 4.9. The change between VH and VM plane are relatively small while the change in HM plane are very large because the scaling factors on H axes and M axes are very different for linear increase $\tau_{f,cy}$ with depth and constant $\tau_{f,cy}$ with depth. The trend of failure envelopes seem very similar when looking at the real number in left of Figure 4.9.

4.4.2 Failure envelopes for different h/D

The failure envelopes for h/D=0.5 and 1 were presented here to confirm the same effect from geometry change of bucket foundation. Figure 4.10 shows the failure envelopes in 3 different load plane for h/D=0.5 and 1. The results agree well with failure envelopes for linear increasing cyclic shear strength in section 4.3.3.

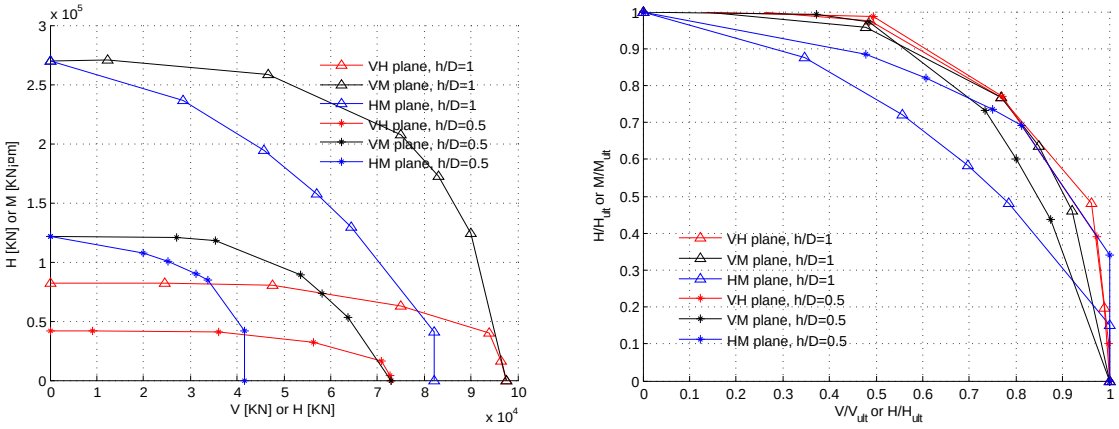

Figure 4.10: *Failure envelopes for* $N_{eq} = 10$, $\tau_{cy}/\tau_a = 2$,*OCR=40*

4.5 Failure envelopes comparison

The failure envelopes are also plotted using the formula from Gourvenec and Barnett[17]. In their paper, the proposed envelope formula are shown below:

For HVM plane:

$$(\frac{h}{h^*})^\alpha + (\frac{m^*}{m})^\alpha + 2\beta(\frac{hm}{h^*m^*}) = 1 \tag{4.1}$$

For only HV plane:

$$h^* = 1 - 0.217v + 1.009v^2 - 1.792v^3 \tag{4.2}$$

For only HM plane:

$$m^* = 1 - 0.112v + 0.535v^2 - 1.423v^3 \tag{4.3}$$

Fitting parameters:

$$\alpha = 1.30 + 1.05(\frac{D}{B}) - 0.55(\frac{D}{B})^2 \tag{4.4}$$

$$\beta = 0.15 - 1.45(\frac{D}{B}) + 0.67(\frac{D}{B})^2 \tag{4.5}$$

Where, D is the embedment depth of the bucket foundation; B is the width of the bucket foundation The failure envelopes were compared for $N_{eq} = 0, 10, 100$, $\tau_{cy}/\tau_a = 0, 1, 2$ & $\tau_a = 0$ for OCR=1 and h/D=1. The results are ouside the failure envelopes in VH and VM plane from Gourvenec and Barnett which are shown in Figure 4.11. This is because the failure envelopes from Gourvenec and Barnett was a conservative solution.

The comparison in HM load plane cannot do directly because the reference points are different from Gourvenec and Barnett which they chose the tip of the bucket foundation

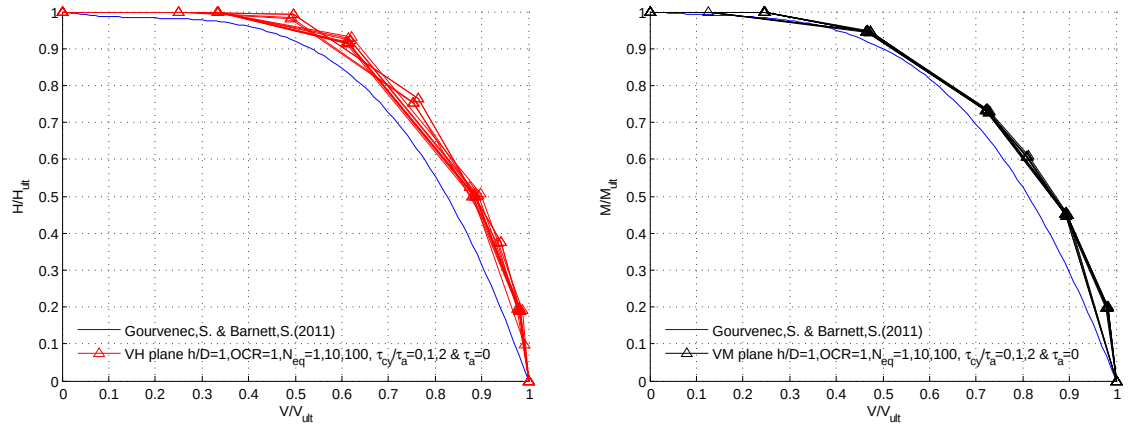

Figure 4.11: *Failure envelopes for OCR=1,* $\tau_{cy}/\tau_a = 1$

as RP instead of the approximate decoupling point in this thesis project. This comparison was carried out by transferring the load from decoupling point to the tip of the bucket foundation. Figure 4.12 shows that the failure envelope from Gourvenec and Barnett overestimates the capacity in HM load plane. And the blue line was a proposed solution to shrink the numerical failure envelope around the failure envelopes from this project. The improved formulas are in the following:

$$(\frac{h}{h^*})^\alpha + (\frac{m^*}{m})^\alpha + 3.2\beta(\frac{hm}{h^*m^*}) = 1 \tag{4.6}$$

$$h^* = 1 - 0.217v + 1.009v^2 - 1.792v^3 \tag{4.7}$$

$$m^* = 1 - 0.112v + 0.535v^2 - 1.423v^3 \tag{4.8}$$

$$\alpha = 0.75 + 1.5(\frac{D}{B}) - 0.3(\frac{D}{B})^2 \tag{4.9}$$

$$\beta = 0.2 - 1.47(\frac{D}{B}) + 0.9(\frac{D}{B})^2 \tag{4.10}$$

The failure envelope from Gourvenec and Barnett did not considered the physical situation that the failure mechanism is dominate by the horizontal movement failure until overturning moment is big than a certain level.

4.6 Full failure envelopes and 3D failure surface

The 3D failure surface can be plotted using the bearing capacity analysis results under general loading conditions. Before plotting the 3D failure surface, it is necessary to check the failure envelopes symmetrical characteristic in each load plane to be able to properly produce the 3D failure surface.

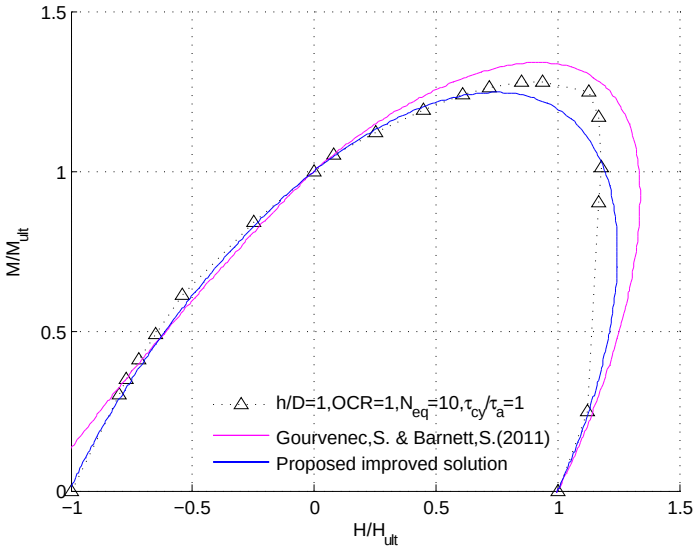

Figure 4.12: *HM plane comparison with load at skirt tip*

4.6.1 Full failure envelopes

This section analyzes the full failure envelopes in HM,VH,VM load planes.

VH and VM load plane symmetrically in four quadrants because the failure mechanisms in VH and VM load plane do not change for different direction of the loads. It means that the failure envelopes in previous section for VH and VM load plane are enough to express the full failure envelopes.

For HM load plane, the failure mechanism is different between the first quadrant and the second quadrant. Figure 4.13 shows that the failure mechanism in the first quadrant is clockwise rotation with right horizontal displacement while in the second quadrant, the failure mechanisms is clockwise rotation with left horizontal displacement. Figure 4.14 shows the full HM failure envelope for OCR=1,$N_{eq} = 20$, $\tau_{cy}/\tau_a = 1$.

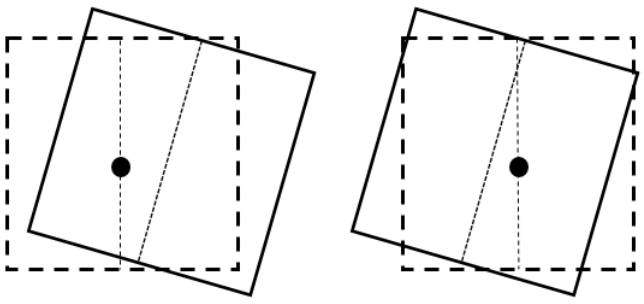

Figure 4.13: *Different failure mechanisms in HM plane, first quadrant(left),second quadrant(right)*

Figure 4.15 shows the comparison of the full failure envelope in HM load plane and the main difference is in the first quadrant.

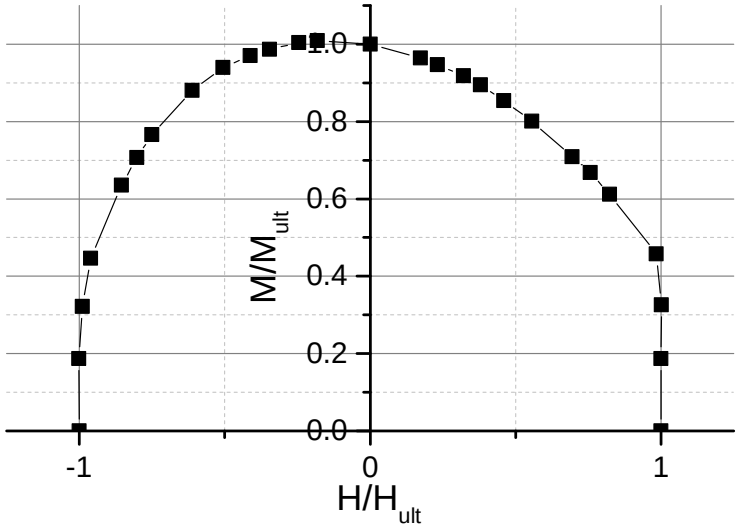

Figure 4.14: *Full failure envelope in HM load plane for OCR=1,$N_{eq} = 10$ $\tau_{cy}/\tau_a = 1$*

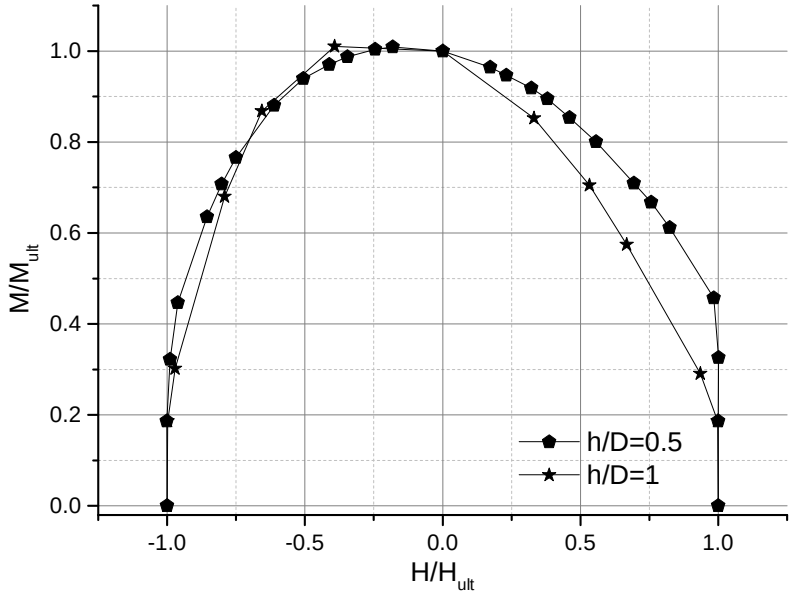

Figure 4.15: *Full failure envelope in HM load plane for h/D=1,0.5*

4.6.2 3D failure surface

Normally three combined loading situations are experienced by the OWT. The full 3D failure surface from combined cyclic loading conditions are presented in this section. The results were produced by a series of analysis run by batch processing script in MATLAB to calculate the bearing capacity for bucket foundation. The 3D failure surface and several cross section are presented in this section. The MATLAB script used linear interpolation function from the output data to derive cross sections of failure surface.The MATLAB script is in Appendix C.2

Figure 4.16 shows cross section of 3D failure surface for a given normalised moment load in HV load plane. Blue failure envelopes are the cross sections for M/M_{ult} from 0.7 down to 0.3 with a interval of 0.1. The red failure envelopes is in HV plane with overturning moment equals zero. Figure 4.17 shows the 3D failure surface.

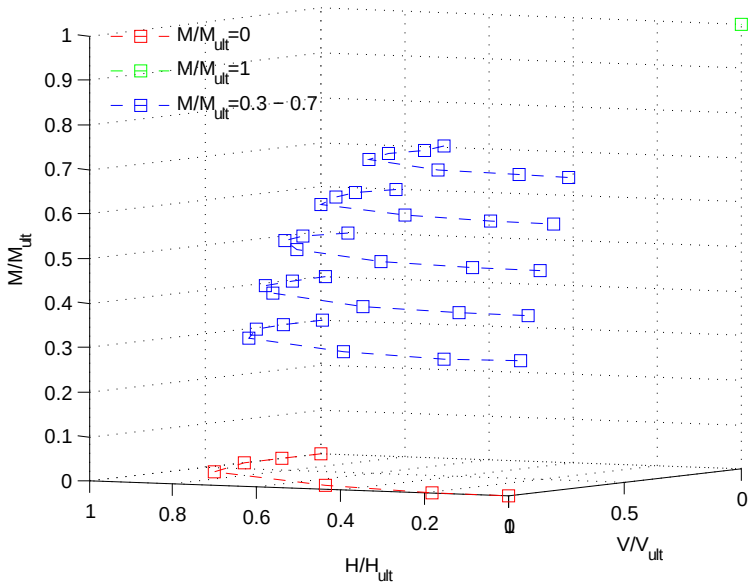

Figure 4.16: *Overturning moment cross section of failure envelopes for OCR=1,*$N_{eq} = 100$*,* $\tau_{cy}/\tau_a = 1$

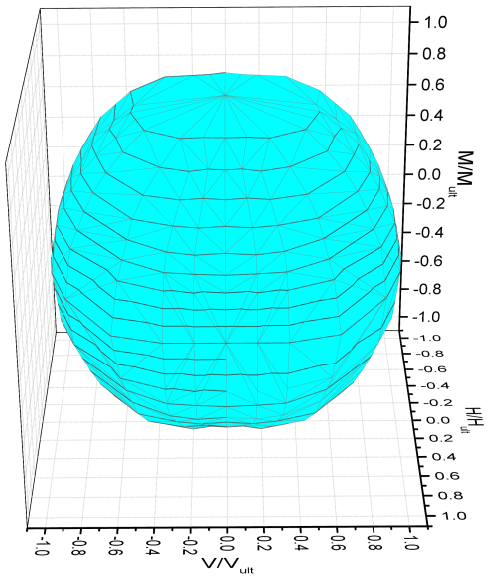

Figure 4.17: *HVM failure surface for OCR=1,*$N_{eq} = 100$*,* $\tau_{cy}/\tau_a = 1$

4.7 Conclusions

The bearing capacity under cyclic loading were compared to static capacity. It shows that the cyclic bearing capacity can be higher or lower than the static capacity which depends on the loading types and cyclic to average ratio τ_{cy}/τ_a.

The normalized failure envelopes by giving different N_{eq} and τ_{cy}/τ_a, bucket foundation geometry h/D and soil shear strength profiles. The failure envelopes does not change duo to cyclic loading history. However, it changes for different h/D and soil shear strength profiles.

The next chapter uses MATLAB to interpolate the bearing capacity analysis results to plot the displacement contours. The displacement contour diagrams will be produced for two load space and HVM three load space.

Chapter 5

Displacement contour diagrams determination

This chapter interpolates the load displacement results from bearing capacity analysis in last chapter to plot the displacement contours. The load displacement results are written into MATLAB workspace. The displacement contour diagrams are produced using MATLAB code. This code uses linear interpolation the corresponding loads for a given displacement level.

The displacement is the total displacement including cyclic and average displacement. The secant stiffness can be calculated from the displacement contour diagrams for a given load level.This secant stiffness for example can be used as boundary conditions for buckets on a jacket structure in analysis performed to calculate the load distribution in the structure.

5.1 2D dispalcement contour diagrams

The failure displacement are 1m for pure horizontal and pure vertical loading and 0.14 rad for moment loading. The load-displacement curve goes flat at 1m displacement and 0.14 rad.

The displacement contours are plotted in VM, VH and HM load plane respectively. Figure 5.1 shows the displacement contours in VM plane with horizontal load equals zero. The dash lines with circles shows the rotational radian, where the solid lines with asterisk shows the vertical displacement.

Figure 5.2 shows the displacement contours in VH plane with overturning moment equals zero. The horizontal displacement u and vertical displacement w were chose from 0.01m

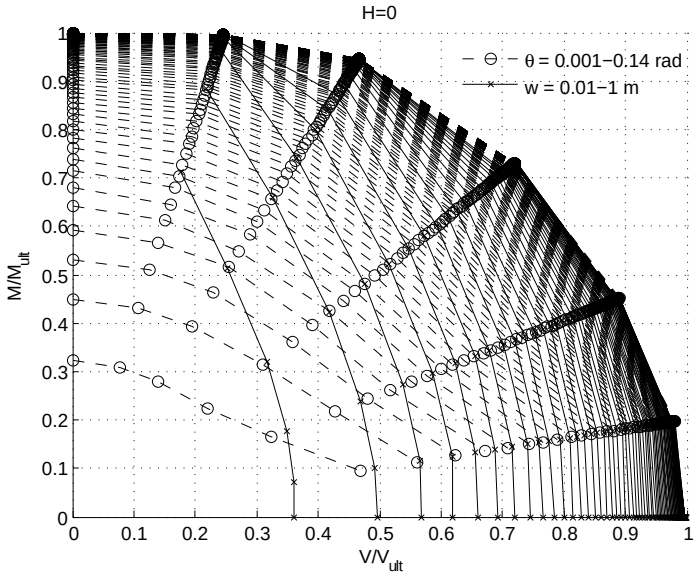

Figure 5.1: *Displacement contour diagrams for h/D=1, OCR=1,$N_{eq} = 1$ $\tau_{cy}/\tau_a = 1$ in VM plane, vertical displacement w is from 0.01-1m, rotational rad θ is from 0.001-0.14 rad*

to 1m with an interval of 0.01m. The most outside line where two lines overlap each other is the defined failure line in VH plane.

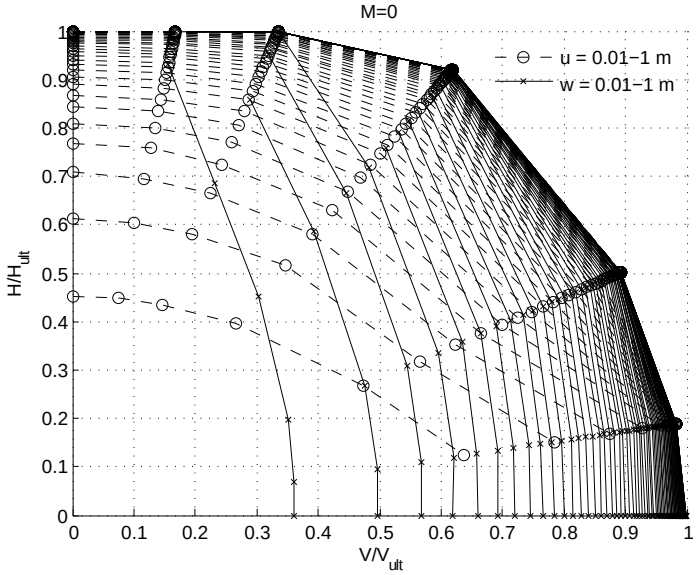

Figure 5.2: *Displacement contour diagrams for h/D=1, OCR=1, $N_{eq} = 1$, $\tau_{cy}/\tau_a = 1$ in HV plane, vertical displacement w and horizontal displacement u are from 0.01-1m*

Figure 5.3 shows the displacement contours in HM plane with vertical load equals zero. The contour expand when the horizontal displacement and rotation become small. One of the reasons might because the reference point was changed in the reality while it is

fixed in this thesis project.

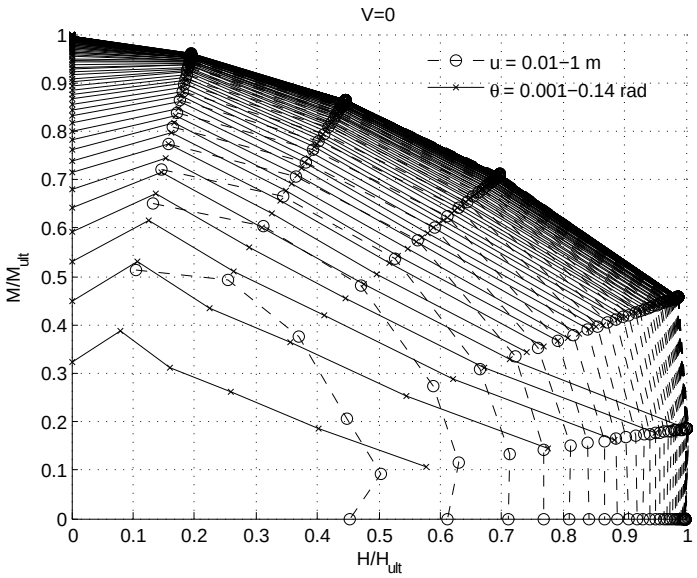

Figure 5.3: *Displacement contour diagrams for h/D=1, OCR=1, $N_{eq} = 1$ $\tau_{cy}/\tau_a = 1$ in HM plane, horizontal displacement u is from 0.01-1m, rotational rad θ is from 0.001-0.14 rad*

5.1.1 Displacement contours as functions of N_{eq} and τ_{cy}/τ_a for OCR=1 & 40

The displacement contour diagrams were not produced for OCR=40 with linear increasing shear strength since it is somewhat unrealistic. This section compared the displacement contours for OCR=1 with linear increasing cyclic shear strength with depth to OCR=40 with constant cyclic shear strength with depth. The displacement contours changed due to change of OCR. Figure 5.4 to Figure 5.6 show the displacement contours in VM, VH and HM load planes for OCR=1 & 40, $N_{eq} = 10$ and $\tau_{cy}/\tau_a = 1$. The displacement contours changed due to the change of the stress strain curve for different OCR.

5.1.2 Displacement contours for different bucket foundation geometry

The increase of embedment depth to diameter ratio, h/D causes the failure envelopes change in HM load plane. According to Figure 5.7 to Figure 5.9, the geometry change also causes the displacement contours change in horizontal displacement and rotational radians. The increased embedment depth do not influence the vertical displacement contours because the vertical displacement contours related to the diameter of the bucket foundation.

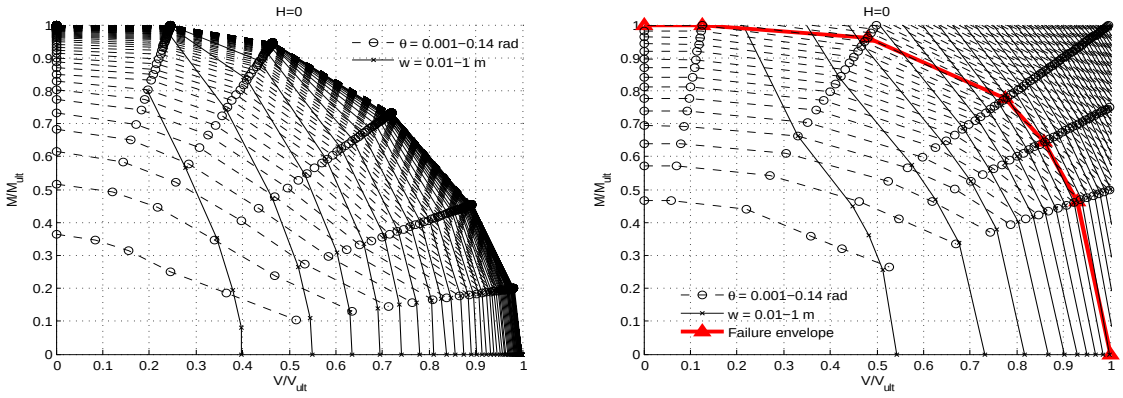

Figure 5.4: *Displacement contours for h/D=1,* $N_{eq} = 10$, $\tau_{cy}/\tau_a = 1$, *OCR=1(left)OCR=40(right)*

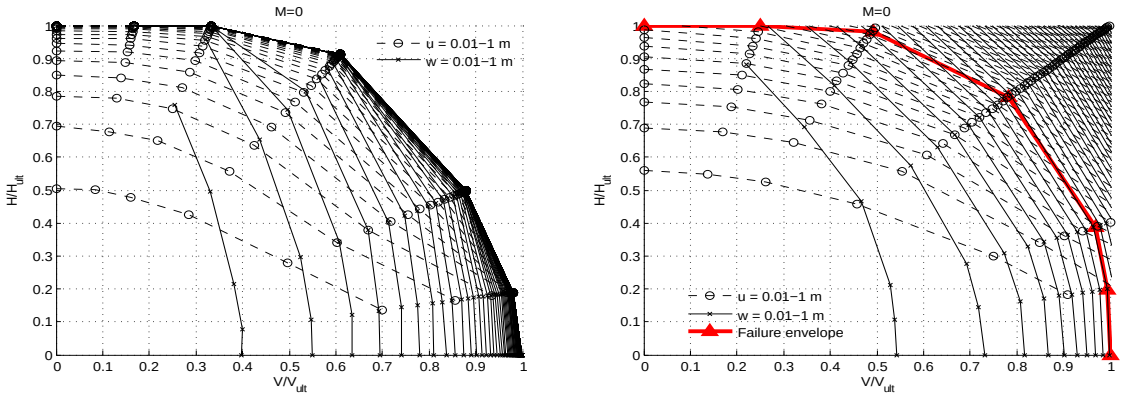

Figure 5.5: *Displacement contours for h/D=1,* $N_{eq} = 10$, $\tau_{cy}/\tau_a = 1$, *OCR=1(left)OCR=40(right)*

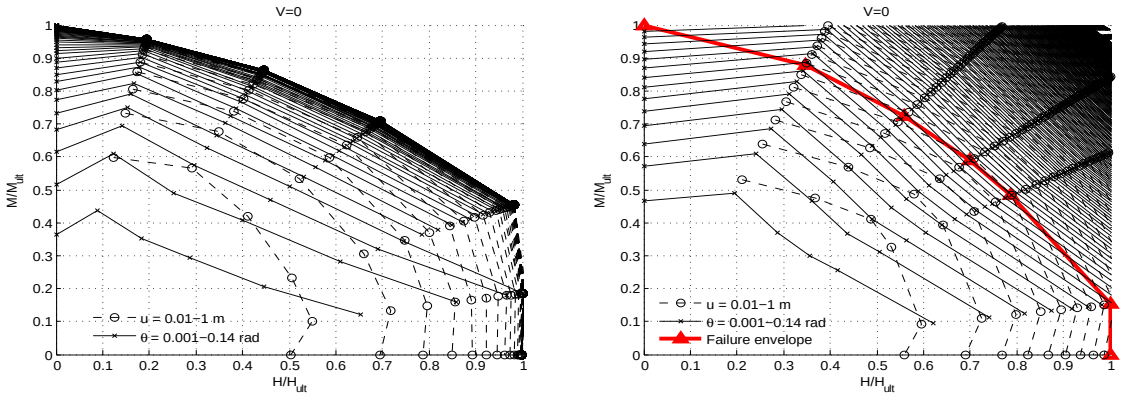

Figure 5.6: *Displacement contours for h/D=1,* $N_{eq} = 10$, $\tau_{cy}/\tau_a = 1$, *OCR=1(left)OCR=40(right)*

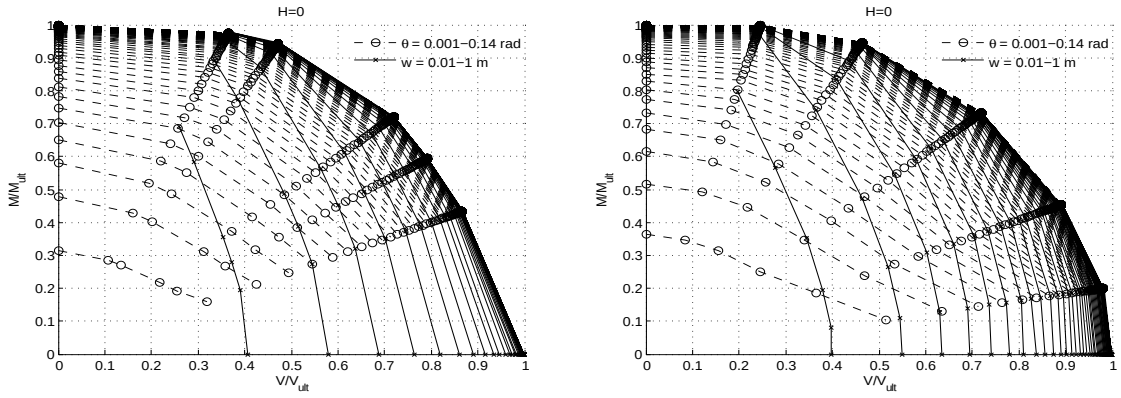

Figure 5.7: *Displacement contours for OCR=1,$N_{eq} = 10$,*
$\tau_{cy}/\tau_a = 2$,h/D=0.5(left)h/D=1(right)

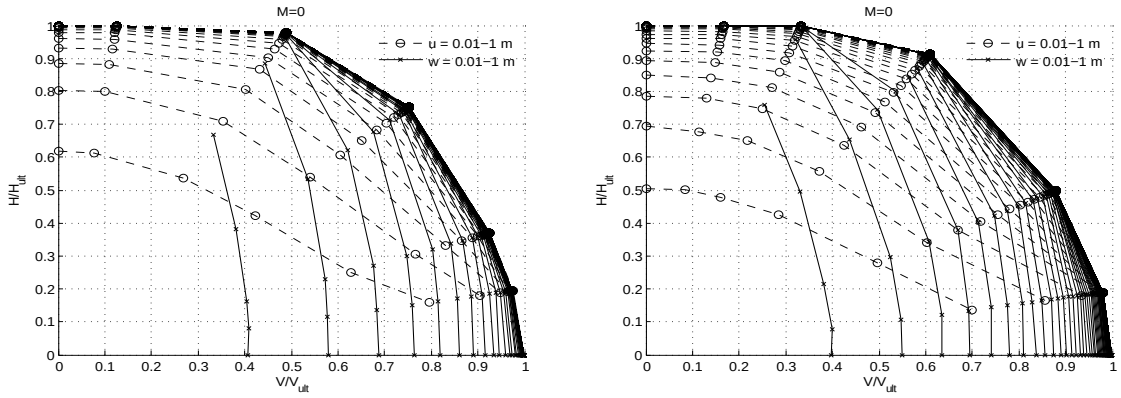

Figure 5.8: *Displacement contours for OCR=1,$N_{eq} = 10$,*
$\tau_{cy}/\tau_a = 2$,h/D=0.5(left)h/D=1(right)

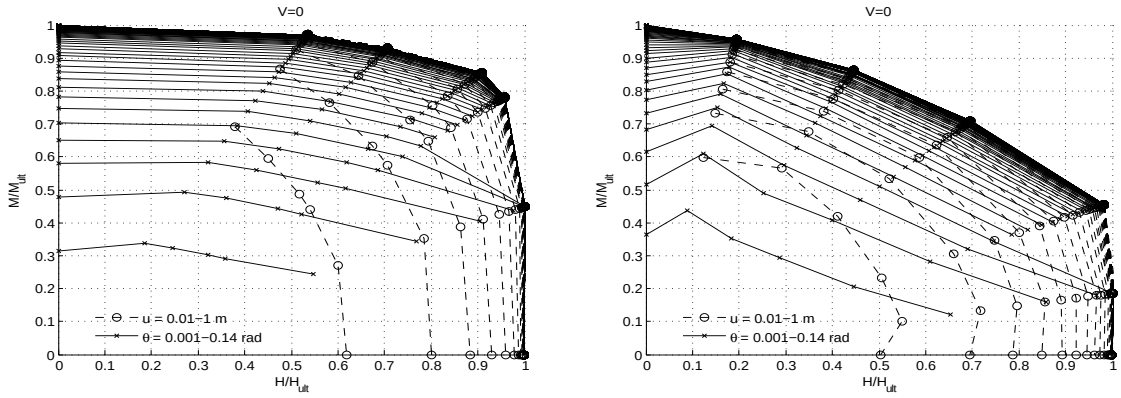

Figure 5.9: *Displacement contours for OCR=1,$N_{eq} = 10$,*
$\tau_{cy}/\tau_a = 2$,h/D=0.5(left)h/D=1(right)

5.2 3D displacement contour diagrams

The 3D displacement contours on HV load plane with different constant moment loads are presented in this section. Figure 5.10 shows the displacement contours in HV load plane with a constant moment load $M = 0.5M_{ult}$. The rotation θ is in a range from 0.001 rad to 0.14 rad with an interval of 0.001 rad. The interpolation method used herein was linear interpolation function from MATLAB. The corresponding MATLAB code was in Appendix C.3. The core interpolations in this section has two steps.

1) Interpolate θ to acquire horizontal load and vertical load for all the combined loading conditions. In addition, the capacity should also add to previous parameters which need to do the moment interpolation in next step. The parameters needed for each load combinations is (θ,M_{load}, H_{load}, V_{load},M_{capa}, H_{capa}, V_{capa});

2) For the same θ, the parameter sets were divided into 5 groups with 7 points in each group. For each group, horizontal load and vertical load were calculated by interpolate moment capacity M_{capa}. The parameter sets changed into (θ,M_{load}, H_{load}, V_{load},0.5, H_{capa}, V_{capa}). Each group generates one point on the displacement contours for a specific θ and M/M_{ult}. 5 groups give 5 points on the contour diagrams. The points on the axis were derived in two load plan which are HM load plane and VM load plane used the method in plotting 2D displacement contours diagram from Section 5.1.

The displacement contours for horizontal displacement and vertical displacement were used the same method. Figure 5.10 shows the displacement contours for θ,u and w in HVM load plane.

The load-displacement curves for a bucket foundation can be determined from Figure 5.10 for a given combined cyclic loading. The detailed procedure for calculating the bearing capacity and stiffness of bucket foundation was presented in next section.

5.3 Procedure for determining cyclic bearing capacity and stiffness

From previous analysis, the failure envelopes and corresponding displacement contours obtained can be used for the preliminary design of bucket foundation for OWT subjected to cyclic loads. This section gives detailed procedure to use the failure envelopes and displacement contour diagrams which were produced in this thesis report to calculate the bearing capacity and soil structure stiffness by giving a specific irregular load history.This procedure is shown in Figure 5.11.

Irregular load history transform into load parcels where each load parcel has a constant average and cyclic load. Load parcels uses NGI cyclic shear strain accumulation procedure to get a cyclic and average stress τ_{cy}/τ_a and equivalent cycles N_{eq}. Those are the input parameters for the procedure introduced in this section.

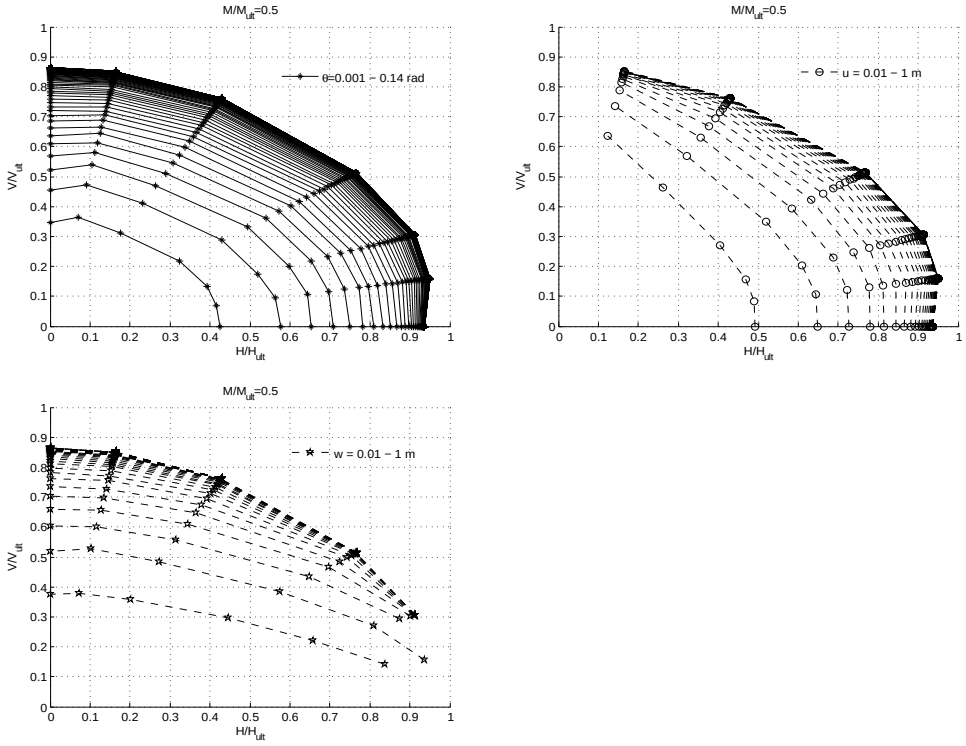

Figure 5.10: *3D displacement contours for OCR=1,*$N_{eq} = 100$*,* $\tau_{cy}/\tau_a = 2$

The static capacity analysis for pure horizontal H_{Static}, pure vertical V_{Static} and pure overturning moment M_{Static} should performe at first. The cyclic ultimate capacity for pure horizontal H_{ult}, vertical V_{ult} and overturning moment M_{ult} can be determined from N_{eq} and F_{cy}/F_a. This calculation can be carried out using Figure 4.5.

Therefore, the failure envelopes were determined using Figure 5.12.

Finally, the soil structure stiffness were determined from Figure 5.10.

5.4 Summary

This chapter presented the displacement contour diagrams for different N_{eq} and τ_{cy}/τ_a, h/D and soil profiles. In the end of this chapter, a procedure was introduced to guide how to use the data produced and plotted in this thesis report.

In the next chapter, the conclusions and suggestions will be presented.

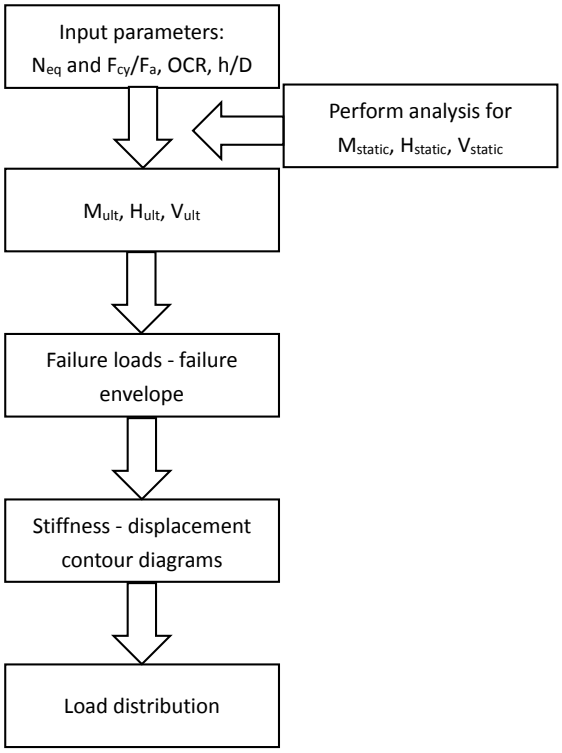

Figure 5.11: *Procedure for determining cyclic bearing capacity and stiffness for bucket foundation*

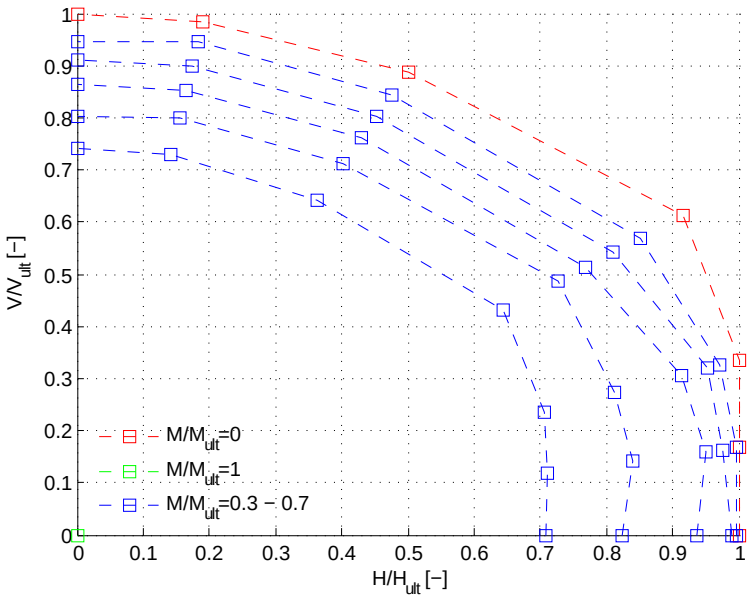

Figure 5.12: *Failure envelopes in 3D load space*

Chapter 6

Conclusions and suggestions

6.1 Conclusions

The research presented in this report has studied the response of bucket foundation for OWT subjected to combined cyclic loads. Normal consolidated clay and heavily consolidated clay have been considered for bucket foundation geometry h/D=0.5 and h/D=1. The research has successfully revealed several characteristics of the behaviour of a cyclically loaded bucket foundation. Based on the results, simplified design diagrams showing foundation failure and foundation displacements are established.

The ultimate cyclic bearing capacity M_{ult}, H_{ult} and V_{ult} were investigated for different number of cycles N_{eq} and average to cyclic load ratio F_{cy}/F_a. The ultimate cyclic bearing capacity can be higher or lower than the ultimate static bearing capacity depending on N_{eq} and F_{cy}/F_a. The ultimate cyclic bearing capacity normalized by the ultimate static corresponding capacity are almost identical for M_{ult}/M_{static}, H_{ult}/H_{static} and V_{ult}/V_{static} and therefore only one diagram is needed for determining ultimate cyclic bearing capacity for the same soil profile.

The effects from different parameters on the normalized failure envelopes in VM,VH and HM plane are studied.

The equivalent number of cycles N_{eq} and cyclic to average load ratio F_{cy}/F_a do not influence the normalized failure envelopes significantly. The soil profile with constant cyclic shear strength with depth influences the failure envelopes in HM plane when compared to the soil profile with linear increasing cyclic shear strength with depth.

The bucket foundation geometry also effects the failure envelopes in HM plane both for normal consolidated clay and over consolidated clay.

Since the failure envelopes only depends on the soil profile and bucket geometry, only four failure envelopes are sufficient to describe the variation considered in this study.

However, this conclusion is only validate for the the foundation studied in this thesis. The normalized failure envelopes for deep bucket may be more sensitive to increasing N_{eq} than the findings in this study.

Based on the conclusions above, it is possible to estimate the capacity for any load combinations if the static capacity M_{static}, H_{static} and V_{static}, degradation expressed as N_{eq} and F_{cy}/F_a are known. The procedure can be used for preliminary design for the range of parameters considered in this report. Layered soil and other bucket geometries may give other relations.

The failure envelopes are symmetry in first quadrant in VM and VH plane and symmetry around first and second quadrant in HM plane which has been discussed in Section 4.6.1.

The coupling of three loads, which are horizontal, vertical and moment loads, in each load plane are different which can be seen from the failure envelopes in VM, VH and HM plane. The coupling of the failure load in VH and VM plane are almost the same while the coupling of failure loads in HM plane is different and significantly influenced by bucket foundation geometry h/D.

The failure envelopes in VM and VH plane have a good agreement to the proposed analytical failure envelopes from Gourvenec and Barnett[17].

Displacement contour diagrams have been developed by the similar procedure and based on Drammen clay stress train data. The trends of the displacement contour diagrams have a good agreement to the displacement contour diagrams for a spud can from Jostad[18]. The general displacement contour diagrams also fits well in terms of the strain contour diagrams in soil element level from Andersen[14].

The displacement data are represented in diagrams as total numbers and not normalized, but can be used for preliminary design of bucket geometries close to the geometries considered. The load data in the diagrams are however normalized and based on the study of the normalized failure envelopes is reasonable to assume that the displacement contours can be scaled according to the same rules by the ultimate pure capacities.

The displacement contour diagrams are sensitive to the cyclic parameters N_{eq} and F_{cy}/F_a as well as bucket geometry h/D and soil profiles.

The decoupling between horizontal displacement and moment rotation for h/D=0.5 is more obvious than h/D=1. The coupling of the displacement contours in VH and VM plane are more or less the same.

6.2 Suggestions for further work

Due to time limitation, this thesis project was not cover all the aspects related to bucket foundation design subjected to combined cyclic loads for OWT. Therefore, several suggestions for the further work are listed in this section.

The geometry of bucket foundation of h/D =0.5 and 1 were analysed from previous chapters. The h/D ratio has a significant influence on the normalized failure envelopes and corresponding displacement contours which means it effects the failure mode and stiffness

of the soil-structure system. Future work should study different bucket geometries and produce the capacity envelopes and displacement contours.

The displacements given in contour diagrams are the total displacement and not normalized by any parameters. In future work, the displacement contour diagrams may use a similar normalized approach as used for establishing the failure envelopes. The displacement may be normalized by e.g. geometry parameters h or D. This will make the displacement contour diagrams more general and applicable to more situations. To incease the possible applicability, it is also necessary to produce displacement contours for other cyclic to average load ratios F_{cy}/F_a and OCR values between 1 and 40.

The failure envelopes and displacement contours can be analysed in the future for bucket foundation in layered soil.

The soil-skirt roughness factors were the same which is α=0.65 for all the cases studied in this thesis. A different parameter is not expected to violate the main conclusions but the effect should be studied and qualified.

References

[1] Lars Bo Ibsen, S Liingaard, and Søren A Nielsen. Bucket foundation, a status. *Proceedings of the Copenhagen Offshore Wind*, 2005.

[2] Knut H Andersen and R Dyvik. Clay behaviour under irregular cyclic loading. 1992.

[3] H.P. Jostad. Bifurc - version 3 undrained capacity analyses of clay. Technical report, Norwegian Geotechnical Institute, 1997.

[4] European Wind Energy Association et al. Wind in power, 2012 european statistics, 2013. *Available online a t http://www. ewea. org/fileadmin/files/library/publications/statistics/Wind_in_power_annual_statistics_2012. pdf*, 2012.

[5] Crown Estate. Offshore wind cost reduction: Pathways study. *Study in partnership with the Secretary of State for Energy and Climate Change in the UK*, 2012.

[6] Byron Byrne. Foundation design for offshore wind turbines. Technical report, University of Oxford, 2011.

[7] IRENA. Renewable energy technologies: Cost analysis series. Technical report, International Renewable Energy Agency, 2012.

[8] Lars Bo Ibsen and Rune Brincker. Design of a new foundation for offshore wind turbines. In *Proceedings of The 22nd International Modal Analysis Conference (IMAC), Detroit, Michigan*, 2004.

[9] Det Norske Veritas. *Design of offshore wind turbine structures*. Det Norske Veritas, 2013.

[10] KH Andersen. Cyclic clay data for foundation design of structures subjected to wave loading. In *Proceedings of the International Conference on Cyclic Behaviour of Soils and Liquefaction Phenomena, CBS04, Bochum, Germany*, volume 31, pages 371–387, 2004.

[11] Knut H Andersen, Hans Petter Jostad, et al. Foundation design of skirted foundations and anchors in clay. In *Offshore Technology Conference*. Offshore Technology Conference, 1999.

[12] Knut H Andersen. Bearing capacity under cyclic loading-offshore, along the coast, and on land. the 21st bjerrum lecture presented in oslo, 23 november 2007 this paper represents the written version of the 21st bjerrum lecture. while it has been edited for the present publication, it retains the general structure of the original lecture, which was intended for a general geotechnical audience. the bjerrum lecture is presented in oslo in alternate years by the norwegian geotechnical society with the support of the bjerrum memorial fund (laurits bjerrums minnefond). *Canadian Geotechnical Journal*, 46(5):513–535, 2009.

[13] Knut H Andersen and Rolf Lauritzsen. Bearing capacity for foundations with cyclic loads. *Journal of Geotechnical Engineering*, 114(5):540–555, 1988.

[14] Knut H Andersen, Arne Kleven, and Dag Heien. Cyclic soil data for design of gravity structures. *Journal of Geotechnical Engineering*, 114(5):517–539, 1988.

[15] KH Andersen, SF Brown, I Foss, JH Poul, and WF Rosenbrand. Effect of cyclic loading on clay behaviour. *Norwegian Geotechnical Institute Publication*, (113), 1976.

[16] CC Ladd. Stress-deformation and strength characteristics, state of the art report. *Proc. of 9th ISFMFE., 1977*, 4:421–494, 1977.

[17] S Gourvenec and S Barnett. Undrained failure envelope for skirted foundations under general loading. *Géotechnique*, 61(3):263, 2011.

[18] HP Jostad, F Nadim, and KH Andersen. A computational model for fixity of spud cans on stiff clay. In *International Journal of Rock Mechanics and Mining Sciences and Geomechanics Abstracts*, volume 32. Elsevier Science, 1995.

Appendix A

Soil normalized cyclic shear strength

Table A.1: *Normalized cyclic shear strength*

τ_{cy}/τ_a	N_{eq}		OCR =1			OCR =40		
			$\tau_{cy,f}$	$\tau_{a,f}$	$\tau_{f,cy}$	$\tau_{cy,f}$	$\tau_{a,f}$	$\tau_{f,cy}$
0	1	$\tau^C_{cy,f}/s^C_u$	0	1	1	0	1	1
		$\tau^E_{cy,f}/s^C_u$	0	0.48	0.48	0	0.52	0.52
		$\tau^{DSS}_{cy,f}/s^{DSS}_u$	0	1	1	0	1	1
	10	$\tau^C_{cy,f}/s^C_u$	0	1	1	0	1	1
		$\tau^E_{cy,f}/s^C_u$	0	0.48	0.48	0	0.52	0.52
		$\tau^{DSS}_{cy,f}/s^{DSS}_u$	0	1	1	0	1	1
	100	$\tau^C_{cy,f}/s^C_u$	0	1	1	0	1	1
		$\tau^E_{cy,f}/s^C_u$	0	0.48	0.48	0	0.52	0.52
		$\tau^{DSS}_{cy,f}/s^{DSS}_u$	0	1	1	0	1	1
0.5	1	$\tau^C_{cy,f}/s^C_u$	0.25	0.95	1.2	0.52	0.76	1.28
		$\tau^E_{cy,f}/s^C_u$	0.18	0.38	0.56	0.2	0.46	0.66
		$\tau^{DSS}_{cy,f}/s^{DSS}_u$	0.44	0.87	1.31	0.47	0.94	1.41
	10	$\tau^C_{cy,f}/s^C_u$	0.23	0.93	1.16	0.44	0.6	1.04
		$\tau^E_{cy,f}/s^C_u$	0.17	0.31	0.48	0.15	0.43	0.58
		$\tau^{DSS}_{cy,f}/s^{DSS}_u$	0.4	0.8	1.2	0.38	0.77	1.15
	100	$\tau^C_{cy,f}/s^C_u$	0.22	0.82	1.04	0.32	0.44	0.76
		$\tau^E_{cy,f}/s^C_u$	0.16	0.25	0.41	0.1	0.36	0.46
		$\tau^{DSS}_{cy,f}/s^{DSS}_u$	0.35	0.7	1.05	0.27	0.54	0.81

τ_{cy}/τ_a	N_{eq}		OCR =1			OCR =40		
			$\tau_{cy,f}$	$\tau_{a,f}$	$\tau_{f,cy}$	$\tau_{cy,f}$	$\tau_{a,f}$	$\tau_{f,cy}$
1	1	$\tau^C_{cy,f}/s^C_u$	0.75	0.66	1.41	0.7	0.5	1.2
		$\tau^E_{cy,f}/s^C_u$	0.3	0.3	0.6	0.4	0.35	0.75
		$\tau^{DSS}_{cy,f}/s^{DSS}_u$	0.76	0.76	1.52	0.76	0.76	1.52
	10	$\tau^C_{cy,f}/s^C_u$	0.5	0.62	1.12	0.52	0.39	0.91
		$\tau^E_{cy,f}/s^C_u$	0.3	0.1	0.4	0.22	0.37	0.59
		$\tau^{DSS}_{cy,f}/s^{DSS}_u$	0.64	0.64	1.28	0.58	0.58	1.16
	100	$\tau^C_{cy,f}/s^C_u$	0.36	0.58	0.94	0.33	0.3	0.63
		$\tau^E_{cy,f}/s^C_u$	0.2	0.2	0.4	0.08	0.33	0.41
		$\tau^{DSS}_{cy,f}/s^{DSS}_u$	0.51	0.51	1.02	0.36	0.36	0.72
2	1	$\tau^C_{cy,f}/s^C_u$	0.84	0.42	1.26	0.72	0.16	0.88
		$\tau^E_{cy,f}/s^C_u$	0.57	0.13	0.7	0.61	0.12	0.73
		$\tau^{DSS}_{cy,f}/s^{DSS}_u$	1.16	0.58	1.74	1	0.5	1.5
	10	$\tau^C_{cy,f}/s^C_u$	0.56	0.42	0.98	0.52	0.15	0.67
		$\tau^E_{cy,f}/s^C_u$	0.4	0.007	0.407	0.42	0.1	0.52
		$\tau^{DSS}_{cy,f}/s^{DSS}_u$	0.84	0.42	1.26	0.74	0.37	1.11
	100	$\tau^C_{cy,f}/s^C_u$	0.43	0.43	0.86	0.24	0.1	0.34
		$\tau^E_{cy,f}/s^C_u$	0.3	0.05	0.35	0.3	0.09	0.39
		$\tau^{DSS}_{cy,f}/s^{DSS}_u$	0.66	0.34	1	0.43	0.23	0.66
$\tau_a = 0$	1	$\tau^C_{cy,f}/s^C_u$	0.8	0	0.8	0.67	0	0.67
		$\tau^E_{cy,f}/s^C_u$	0.8	0	0.8	0.67	0	0.67
		$\tau^{DSS}_{cy,f}/s^{DSS}_u$	1.28	0	1.28	1.1	0	1.1
	10	$\tau^C_{cy,f}/s^C_u$	0.55	0	0.55	0.47	0	0.47
		$\tau^E_{cy,f}/s^C_u$	0.55	0	0.55	0.47	0	0.47
		$\tau^{DSS}_{cy,f}/s^{DSS}_u$	0.92	0	0.92	0.78	0	0.78
	100	$\tau^C_{cy,f}/s^C_u$	0.4	0	0.4	0.28	0	0.28
		$\tau^E_{cy,f}/s^C_u$	0.4	0	0.4	0.28	0	0.28
		$\tau^{DSS}_{cy,f}/s^{DSS}_u$	0.69	0	0.69	0.45	0	0.45

Appendix B

Soil stress strain curves

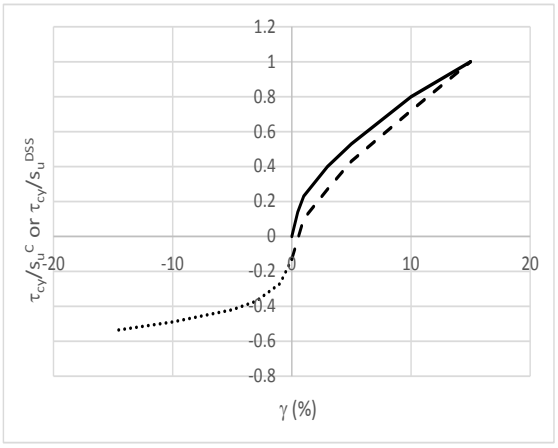

(a) $\tau_{cy} = 0$

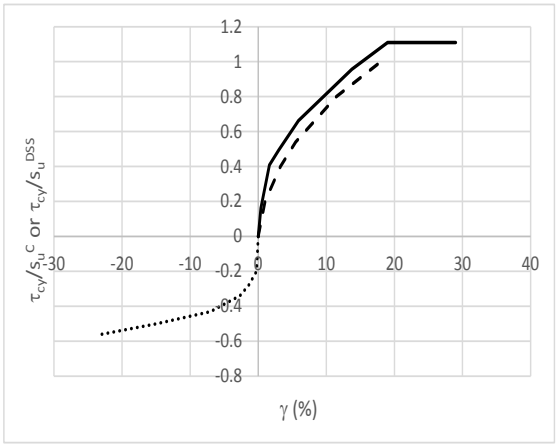

(b) $\tau_{cy}/\tau_a = 1$

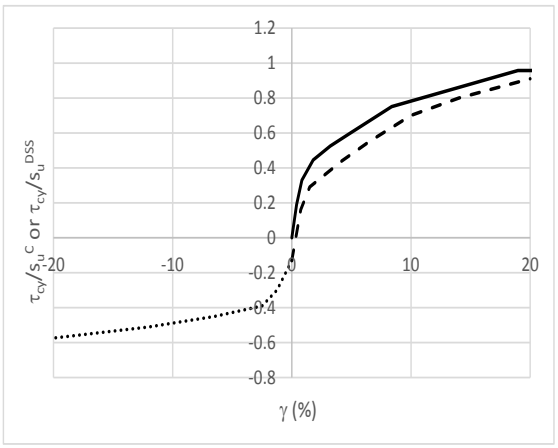

(c) $\tau_{cy}/\tau_a = 2$

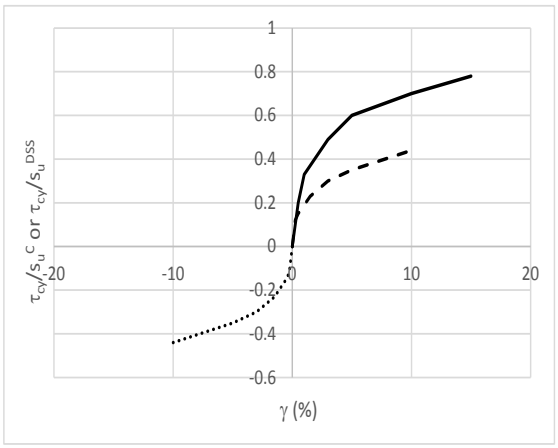

(d) $\tau_a = 0$

Figure B.1: *Stress strain curve for OCR=40,*$N_{eq} = 10$

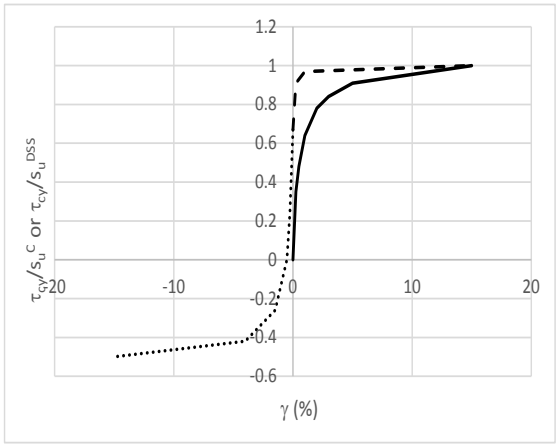

(a) $\tau_{cy} = 0$

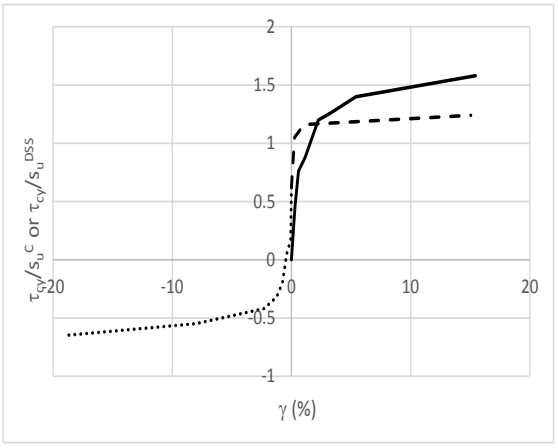

(b) $\tau_{cy}/\tau_a = 1$

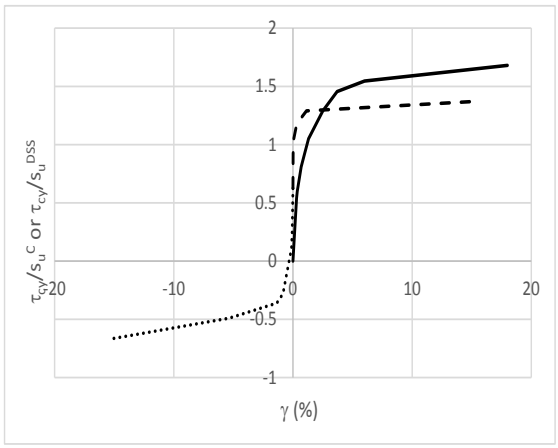

(c) $\tau_{cy}/\tau_a = 2$

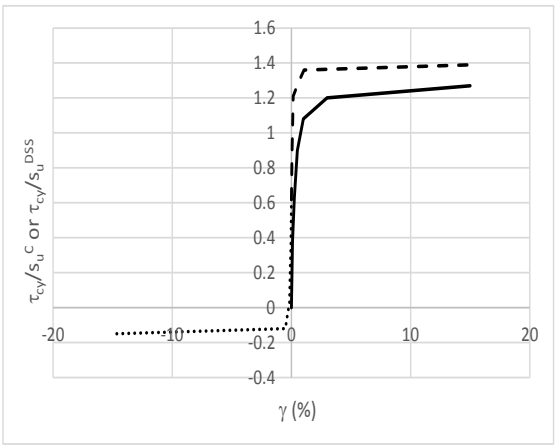

(d) $\tau_a = 0$

Figure B.2: *Stress strain curve for OCR=1,*$N_{eq} = 1$

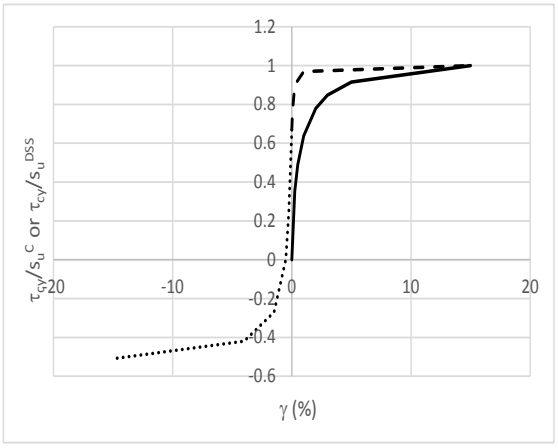

(a) $\tau_{cy} = 0$

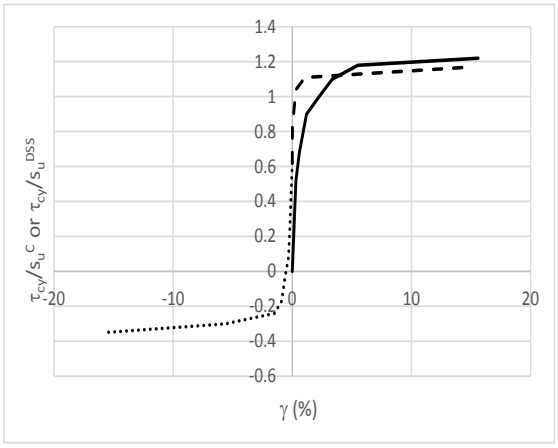

(b) $\tau_{cy}/\tau_a = 1$

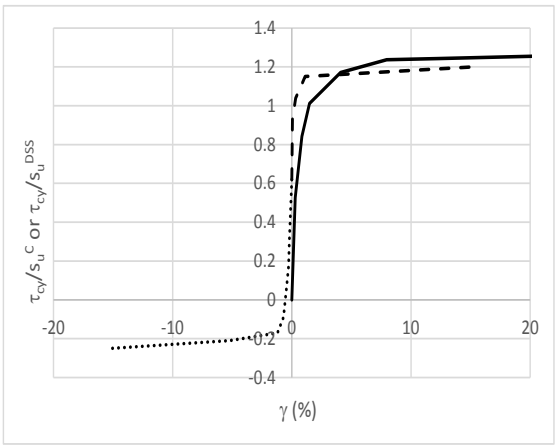

(c) $\tau_{cy}/\tau_a = 2$

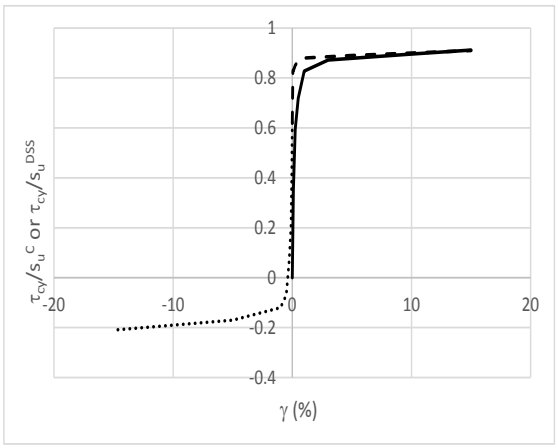

(d) $\tau_a = 0$

Figure B.3: *Stress strain curve for OCR=1,*$N_{eq} = 10$

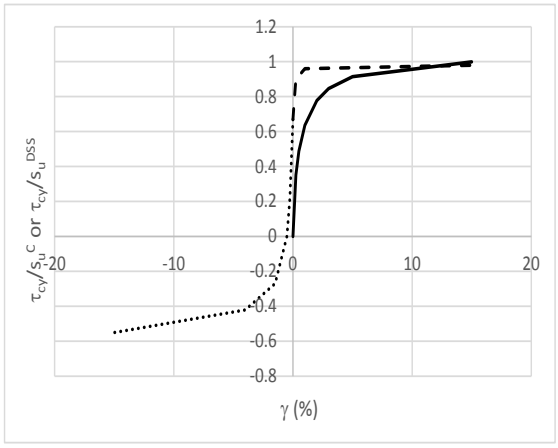

(a) $\tau_{cy} = 0$

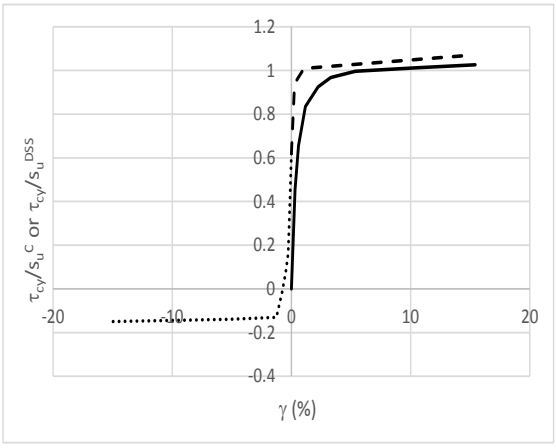

(b) $\tau_{cy}/\tau_a = 1$

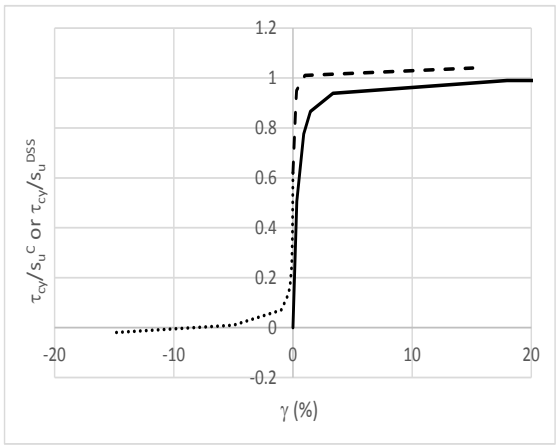

(c) $\tau_{cy}/\tau_a = 2$

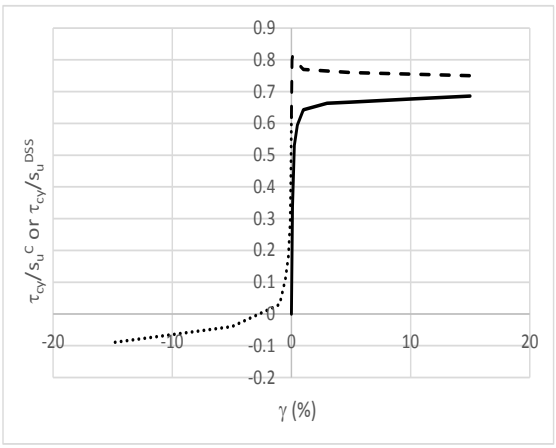

(d) $\tau_a = 0$

Figure B.4: *Stress strain curve for OCR=1,*$N_{eq} = 100$

Appendix C

MATLAB code

C.1 MATLAB code for batch processing

```
%% This MATLAB script is for batch processing in BIFURC by giving a series of
    predefined ultimate loads
clear all
clc
close all
%% read data into matlab for next calculating
filename='LOADS.DAT';
filename_readdata='Read_data.xlsx';
load_combUlt=xlsread('C:\Users\yic\Dropbox\NTNU\Master Thesis\HVMCap for
    matlab programming\Load_combinations_OCR40_geom1_2LoadPlane_const_su.xlsx'
    ,'sheet1');
filename_loadcomb='Load_combinations_OCR40_geom1_2LoadPlane_const_su.xlsx';
%% Read load input from excel file which loaded before
H_Bload=load_combUlt(1:3,1);% read Horizontal bottom load
H_Tload=load_combUlt(1:3,2);% read horizontal top load
M_load=load_combUlt(21:23,1);% input Moment load
H_load=load_combUlt(21:23,2);% input horizontal load
```

```
V_load=load_combUlt(1:3,3);% read vertical load
H_posi=load_combUlt(1:3,4);% read horizontal load position
output=zeros(1000,1000); M_ult=zeros(1,3);H_ult=zeros(1,3);V_ult=zeros(1,3);
for j=0:2;% calculate first three loads conditions% %
fid=fopen(filename,'r+');
for i=1:4;
    fgetl(fid);
end
%change Loads
fseek(fid,7,'cof');% search the M_load data position
fprintf(fid,'%+6.15E',H_Bload(j+1));
fgetl(fid);
fseek(fid,7,'cof');
fprintf(fid,'%+6.15E',H_Tload(j+1));
fgetl(fid);
fseek(fid,7,'cof');
fprintf(fid,'%+6.15E',V_load(j+1));
fclose(fid);
% execute bifurc
system('S:\Sw\NGIPRG\Hvmcap\v3_0\AddIn\BifurcW.exe');% for NGI PC
pause(30);
a=importdata('C:\Users\yic\Dropbox\NTNU\Master Thesis\HVMCap for matlab
    programming\OUTHIST.DAT');% from NGI PC
nrows=size(a,1);% number of rows from results
output(1:nrows,8*j+1)=a(:,1);%load factors
output(1:nrows,8*j+2)=a(:,2);% x_top disp
output(1:nrows,8*j+3)=a(:,3);%z_top disp
output(1:nrows,8*j+4)=a(:,4);%x_bottom disp
output(1:nrows,8*j+5)=a(:,5);%z_bottom disp
output(1:nrows,8*j+6)=output(1:nrows,8*j+1)*M_load(j+1);% M_load
M_ult(:,j+1)=max(output(1:nrows,8*j+6));%M_ult load
output(1:nrows,8*j+7)=output(1:nrows,8*j+1)*H_load(j+1);% H_load
H_ult(:,j+1)=max(output(1:nrows,8*j+7));%H_ult load
output(1:nrows,8*j+8)=output(1:nrows,8*j+1)*V_load(j+1);% V_load
V_ult(:,j+1)=max(abs(output(1:nrows,8*j+8)));%V_ult load%
end
```

```
%write three ultimate loads into load combination file
xlswrite(filename_loadcomb,M_ult(1),'sheet1','A42');% write moment load
xlswrite(filename_loadcomb,H_ult(2),'sheet1','B43');% write Horizontal load
xlswrite(filename_loadcomb,V_ult(3),'sheet1','C44');% write Vertical load
pause(10);
load_comb=xlsread('C:\Users\yic\Dropbox\NTNU\Master Thesis\HVMCap for matlab
    programming\Load_combinations_OCR40_geom1_2LoadPlane_const_su.xlsx','
    sheet1');
H_Bload_re=load_comb(1:18,1);% read Horizontal bottom load
H_Tload_re=load_comb(1:18,2);% read horizontal top load
M_load_re=load_comb(21:38,1);% input Moment load
H_load_re=load_comb(21:38,2);% input horizontal load
V_load_re=load_comb(1:18,3);% read vertical load
%% Do the iteration for the rest of the load combination
for j=3:17;
fid=fopen(filename,'r+');
for i=1:4;
    fgetl(fid);
end
%change load
fseek(fid,7,'cof');% search the M_load data position
fprintf(fid,'%+6.15E',H_Bload_re(j+1));
fgetl(fid);
fseek(fid,7,'cof');
fprintf(fid,'%+6.15E',H_Tload_re(j+1));
fgetl(fid);
fseek(fid,7,'cof');
fprintf(fid,'%+6.15E',V_load_re(j+1));
fclose(fid);
% execute bifurc
system('S:\Sw\NGIPRG\Hvmcap\v3_0\AddIn\BifurcW.exe');
pause(60);
a=importdata('C:\Users\yic\Dropbox\NTNU\Master Thesis\HVMCap for matlab
    programming\OUTHIST.DAT');
nrows=size(a,1);% number of rows in the results
output(1:nrows,8*j+1)=a(:,1);%load factors
```

```
output(1:nrows,8*j+2)=a(:,2);% x_top disp
output(1:nrows,8*j+3)=a(:,3);%z_top disp
output(1:nrows,8*j+4)=a(:,4);%x_bottom disp;
output(1:nrows,8*j+5)=a(:,5);%z_bottom disp

output(1:nrows,8*j+6)=output(1:nrows,8*j+1)*M_load_re(j+1)/M_ult(1);% M_load
output(1:nrows,8*j+7)=output(1:nrows,8*j+1)*H_load_re(j+1)/H_ult(2);% H_load
output(1:nrows,8*j+8)=output(1:nrows,8*j+1)*abs(V_load_re(j+1))/V_ult(3);%
    V_load
end
%% read output data to excel
xlswrite(filename_readdata,output,'sheet36');%,xlRange);
```

C.2 MATLAB code for plotting 3D failure surface

```
%% The MATLAB code in this section was made for linear interpolation bearing
    capacity analysis results for general loading condition to plot the cross-
    section failure envelopes in 3D failure surface.
clear all
clc
close all
%% plot three loading combined situation
n_M=0.2:0.1:0.90;
cols_n_M=size(n_M,2);
% caculate the H loads for M/M_max=0.4:0.1:0.7 without vertical loading
N_100data=xlsread('C:\Users\yo\Dropbox\NTNU\Master Thesis\HVMCap for matlab
    programming\Read_data.xlsx','sheet5');
% HMdata=N_100data(:,(8*(14-1)+1):(8*(18-1)+8));
HMdata=N_100data(:,(8*(14-1)+1):(8*(25-1)+8));

MVdata=N_100data(:,(8*(4-1)+1):(8*(8-1)+8));
HVdata=N_100data(:,(8*(9-1)+1):(8*(13-1)+8));
cols_HMdata=40;% coloumns of the HMdata sets
for i=1:5 % caculate the maximum HVM loads for different combinations for HM&
    MV plane
```

```
H_load(i)=max(HMdata(:,8*(i-1)+7));% Hori. load in HM plane
M_loadH(i)=max(abs(HMdata(:,8*(i-1)+6)));% Moment loads in HM Plane
V_load(i)=max(abs(MVdata(:,8*(i-1)+8)));% Vert. load in MV plane
if V_load(i)>1;V_load(i)=1;end
M_loadV(i)=max(abs(MVdata(:,8*(i-1)+6)));% moment load in MV Plane
if M_loadV(i)>1;M_loadV(i)=1;end
H_loadV(i)=max(HVdata(:,8*(i-1)+7));% Hori. load in HV plane
if H_loadV(i)>1;H_loadV(i)=1;end
V_loadH(i)=max(abs(HVdata(:,8*(i-1)+8)));% Vert. load in HV plane
if V_loadH(i)>1;V_loadH(i)=1;end
end
M_loadH=[1 M_loadH 0];
M_loadV=[1 M_loadV 0];
H_load=[0 H_load 1];% HMplane
V_load=[0 V_load 1];% VM plane
for i=1:cols_n_M
[M_loadH,ia]=unique(M_loadH,'stable');
H_load=H_load(ia);
H_loadVsM(i)=interp1(M_loadH,H_load,n_M(i));% Hori. loads for diff. M/M_max in
     HM plane
V_loadVsM(i)=interp1(M_loadV,V_load,n_M(i));% vert. loads for diff. M/M_max in
     MV plane
end
% % plot cross section for different moment load (should interpolate between
    maximum load for each cases for all the load combinations)
N_1data=xlsread('C:\Users\yo\Dropbox\NTNU\Master Thesis\HVMCap for matlab
    programming\Read_data.xlsx','sheet12');
cols_N1=304;
% read all the data and pick up the maximum load for each load combinations
for i=4:(cols_N1/8)
M_N1(i-3)=max(abs(N_1data(:,8*(i-1)+6)));
if M_N1(i-3)>1;M_N1(i-3)=1;end
H_N1(i-3)=max(abs(N_1data(:,8*(i-1)+7)));
V_N1(i-3)=max(abs(N_1data(:,8*(i-1)+8)));
if V_N1(i-3)>1;V_N1(i-3)=1;end
end
```

```
for i=1:7
for j=1:5
H_N1_re(j,i)=H_N1(5*(i-1)+j);
V_N1_re(j,i)=V_N1(5*(i-1)+j);
M_N1_re(j,i)=M_N1(5*(i-1)+j);
end
end
zero=zeros(1,cols_n_M);% for compensate the 0 values for V_load in HM plane
    and H_load in MV Plane
one=ones(5,1);% for compensate the 1 values for pure moment loading
zerore=zeros(5,1);
rows_M_N1=size(M_N1_re,1);
for i=1:cols_n_M
for j=1:rows_M_N1
H_N1VsM(j,i)=interp1(M_N1_re(j,:),H_N1_re(j,:),n_M(i));
V_N1VsM(j,i)=interp1(M_N1_re(j,:),V_N1_re(j,:),n_M(i));
end
end
one=ones(7,1);% for compensate the 1 values for pure moment loading
zerore=zeros(7,1);
H_loadV_re=[1 H_loadV 0];% h load only in HV plane M/Mmax=0
V_loadH_re=[0 V_loadH 1];% v load only in HV plane M/Mmax=0
H_N1VsM_re=[H_loadVsM;H_N1VsM;zero];
V_N1VsM_re=[zero;V_N1VsM;V_loadVsM];
H_N1VsM_ne=[(H_loadV_re)' H_N1VsM_re zerore];
V_N1VsM_ne=[(V_loadH_re)' V_N1VsM_re zerore];
rows_M_N1=size(M_N1_re,1);
n_M_zero=zeros(1,1);
n_M_one=ones(1,1);
n_M_ne=[n_M_zero n_M n_M_one];
n_M_re=[n_M_ne;n_M_ne;n_M_ne;n_M_ne;n_M_ne;n_M_ne;n_M_ne];
% plot HV load combination for constant moment loading
figure(1)
hold on
plot3(H_N1VsM_ne(:,1),V_N1VsM_ne(:,1),n_M_re(:,1),'--rs');
plot3(H_N1VsM_ne(:,cols_n_M+2),V_N1VsM_ne(:,cols_n_M+2),n_M_re(:,cols_n_M+2),'
```

```
    --gs');
for v=2:(cols_n_M+1)% suppose 1:cols_n_M+2
plot3(H_N1VsM_ne(:,v),V_N1VsM_ne(:,v),n_M_re(:,v),'--bs');
xlabel('H/H_u_l_t');
ylabel('V/V_u_l_t');
zlabel('M/M_u_l_t');
legend('M/M_u_l_t=0','M/M_u_l_t=1','M/M_u_l_t=0.3 - 0.7','Location','NorthWest
    ');
legend('boxoff');
grid on
```

C.3 MATLAB code for plotting 3D displacement contour diagrams

```
%% The following MATLAB script was made for plotting displacement for combined
     horizontal, vertical and overturning moment load
clear all
clc
close all
%% load 3D combined load situations results into workspace
% define the interval of rotational rad
n_theta=0.001:0.001:0.14;% rotational rad
cols_n_theta=size(n_theta,2);% cols of n_M
n_comb=35;%number of load combinations
n_M=0.7;%:0.1:1;%M/M_max=0.3,0.4,0.5
cols_n_M=size(n_M,2);%cols of n_M
% read data
N_100data=xlsread('C:\Users\yo\Dropbox\NTNU\Master Thesis\HVMCap for matlab
    programming\Read_data.xlsx','sheet10');
depth=xlsread('C:\Users\yo\Dropbox\NTNU\Master Thesis\HVMCap for matlab
    programming\Load_combinations_allPlane_Geo.1.xlsx','sheet1','E2');% bucket
     foundation height
% read the M_ult,V_ult,H_ult
M_ult=max(N_100data(:,8*(1-1)+6));
H_ult=max(N_100data(:,8*(2-1)+7));
```

```
V_ult=max(abs(N_100data(:,8*(3-1)+8)));
% interpolate each data set for different rotational rad
interp_data=zeros(35*cols_n_theta,7);% workspace for putting interpolate
    results
for i=4:38
x_Tdisp=N_100data(:,8*(i-1)+2);% top hori. disp.
x_Tdisp(x_Tdisp==0)=[];% delete zero
x_Bdisp=N_100data(:,8*(i-1)+4);% bottom hori. disp.
x_Bdisp(x_Bdisp==0)=[];% delete zero
z_Tdisp=N_100data(:,8*(i-1)+3);% top vert. disp.
z_Tdisp(z_Tdisp==0)=[];% delete zero
z_Bdisp=N_100data(:,8*(i-1)+5);% bottom vert. disp.
z_Bdisp(z_Bdisp==0)=[];% delete zero
M=N_100data(:,8*(i-1)+6);% moment load
M(M==0)=[];% delete zero
M_max=max(abs(M));% read the maximum moment for each load combination
H=N_100data(:,8*(i-1)+7);% hori. load
H(H==0)=[];% delete zero
H_max=max(abs(H));% read the maximum moment for each load combination
V=N_100data(:,8*(i-1)+8);% Vertical load
V(V==0)=[];% delete zero
V_max=max(abs(V));% read the maximum moment for each load combination
%calculate theta;
H_disp=0.67*x_Bdisp+0.33*x_Tdisp;%calculate horizontal disp
theta=atan((x_Tdisp-H_disp)./(2/3*depth)); %calculate rotation rad
[thetaUni,ia]=unique(theta,'stable');% monotonic increase
MUni=M(ia);% pick out moment according to monotonic increase theta
HUni=H(ia);% pick out horizontal load according to monotonic increase theta
VUni=V(ia);% pick out vertical load according to monotonic increase theta
interp_data(1:cols_n_theta,7*(i-4)+1)=n_theta;% read correspoding maximum
    vertical load for each load combinations
interp_data(1:cols_n_theta,7*(i-4)+2)=interp1(thetaUni,MUni,n_theta);%
    interpolate theta to get moment load
interp_data(1:cols_n_theta,7*(i-4)+3)=interp1(thetaUni,HUni,n_theta);%
    interpolate theta to get moment load
interp_data(1:cols_n_theta,7*(i-4)+4)=interp1(thetaUni,VUni,n_theta);%
```

```
    interpolate theta to get moment load
interp_data(1:cols_n_theta,7*(i-4)+5)=M_max;% read correspoding maximum moment
     for each load combinations
interp_data(1:cols_n_theta,7*(i-4)+6)=H_max;% read correspoding maximum
    horizontal load for each load combinations
interp_data(1:cols_n_theta,7*(i-4)+7)=V_max;% read correspoding maximum
    vertical load for each load combinations
end
%% pick data for same theta
for i=1:cols_n_theta
for j=1:n_comb
theta_re((j+n_comb*(i-1)),:)=interp_data(i,(7*(j-1)+1));
M_re((j+n_comb*(i-1)),:)=interp_data(i,(7*(j-1)+2));
H_re((j+n_comb*(i-1)),:)=interp_data(i,(7*(j-1)+3));
V_re((j+n_comb*(i-1)),:)=interp_data(i,(7*(j-1)+4));
M_max_re((j+n_comb*(i-1)),:)=interp_data(i,(7*(j-1)+5));
H_max_re((j+n_comb*(i-1)),:)=interp_data(i,(7*(j-1)+6));
V_max_re((j+n_comb*(i-1)),:)=interp_data(i,(7*(j-1)+7));
end
end
% divide different theta into different conlumns
for i=1:cols_n_theta
    theta_new(:,i)=theta_re((n_comb*(i-1)+1):(n_comb*(i-1)+n_comb));
    H_new(:,i)=H_re((n_comb*(i-1)+1):(n_comb*(i-1)+n_comb));
    M_new(:,i)=M_re((n_comb*(i-1)+1):(n_comb*(i-1)+n_comb));
    V_new(:,i)=V_re((n_comb*(i-1)+1):(n_comb*(i-1)+n_comb));
    M_max_new(:,i)=M_max_re((n_comb*(i-1)+1):(n_comb*(i-1)+n_comb));
    H_max_new(:,i)=H_max_re((n_comb*(i-1)+1):(n_comb*(i-1)+n_comb));
    V_max_new(:,i)=V_max_re((n_comb*(i-1)+1):(n_comb*(i-1)+n_comb));
end
% divide all the same theta into 7 series, select one in every 5 data sets
for i=1:cols_n_theta
    for k=1:5
    for j=1:7
    theta_fi(7*(k-1)+j,i)=theta_new(5*(j-1)+k,i);
    M_fi(7*(k-1)+j,i)=M_new(5*(j-1)+k,i);
```

```
    H_fi(7*(k-1)+j,i)=H_new(5*(j-1)+k,i);
    V_fi(7*(k-1)+j,i)=V_new(5*(j-1)+k,i);
    M_max_fi(7*(k-1)+j,i)=M_max_new(5*(j-1)+k,i);
    H_max_fi(7*(k-1)+j,i)=H_max_new(5*(j-1)+k,i);
    V_max_fi(7*(k-1)+j,i)=V_max_new(5*(j-1)+k,i);
    end
    end
    % interpolate the M/M_max to get different H,V for the same theta
   for m=1:5
    H_fi_new(1:7,1)=H_fi(((7*(m-1)+1):(7*(m-1)+7)),i);
    V_fi_new(1:7,1)=V_fi(((7*(m-1)+1):(7*(m-1)+7)),i);
    M_max_fi_new(1:7,1)=M_max_fi(((7*(m-1)+1):(7*(m-1)+7)),i);
    H_max_fi_new(1:7,1)=H_max_fi(((7*(m-1)+1):(7*(m-1)+7)),i);
    V_max_fi_new(1:7,1)=V_max_fi(((7*(m-1)+1):(7*(m-1)+7)),i);

    [H_fi_new,ia]=unique(H_fi_new,'stable');
    V_fi_new=V_fi_new(ia);
    M_max_fi_new=M_max_fi_new(ia);
    H_fi_new_re(m,i)=interp1(M_max_fi_new,H_fi_new,n_M);
    V_fi_new_re(m,i)=interp1(M_max_fi_new,V_fi_new,n_M);
    H_max_fi_new_re(m,i)=interp1(M_max_fi_new,H_max_fi_new,n_M);
    V_max_fi_new_re(m,i)=interp1(M_max_fi_new,V_max_fi_new,n_M);
   end
end
%% select H & V for different M/M_max and theta in HM and VM plan,seperately
%read data in HM plane and VM plane
two_plane_data=xlsread('C:\Users\yo\Dropbox\NTNU\Master Thesis\HVMCap for
    matlab programming\Read_data.xlsx','sheet9');
HMdata=two_plane_data(:,(8*(14-1)+1):(8*(18-1)+8));
MVdata=two_plane_data(:,(8*(4-1)+1):(8*(8-1)+8));
cols_HMdata=40;% coloumns of the  load plane data sets
%% interpolate theta to get different H,M, H_max & M_max in HM plane
for i=1:cols_HMdata/8% 2D load plane data sets
x_Tdisp=HMdata(:,8*(i-1)+2);% top hori. disp.
x_Tdisp(x_Tdisp==0)=[];% delete zero
x_Bdisp=HMdata(:,8*(i-1)+4);% bottom hori. disp.
```

```
x_Bdisp(x_Bdisp==0)=[];% delete zero
z_Tdisp=HMdata(:,8*(i-1)+3);% top vert. disp.
z_Tdisp(z_Tdisp==0)=[];% delete zero
z_Bdisp=HMdata(:,8*(i-1)+5);% bottom vert. disp.
z_Bdisp(z_Bdisp==0)=[];% delete zero
M=HMdata(:,8*(i-1)+6);% moment load
M(M==0)=[];% delete zero
M_max=max(abs(M));% read the maximum moment for each load combination
H=HMdata(:,8*(i-1)+7);% hori. load
H(H==0)=[];% delete zero
H_max=max(abs(H));% read the maximum moment for each load combination
H_disp=0.67*x_Bdisp+0.33*x_Tdisp;%calculate horizontal disp
theta=atan((x_Tdisp-H_disp)./(2/3*depth)); %calculate rotation rad
[thetaUni,ia]=unique(theta,'stable');% arrage theta monotonic increase
MUni=M(ia);% pick out moment according to monotonic increase theta
HUni=H(ia);% pick out horizontal load according to monotonic increase theta
interp_HMdata(1:cols_n_theta,7*(i-1)+1)=n_theta;% read correspoding maximum
    vertical load for each load combinations
interp_HMdata(1:cols_n_theta,7*(i-1)+2)=interp1(thetaUni,MUni,n_theta);%
    interpolate theta to get moment load
interp_HMdata(1:cols_n_theta,7*(i-1)+3)=interp1(thetaUni,HUni,n_theta);%
    interpolate theta to get moment load
interp_HMdata(1:cols_n_theta,7*(i-1)+5)=M_max;% read correspoding maximum
    moment for each load combinations
interp_HMdata(1:cols_n_theta,7*(i-1)+6)=H_max;% read correspoding maximum
    horizontal load for each load combinations
end
% interplolate M/M_max to get H for the same theta
n_2loadcomb=5;
for i=1:cols_n_theta
for j=1:n_2loadcomb%(35*cols_n_M)
theta_reHM((j+n_2loadcomb*(i-1)),:)=interp_HMdata(i,(7*(j-1)+1));
M_reHM((j+n_2loadcomb*(i-1)),:)=interp_HMdata(i,(7*(j-1)+2));
H_reHM((j+n_2loadcomb*(i-1)),:)=interp_HMdata(i,(7*(j-1)+3));
M_max_reHM((j+n_2loadcomb*(i-1)),:)=interp_HMdata(i,(7*(j-1)+5));
H_max_reHM((j+n_2loadcomb*(i-1)),:)=interp_HMdata(i,(7*(j-1)+6));
```

```
end
end
% divide different theta into different conlumns
for i=1:cols_n_theta
    theta_newHM(:,i)=theta_reHM((n_2loadcomb*(i-1)+1):(n_2loadcomb*(i-1)+
        n_2loadcomb));
    H_newHM(:,i)=H_reHM((n_2loadcomb*(i-1)+1):(n_2loadcomb*(i-1)+n_2loadcomb))
        ;
    M_newHM(:,i)=M_reHM((n_2loadcomb*(i-1)+1):(n_2loadcomb*(i-1)+n_2loadcomb))
        ;
    M_max_newHM(:,i)=M_max_reHM((n_2loadcomb*(i-1)+1):(n_2loadcomb*(i-1)+
        n_2loadcomb));
    H_max_newHM(:,i)=H_max_reHM((n_2loadcomb*(i-1)+1):(n_2loadcomb*(i-1)+
        n_2loadcomb));
end
% interpolate M/M_max in HM plane
for i=1:cols_n_theta;
[H_fi,ia]=unique(H_newHM(:,i),'stable');% delete
M_max_newHM_re=M_max_newHM(:,i);
M_max_HM=M_max_newHM_re(ia);
H_HM(cols_n_M,i)=interp1(M_max_HM,H_fi,n_M);
end
%% interpolate theta to get different V,M, V_max & M_max in VM planeHdisp no
    this part
for i=1:cols_HMdata/8% 2D load plane data sets
x_Tdisp=MVdata(:,8*(i-1)+2);% top hori. disp.
x_Tdisp(x_Tdisp==0)=[];% delete zero
x_Bdisp=MVdata(:,8*(i-1)+4);% bottom hori. disp.
x_Bdisp(x_Bdisp==0)=[];% delete zero
z_Tdisp=MVdata(:,8*(i-1)+3);% top vert. disp.
z_Tdisp(z_Tdisp==0)=[];% delete zero
z_Bdisp=MVdata(:,8*(i-1)+5);% bottom vert. disp.
z_Bdisp(z_Bdisp==0)=[];% delete zero
M=MVdata(:,8*(i-1)+6);% moment load
M(M==0)=[];% delete zero
M_max=max(abs(M));% read the maximum moment for each load combination
```

```
V=MVdata(:,8*(i-1)+8);% Vertical load
V(V==0)=[];% delete zero
V_max=max(abs(V));% read the maximum moment for each load combination
%calculate theta;
theta=atan(x_Tdisp./(2/3*depth)); %calc.rotational angel rad [thetaUni,ia]=
    unique(theta,'stable');% arrage theta monotonic increase
MUni=M(ia);% pick out moment according to monotonic increase theta
VUni=V(ia);% pick out vertical load according to monotonic increase theta
interp_MVdata(1:cols_n_theta,7*(i-1)+1)=n_theta;% read correspoding maximum
    vertical load for each load combinations
interp_MVdata(1:cols_n_theta,7*(i-1)+2)=interp1(thetaUni,MUni,n_theta);%
    interpolate theta to get moment load
interp_MVdata(1:cols_n_theta,7*(i-1)+4)=interp1(thetaUni,VUni,n_theta);%
    interpolate theta to get moment load
interp_MVdata(1:cols_n_theta,7*(i-1)+5)=M_max;% read correspoding maximum
    moment for each load combinations
interp_MVdata(1:cols_n_theta,7*(i-1)+7)=V_max;% read correspoding maximum
    vertical load for each load combinations
end
% interplolate M/M_max to get V for the same theta
for i=1:cols_n_theta
for j=1:n_2loadcomb%(35*cols_n_M)
theta_reHM((j+n_2loadcomb*(i-1)),:)=interp_MVdata(i,(7*(j-1)+1));
M_reHM((j+n_2loadcomb*(i-1)),:)=interp_MVdata(i,(7*(j-1)+2));
V_reHM((j+n_2loadcomb*(i-1)),:)=interp_MVdata(i,(7*(j-1)+4));
M_max_reHM((j+n_2loadcomb*(i-1)),:)=interp_MVdata(i,(7*(j-1)+5));
V_max_reHM((j+n_2loadcomb*(i-1)),:)=interp_MVdata(i,(7*(j-1)+7));
end
end
% divide different theta into different conlumns
for i=1:cols_n_theta
    theta_newHM(:,i)=theta_reHM((n_2loadcomb*(i-1)+1):(n_2loadcomb*(i-1)+
        n_2loadcomb));
    M_newHM(:,i)=M_reHM((n_2loadcomb*(i-1)+1):(n_2loadcomb*(i-1)+n_2loadcomb))
        ;
    V_newHM(:,i)=V_reHM((n_2loadcomb*(i-1)+1):(n_2loadcomb*(i-1)+n_2loadcomb))
```

```
        ;
    M_max_newHM(:,i)=M_max_reHM((n_2loadcomb*(i-1)+1):(n_2loadcomb*(i-1)+
        n_2loadcomb));
    V_max_newHM(:,i)=V_max_reHM((n_2loadcomb*(i-1)+1):(n_2loadcomb*(i-1)+
        n_2loadcomb));
end
% interpolate M/M_max in MV plane
for i=1:cols_n_theta;
 [V_fi,ia]=unique(V_newHM(:,i),'stable');% delete
M_max_newHM_re=M_max_newHM(:,i);
M_max_HM=M_max_newHM_re(ia);
V_HM(cols_n_M,i)=interp1(M_max_HM,V_fi,n_M);
end
%% plot the displacement contours for a specfic M/M_max
zero=zeros(1,cols_n_theta);% compensate the zeros for MV for H=0 and HM for V
    =0
H_plot=[H_HM;H_fi_new_re;zero];% integarate 2load plane data into 3 load plane
     data
V_plot=[zero;V_fi_new_re;V_HM];
figure(1)
hold on
for i=1:cols_n_theta
x=H_plot(:,i);
y=V_plot(:,i);
plot(x,y,'-k*');
axis([0 1 0 1]);
end
title('M/M_u_l_t=0.7');
xlabel('H/H_u_l_t');
ylabel('V/V_u_l_t');
legend('\theta=0.001 - 0.14 rad','Location','Best');%,'k_M');
legend('boxoff');
axis([0 1 0 1]);
grid on
```

Appendix D

Displacement contour diagrams

D.1 2D displacement contour diagrams

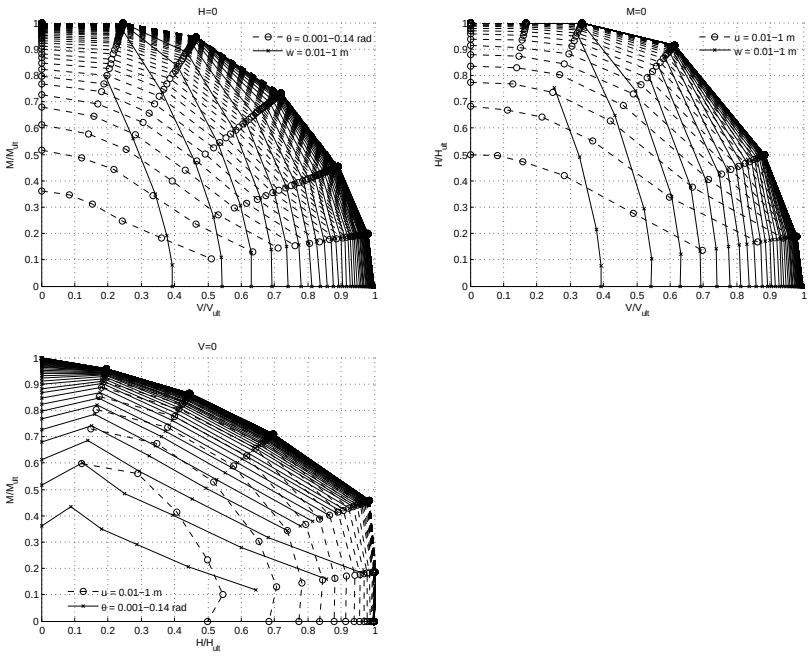

Figure D.1: *2D displacement contours for h/D=1, OCR=1,* $N_{eq} = 10$,$\tau_{cy}/\tau_a = 1$

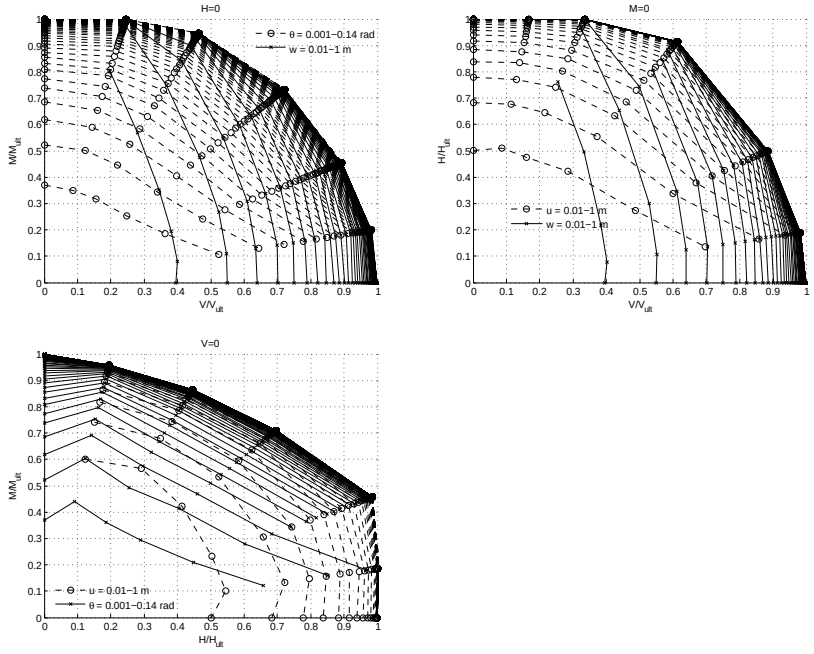

Figure D.2: *2D displacement contours for h/D=1, OCR=1,* $N_{eq} = 100$,$\tau_{cy}/\tau_a = 1$

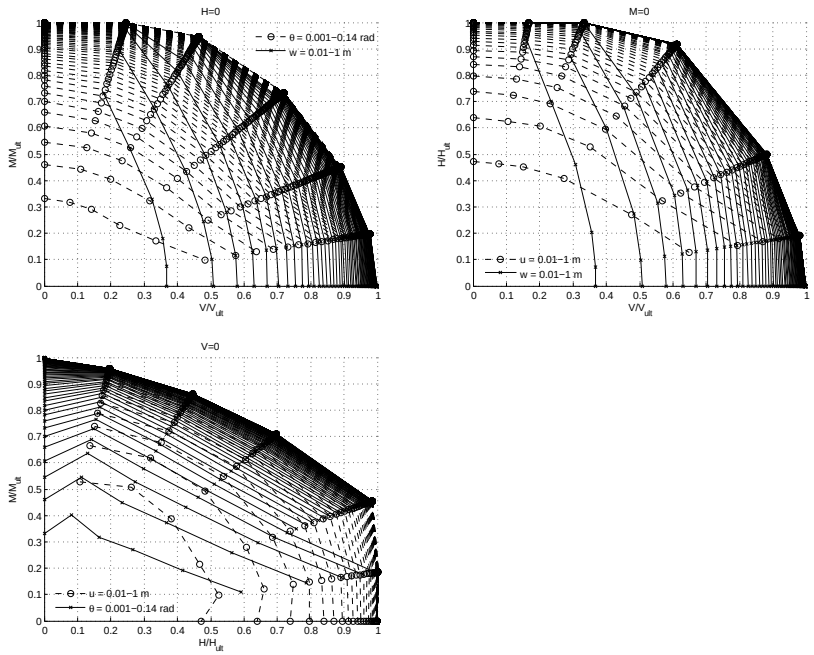

Figure D.3: *2D displacement contours for h/D=1, OCR=1,* $N_{eq} = 100$,$\tau_{cy}/\tau_a = 1$

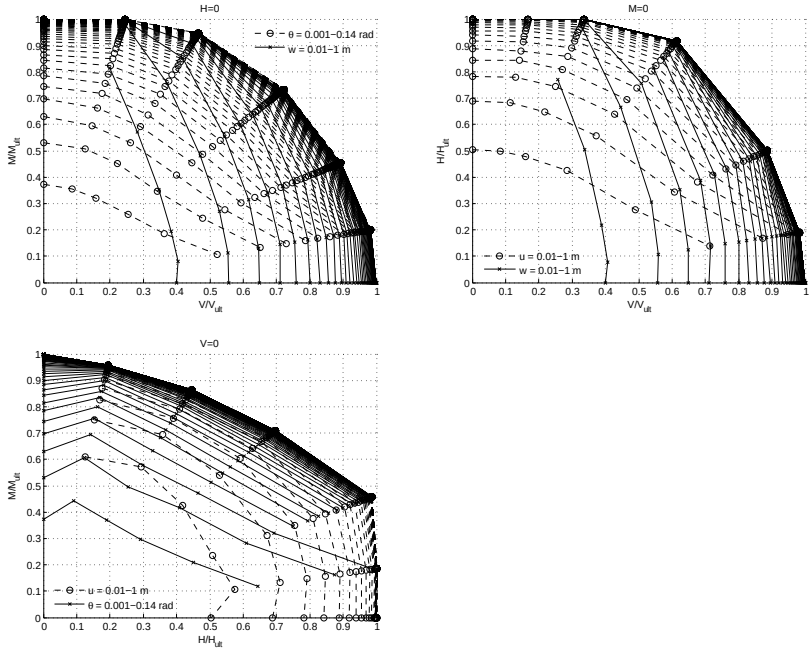

Figure D.4: *2D displacement contours for h/D=1, OCR=1,* $N_{eq} = 100$,$\tau_{cy}/\tau_a = 1$

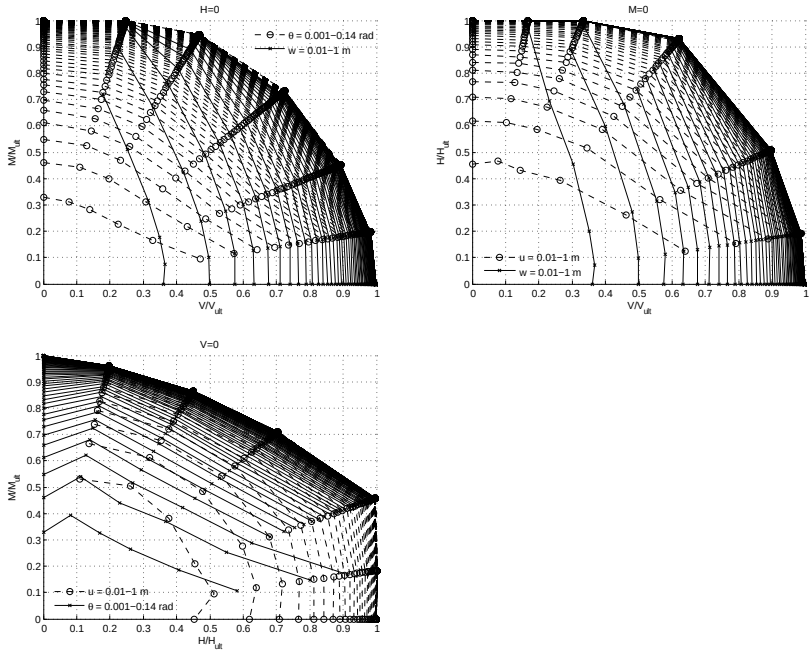

Figure D.5: *2D displacement contours for h/D=1, OCR=1,* $N_{eq} = 1$,$\tau_{cy}/\tau_a = 0$

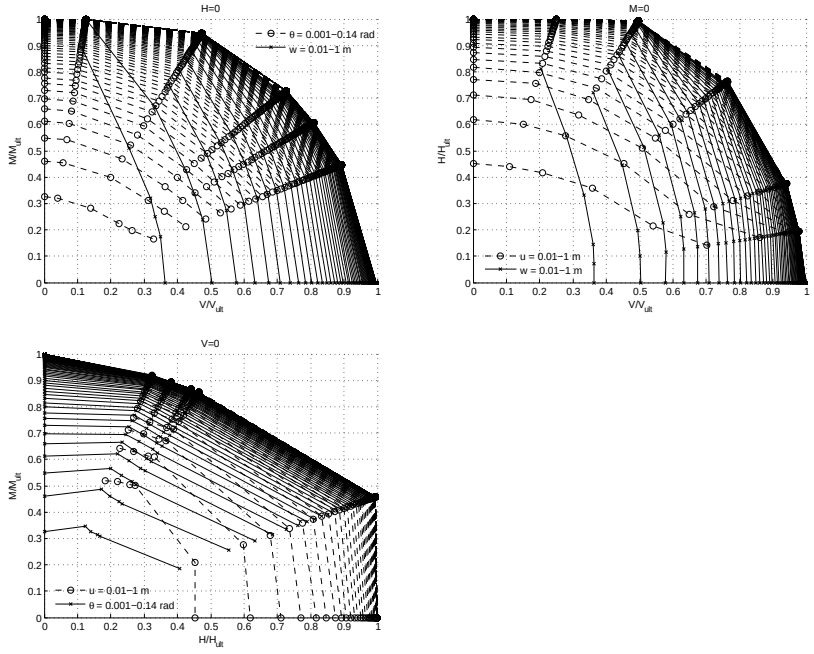

Figure D.6: *2D displacement contours for h/D=1, OCR=1,* $N_{eq} = 10$,$\tau_{cy}/\tau_a = 0$

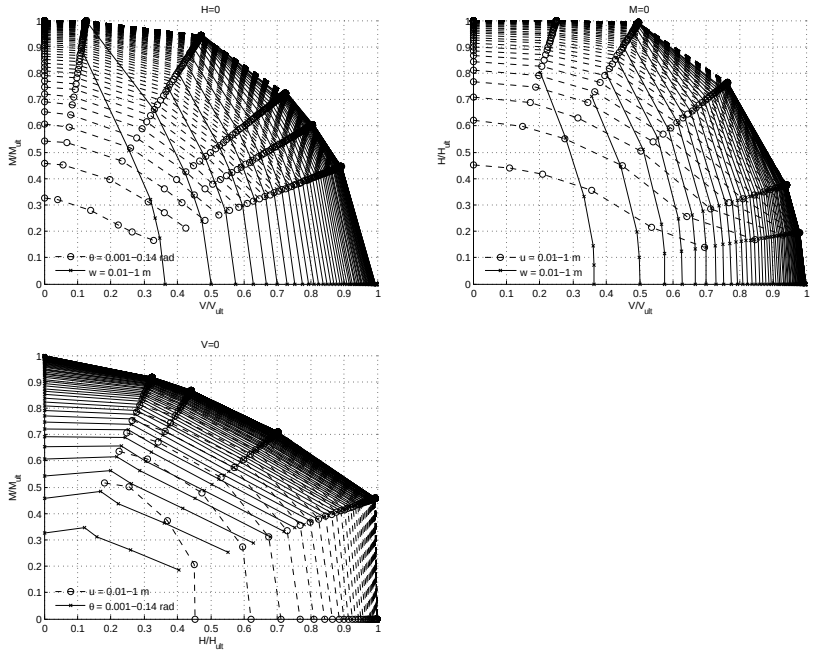

Figure D.7: *2D displacement contours for h/D=1, OCR=1,* $N_{eq} = 100$,$\tau_{cy}/\tau_a = 0$

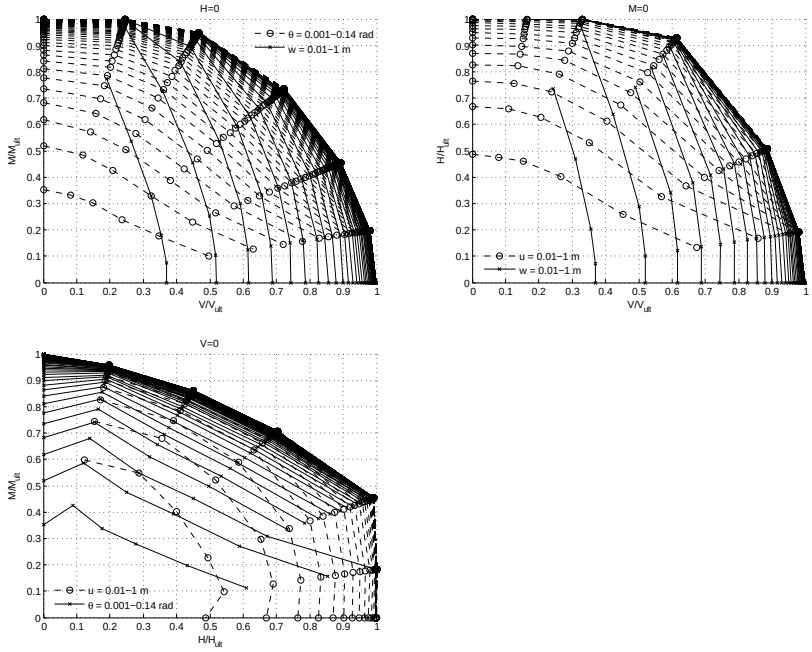

Figure D.8: *2D displacement contours for h/D=1, OCR=1,* $N_{eq} = 1$,$\tau_a = 0$

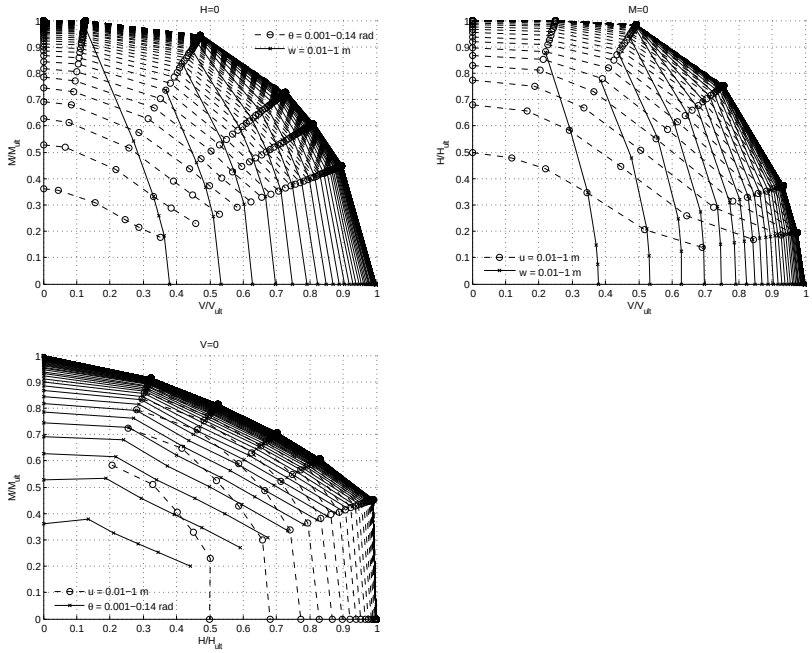

Figure D.9: *2D displacement contours for h/D=1, OCR=1,* $N_{eq} = 10$,$\tau_a = 0$

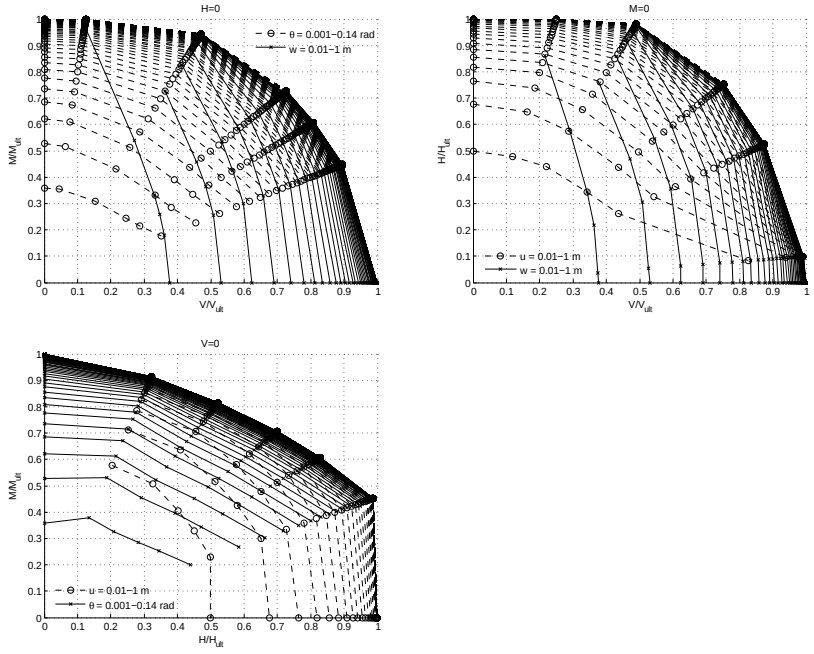

Figure D.10: *2D displacement contours for h/D=1, OCR=1,* $N_{eq} = 100$,$\tau_a = 0$

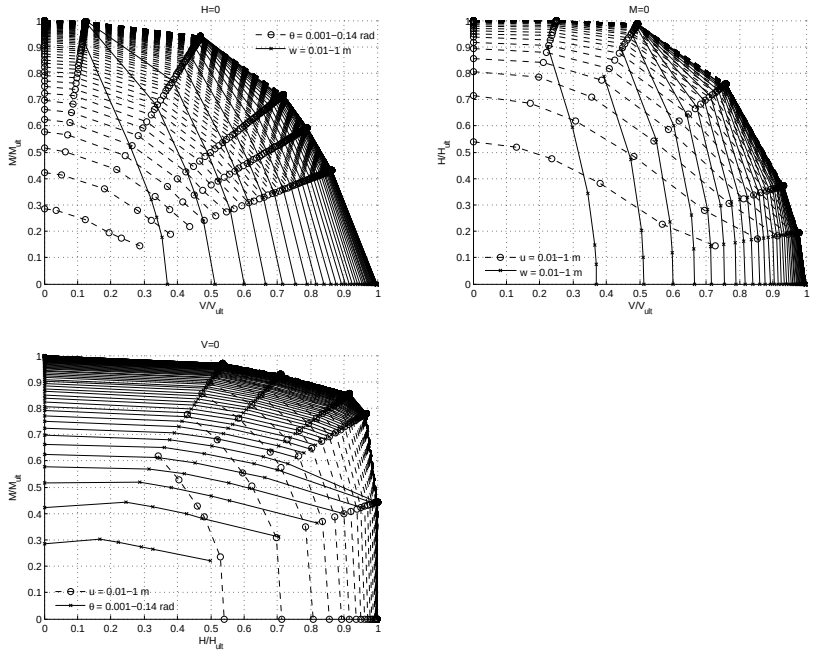

Figure D.11: *2D displacement contours for h/D=0.5, OCR=1,* $N_{eq} = 1$,$\tau_{cy}/\tau_a = 1$

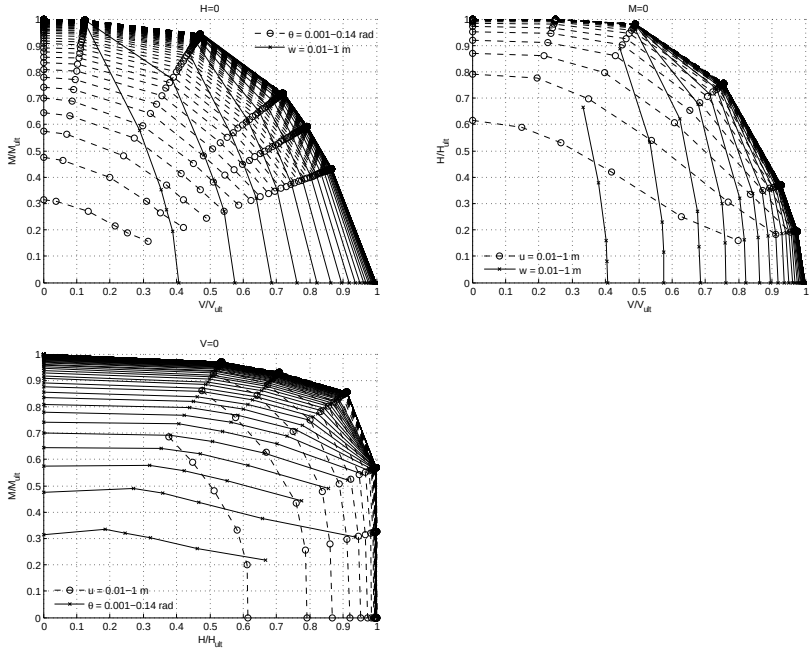

Figure D.12: *2D displacement contours for h/D=0.5, OCR=1,* $N_{eq} = 10$,$\tau_{cy}/\tau_a = 1$

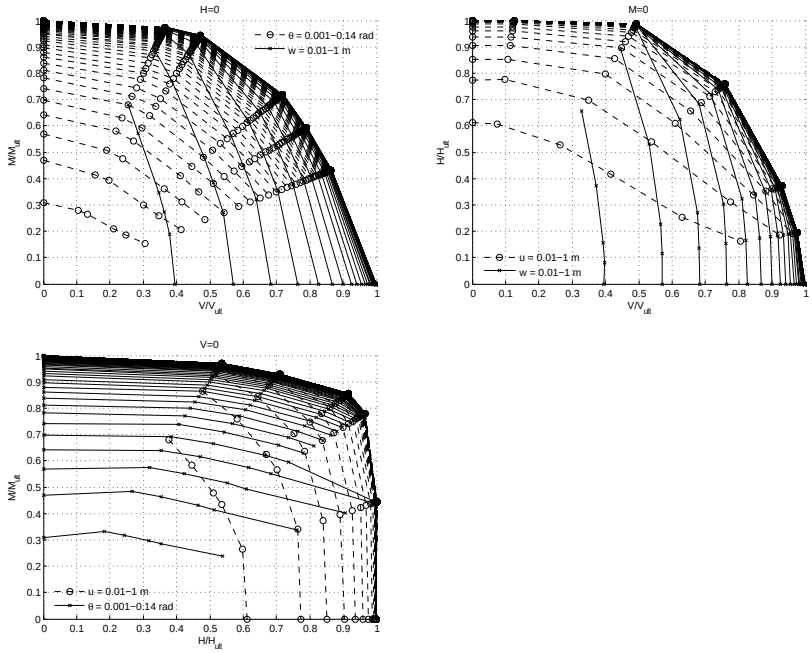

Figure D.13: *2D displacement contours for h/D=0.5, OCR=1,* $N_{eq} = 100$,$\tau_{cy}/\tau_a = 1$

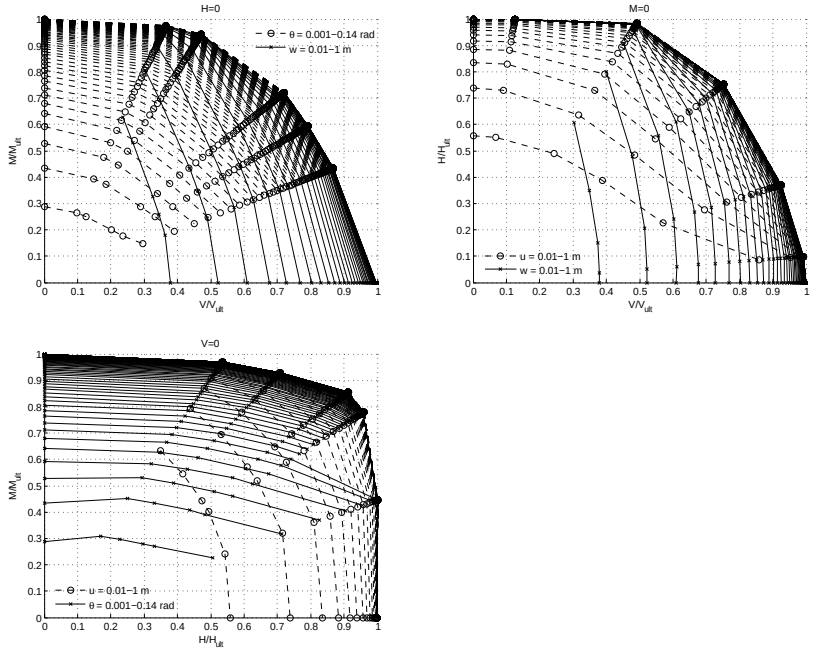

Figure D.14: *2D displacement contours for h/D=0.5, OCR=1,* $N_{eq} = 1$,$\tau_{cy}/\tau_a = 2$

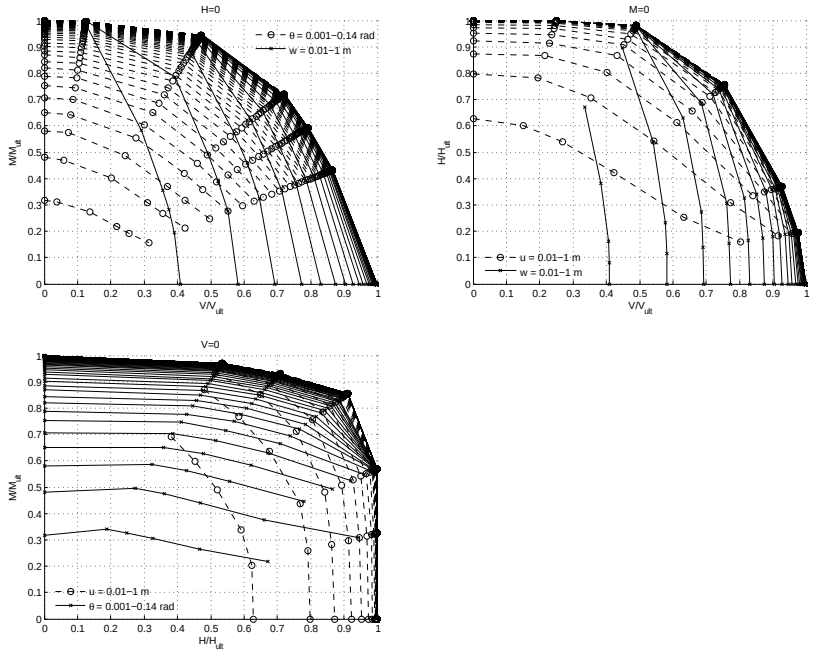

Figure D.15: *2D displacement contours for h/D=0.5, OCR=1,* $N_{eq} = 100$,$\tau_{cy}/\tau_a = 2$

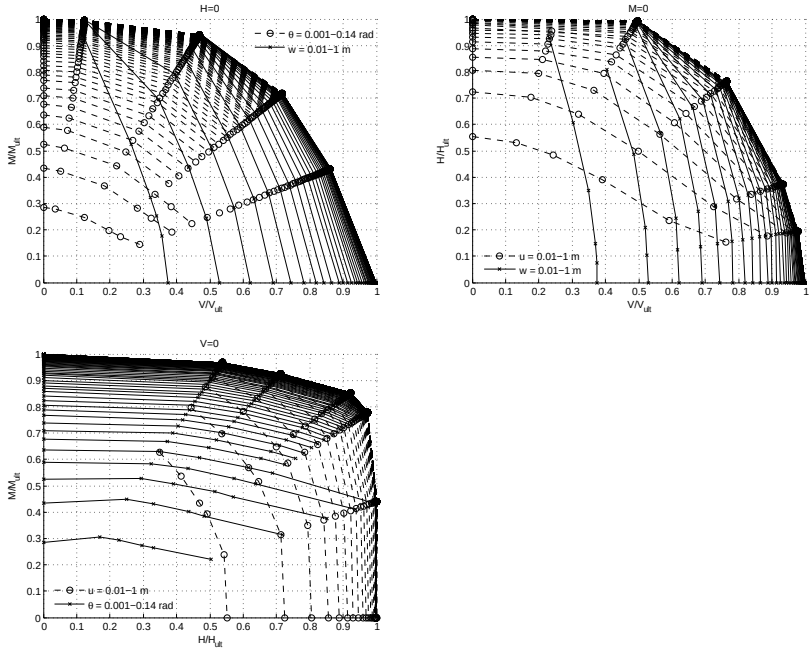

Figure D.16: *2D displacement contours for h/D=0.5, OCR=1,* $N_{eq} = 10$,$\tau_{cy} = 0$

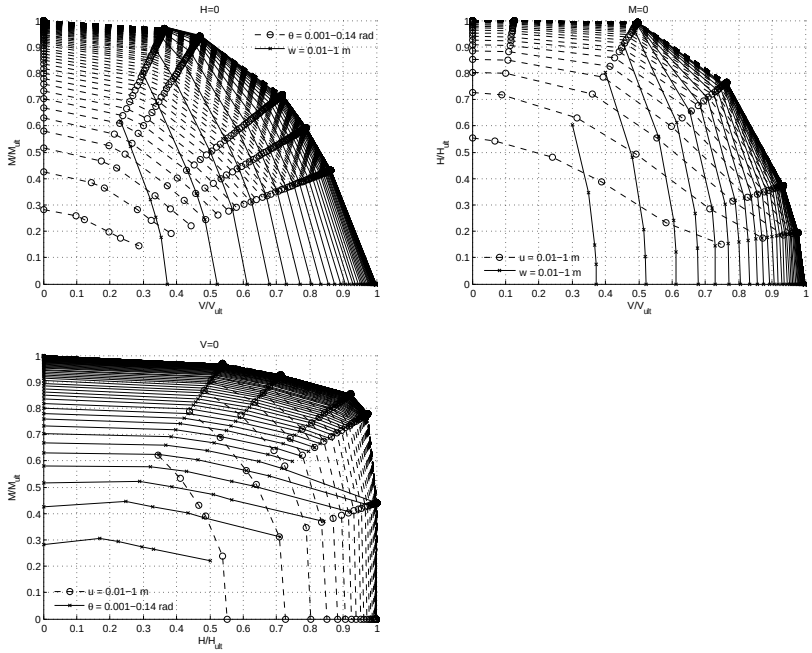

Figure D.17: *2D displacement contours for h/D=0.5, OCR=1,* $N_{eq} = 100$,$\tau_{cy} = 0$

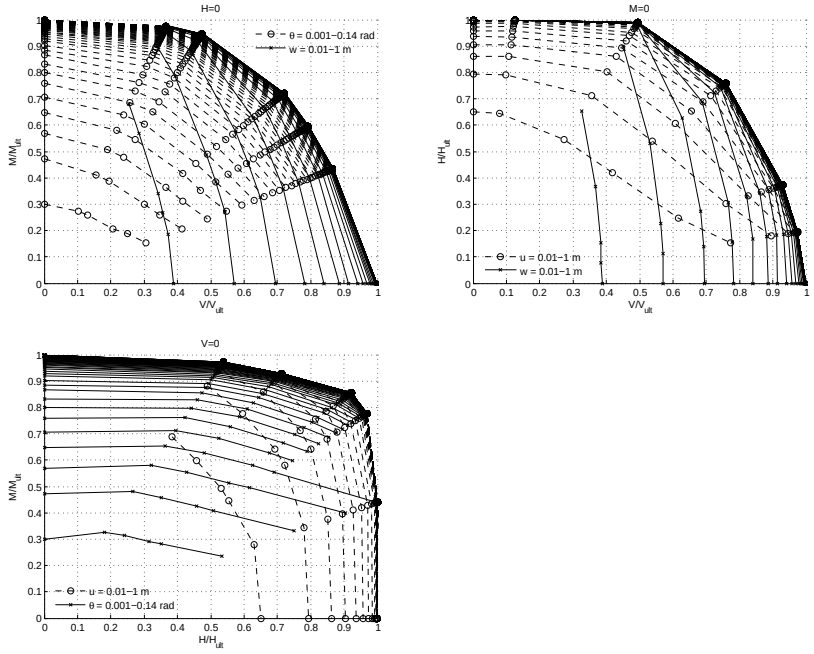

Figure D.18: *2D displacement contours for h/D=0.5, OCR=1,* $N_{eq} = 10$,$\tau_a = 0$

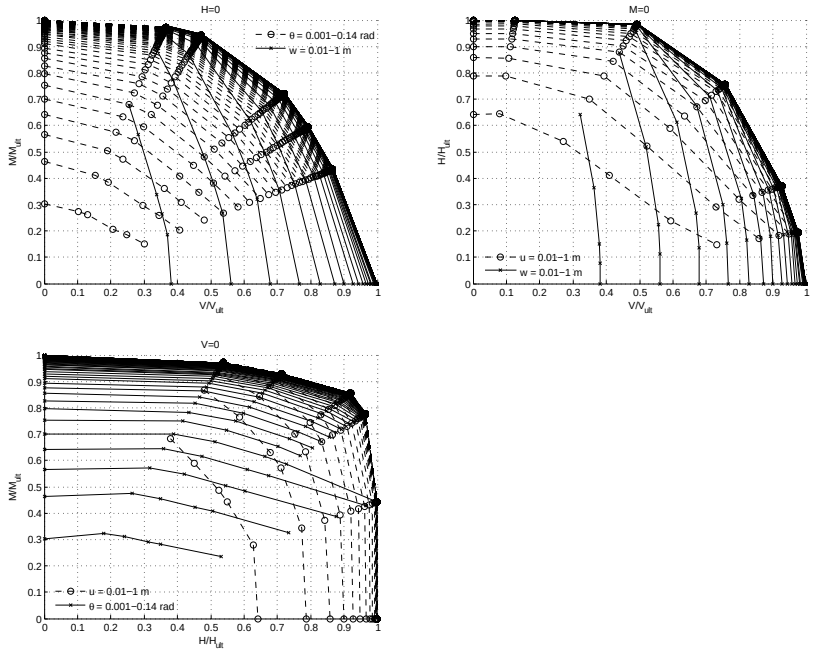

Figure D.19: *2D displacement contours for h/D=0.5, OCR=1,* $N_{eq} = 100$,$\tau_a = 0$

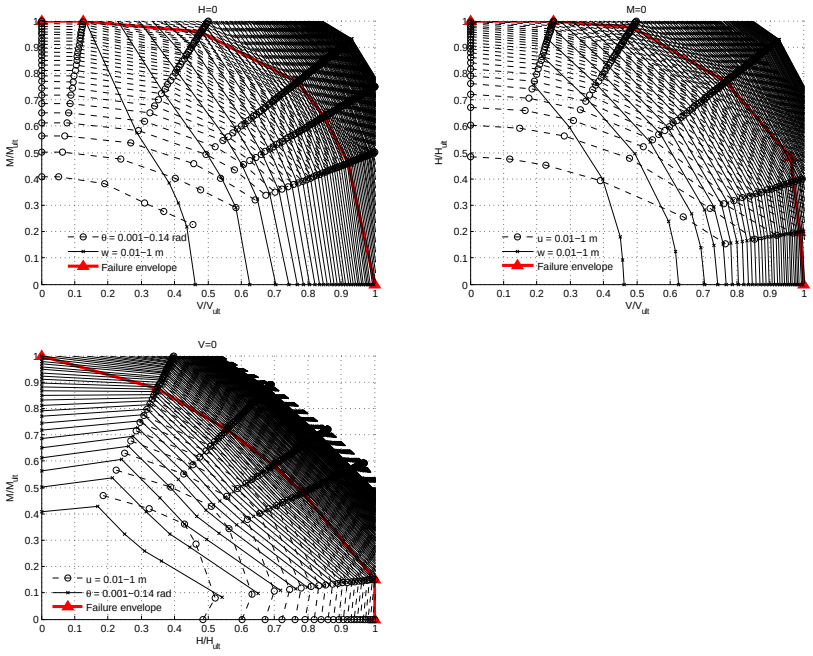

Figure D.20: *2D displacement contours for h/D=1, OCR=40,* $N_{eq} = 10$,$\tau_{cy}/\tau_a = 2$

D.2 3D displacement contour diagrams

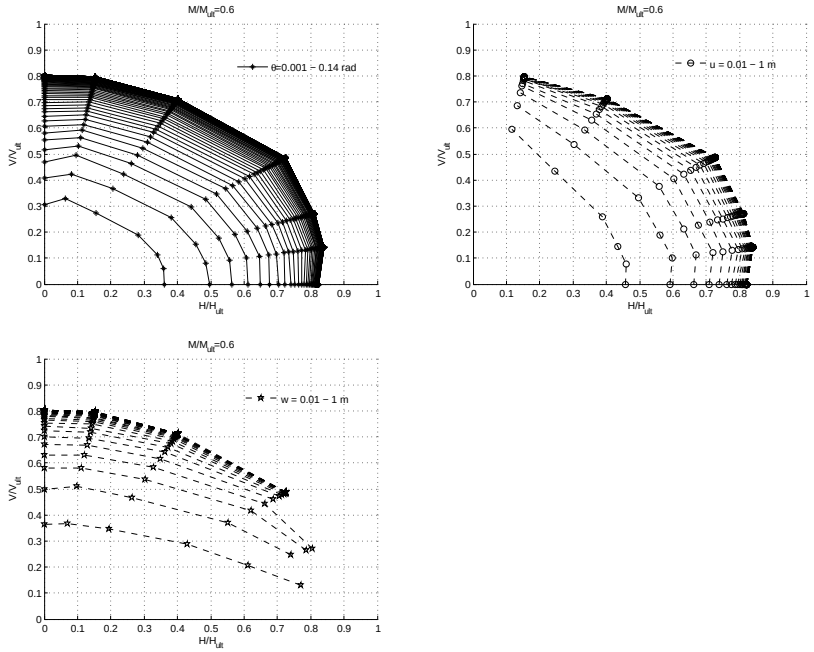

Figure D.21: *3D displacement contours for* $M/M_{ult} = 0.6$*,h/D=1, OCR=1,* $N_{eq} = 100$*,*$\tau_{cy}/\tau_a = 2$

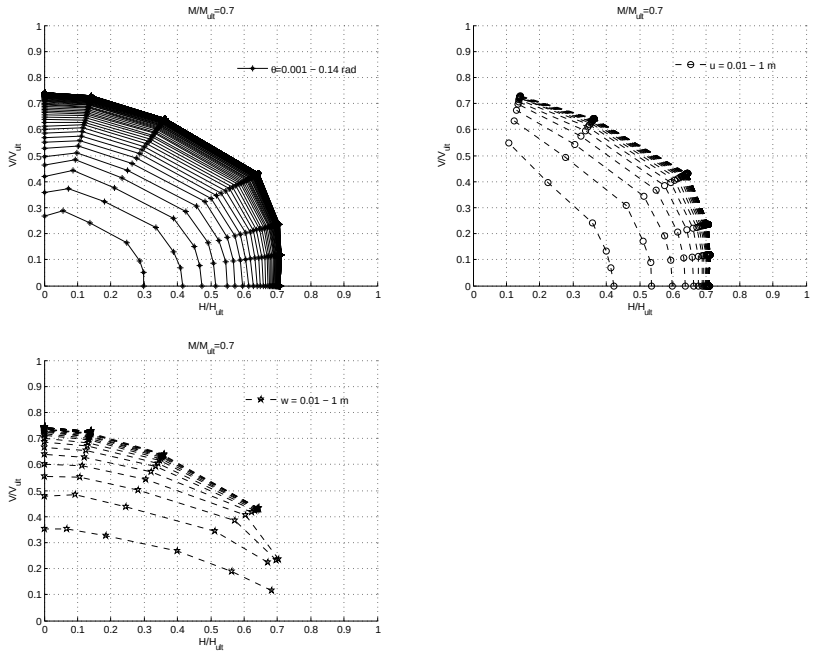

Figure D.22: *3D displacement contours for* $M/M_{ult} = 0.7$